Goethe-Universität Frankfurt am Main

New insights in LUBAC- and OTULIN-mediated M1 poly-ubiquitination in the regulation of bulk and selective autophagy

Dissertation

zur Erlangung des Doktorgrades der Naturwissenschaften

vorgelegt beim Fachbereich 14 Biochemie, Chemie und Pharmazie
der Johann Wolfgang Goethe-Universität
in Frankfurt am Main

von
Laura Zein
aus Trier

Frankfurt am Main, 2024
(D30)

Vom Fachbereich 14 der Johann Wolfgang Goethe-Universität als Dissertation angenommen.

Dekan:	Prof. Dr. Clemens Glaubitz, FB14
Gutachter 1:	Prof. Dr. Stefan Knapp, FB14
Gutachter 2:	PD Dr. Sjoerd J. L. van Wijk, FB16

Datum der Disputation: noch offen

Table of contents

Table of contents ..... **I**

List of figures ..... **V**

List of tables ..... **VI**

Abbreviations ..... **VII**

1 Abstract **1**

2 Introduction **3**

2.1 Autophagy 3
2.1.1 The autophagy pathway 3
2.1.1.1 Autophagy initiation and phagophore nucleation 4
2.1.1.2 Expansion of the phagophore 4
2.1.1.3 Maturation of the autophagosome 5
2.1.2 Role of autophagy 6
2.1.3 Regulation of autophagy 7
2.1.3.1 Post-translational regulation of autophagy 7
2.1.3.2 Transcriptional regulation of autophagy 7
2.1.4 Selective autophagy pathways 8
2.1.5 Selective autophagy of lysosomes (lysophagy) 8
2.1.5.1 Sensing of lysosomal damage and ubiquitination in lysophagy 9
2.1.5.2 Autophagy receptors in lysophagy 11
2.1.5.3 Regulation of lysophagy 11
2.1.6 Selective autophagy of protein aggregates (aggrephagy) 12
2.1.6.1 Autophagy receptors in aggrephagy 12
2.1.6.2 Regulation of aggrephagy 13
2.1.6.3 Chaperone-assisted selective autophagy (CASA) 14
2.1.7 Glioblastoma multiforme (GBM) 14
2.1.7.1 Role of autophagy in GBM 15
2.1.8 Role of autophagy in neurodegenerative diseases 15
2.1.9 Autophagy-inducing drugs 16
2.1.9.1 Loperamide hydrochloride (LOP) 16
2.1.9.2 L-Leucyl-L-Leucine methyl ester (LLOMe) 16
2.2 The ubiquitin code 17
2.2.1 Ubiquitination 17
2.2.2 Deubiquitinating enzymes 19
2.3 M1-linked (linear) ubiquitination 20
2.3.1 Linear ubiquitin chain assembly complex (LUBAC) 20
2.3.2 M1 Ub-specific DUBs 22
2.3.2.1 OTULIN 22
2.3.2.2 CYLD 23
2.3.3 Roles of M1 poly-Ub 23
2.3.3.1 Immune receptor-mediated NF-κB activation 23

2.3.3.2 Cell death 24
2.3.3.3 Autophagy 24
2.3.3.4 Other roles of M1 poly-Ub 24
2.3.4 M1 poly-Ub in human diseases 25

3 Aim of the study 26

4 Materials and methods 27

4.1 Materials 27
4.1.1 Cell lines 27
4.1.2 Cell culture reagents 27
4.1.3 Drugs and inhibitors 28
4.1.4 Chemicals and reagents 29
4.1.5 Fluorescent dyes 30
4.1.6 Buffers and solutions 30
4.1.7 Antibodies 31
4.1.8 qPCR primer 34
4.1.9 siRNA 34
4.1.10 Guide RNA sequences for CRISPR/Cas9 34
4.1.11 Plasmids 35
4.1.12 Kits and cloning reagents 35
4.1.13 Plastic ware and consumables 36
4.1.14 Equipment and instruments 37
4.1.15 Software and algorithms 39
4.2 Methods 39
4.2.1 Cell culture 39
4.2.1.1 Culturing conditions of cell lines 39
4.2.1.2 Freezing and thawing of cell lines 40
4.2.1.3 Cell counting 40
4.2.1.4 Seeding and treatment of cells 40
4.2.2 iPSC culture and neuronal differentiation 41
4.2.3 Culture of primary mouse cortical neurons 41
4.2.4 Generation of CRISPR/Cas9-derived *OTULIN* KO cells 42
4.2.4.1 Viral particle production and target cell transduction 42
4.2.5 Generation of myc-APEX2-LC3B expressing MZ-54 cells 42
4.2.6 Quantification of cell death 43
4.2.7 RNAi-mediated silencing of protein expression 43
4.2.8 Immunofluorescence analysis (confocal microscope) 43
4.2.9 Electron microscopy 44
4.2.10 Western blot analysis 45
4.2.10.1 Cell lysis and Bicinchoninic acid assay (BCA) 45
4.2.10.2 SDS-polyacrylamide gel electrophoresis (SDS-PAGE) 45
4.2.10.3 Western Blotting 45
4.2.10.4 Protein detection by enhanced chemiluminescence (ECL) 46
4.2.11 NP-40-soluble and NP-40-insoluble cell fractionation 46
4.2.12 Organelle (nuclear) fractionation 46

4.2.13 Quantitative real-time PCR (qRT-PCR) 47
4.2.13.1 RNA isolation and cDNA synthesis 47
4.2.13.2 qRT-PCR 47
4.2.14 APEX2-based autophagosome content profiling 48
4.2.14.1 Proximity labeling 48
4.2.14.2 Proteinase K digest 48
4.2.14.3 Streptavidin pulldown 49
4.2.15 Mass spectrometry (MS) data collection and analysis 50
4.2.16 Statistical analysis 51

5 Results 52

5.1 Characterization of the function of OTULIN and LUBAC in autophagy 52
5.1.1 Loss of OTULIN leads to enhanced autophagy induction and increases the autophagic flux 52
5.1.2 OTULIN depletion triggers ultrastructural increases in degradative compartments and autophagosomes 54
5.1.3 Autophagosome content profiling reveals OTULIN-dependent autophagy cargo proteins 55
5.2 Role of OTULIN and M1 poly-Ub in aggrephagy 59
5.2.1 Loss of OTULIN enhances the formation of M1 poly-Ub-positive protein aggregates in response to proteotoxic stress 59
5.2.2 Formation and clearance of puromycin-labeled peptides is regulated in an OTULIN-dependent manner 62
5.3 Role of OTULIN and M1 poly-Ub in lysophagy 64
5.3.1 M1 poly-Ub accumulates at damaged lysosomes 64
5.3.2 TAX1BP1 localizes to M1 poly-Ub modified lysosomes in response to lysosomal damage 65
5.3.3 Effect of OTULIN depletion on the lysophagic flux 66
5.3.4 OTULIN and M1 poly-Ub control TBK1 activation after lysosomal damage 67
5.3.5 OTULIN depletion does not affect nuclear translocation of TFEB in response to lysosomal damage 68
5.3.6 Accumulation of M1 poly-Ub at damaged lysosomes induces local NF-κB activation 69
5.3.7 M1 poly-Ub accumulation and NF-κB activation requires K63 poly-Ub deposited on damaged lysosomes 74
5.3.8 Lysophagy serves pro-survival roles during LMP-induced cell death 77
5.3.9 Role of M1 poly-Ub in the response to lysosomal damage in human dopaminergic neurons and primary mouse cortical neurons 78

6 Discussion 80

6.1 Function of OTULIN in the control of autophagy 80
6.2 OTULIN-dependent effects on autophagy cargo proteins 81
6.3 OTULIN- and M1 poly-Ub-mediated regulation of aggrephagy 82
6.4 Role of OTULIN and M1 poly-Ub in the response to lysosomal damage 83
6.5 TBK1 activation after lysosomal damage is regulated by OTULIN and M1 poly-Ub 85
6.6 Nuclear translocation of TFEB is not controlled by OTULIN 85

6.7 M1 poly-Ub at damaged lysosomes serves as platform for local NF-κB activation 85

6.8 K63 poly-Ub is required for M1 ubiquitination of damaged lysosomes and local NF-κB activation 86

6.9 Lysophagy serves pro-survival functions in the response to lysosomal damage 87

6.10 Modeling the response to lysosomal damage in primary human and mouse neurons 87

6.11 Limitations and Outlook 88

7 Deutsche Zusammenfassung 92

8 References 98

9 Danksagung 121

10 Curriculum vitae 122

11 Erklärung 124

List of figures

Figure 1. The autophagy pathway. 6
Figure 2. The ubiquitin code. 18
Figure 3. Structure of LUBAC subunits and the DUBs OTULIN and CYLD. 21
Figure 4. Loss of OTULIN enhances LC3 lipidation in response to autophagy induction and increases the autophagic flux. 53
Figure 5. OTULIN depletion enhances LOP-induced formation of LC3 and M1 poly-Ub puncta. 54
Figure 6. Loss of OTULIN enhances the formation of degradative compartments and autophagosomes. 55
Figure 7. Generation and validation of myc-APEX2-LC3B-expressing MZ-54 cells. 56
Figure 8. APEX2-based autophagosome content profiling identifies OTULIN-dependent autophagy cargo candidates. 57
Figure 9. Validation of selected cargo candidates. 58
Figure 10. TAX1BP1 degradation is regulated in an OTULIN-dependent manner. 59
Figure 11. Puromycin-induced formation of M1 poly-Ub- and K63 poly-Ub-positive puncta is enhanced in OTULIN-deficient cells. 60
Figure 12. Puromycin induces accumulation of insoluble M1 poly-Ub-modified proteins upon loss of OTULIN. 61
Figure 13. TAX1BP1 and p62 colocalize with M1 Ub-labeled puncta in response to puromycin-induced proteotoxic stress. 62
Figure 14. Loss of OTULIN delays clearance of puromycin-labeled peptides. 63
Figure 15. Clearance of puromycin-labeled peptides is ubiquitin-dependent. 64
Figure 16. M1 poly-Ub accumulates at damaged lysosomes. 65
Figure 17. TAX1BP1 is recruited to damaged lysosomes and colocalizes with LLOMe-induced M1 poly-Ub puncta. 66
Figure 18. Clearance of galectin-3 puncta after lysosomal damage might be affected by loss of OTULIN. 67
Figure 19. Loss of OTULIN increases TBK1 phosphorylation in response to lysosomal damage. 68
Figure 20. LLOMe-induced nuclear translocation of TFEB is not affected by loss of OTULIN expression. 69
Figure 21. M1 poly-Ub accumulation at damaged lysosomes induces local recruitment of NEMO. 70
Figure 22. Lysosomal damage induces IKK phosphorylation on M1 poly-Ub-modified lysosomes in an OTULIN-dependent manner. 71
Figure 23. HOIPIN-8-mediated HOIP inhibition decreases LLOMe-induced formation of NEMO puncta. 72
Figure 24. Inhibition of IKKβ with TPCA-1 prevents IKK phosphorylation at LLOMe-induced M1 poly-Ub puncta. 73
Figure 25. M1 poly-Ub accumulation at damaged lysosomes induces NF-κB target gene activation in an OTULIN-dependent manner. 74
Figure 26. Formation of M1 poly-Ub chains at damaged lysosomes relies on K63 poly-Ub. 75
Figure 27. Local recruitment of NEMO to damaged lysosomes and NF-κB activation depends on K63 poly-Ub. 76
Figure 28. Lysophagy serves pro-survival roles during LMP-induced cell death. 77
Figure 29. M1 poly-Ub increases at damaged lysosomes in human dopaminergic neurons and primary mouse cortical neurons. 79

List of tables

Table 1. Human cell lines 27
Table 2. Media, supplements and additional cell culture reagents 27
Table 3. Drugs and inhibitors 28
Table 4. Chemicals and reagents 29
Table 5. Fluorescent dyes 30
Table 6. Buffers and solutions 30
Table 7. Primary antibodies 31
Table 8. Secondary antibodies for Western Blotting 33
Table 9. Secondary antibodies and other reagents for immunofluorescence 33
Table 10. qPCR primer 34
Table 11. siRNA 34
Table 12. Guide RNA sequences for CRISPR/Cas9 34
Table 13. Plasmids 35
Table 14. Kits and cloning reagents 35
Table 15. Plastic ware and consumables 36
Table 16. Equipment and instruments 37
Table 17. Software and algorithms 39
Table 18. Cell numbers for seeding 41
Table 19. Program for cDNA synthesis 47
Table 20. qRT-PCR Master Mix 48
Table 21. qRT-PCR program 48
Table 22. Reactions for proteinase K protection assay 49

Abbreviations

(m)RNA	(Messenger) ribonucleic acid
(mi)RNA	(Micro) ribonucleic acid
(r)RNA	(Ribosomal) ribonucleic acid
(si)RNA	(Silencer) ribonucleic acid
(t)RNA	(Transfer) ribonucleic acid
A	Adenine
AAA+	ATPase Associated with diverse cellular Activities
ABC-DLBCL	Activated B cell-like subtype of diffuse large B-cell lymphoma
ABIN	Ubiquitin-binding in A20-binding inhibitor of NF-κB
AD	Alzheimer disease
ADCD	Autophagy-dependent cell death
AHA	L-azidohomoalanine
ALFY	Autophagy-linked FYVE protein
ALIX	ALG-2-interacting protein X
ALS	Amyotrophic lateral sclerosis
AMBRA1	Activating molecule in BECN1-regulated autophagy protein 1
AMP	Adenosine monophosphate
AMPK	AMP-activated protein kinase
ANOVA	Analysis of variance
ATF4	Activating transcription factor 4
ATP	Adenosine triphosphate
ATG	Autophagy-related protein
BafA1	Bafilomycin A1
BAG3	Bcl-2 associated athanogene (BAG) family molecular chaperone regulator 3
Bcl-2	B-cell lymphoma 2
BECN1	Beclin-1
BMDM	Bone marrow-derived macrophages
bp	Base pairs
BRD4	Bromodomain-containing protein 4
BSA	Bovine serum albumin
C	Cytosine
CASA	Chaperone-assisted selective autophagy
CCT2	Chaperonin-containing TCP-1 subunit 2
cDNA	Complementary DNA
cIAP	Cellular inhibitor of apoptosis
CHIP	Carboxy terminus of Hsp70-interacting protein

CHMP2A	Charged multivesicular body protein 2a
CHX	Cycloheximide
CMA	Chaperone-mediated autophagy
CNS	Central nervous system
CO_2	Carbon dioxide
CRD	Carbohydrate recognition domain
C_t	Cycle threshold
CRISPR	Clustered regularly interspaced short palindromic repeats
CUL4A	Cullin-4A
CYLD	Cylindromatosis
CYP3A4	Cytochrome P450 3A4
DAPI	4′,6-diamidino-2-phenylindole
DDB1	DNA damage-binding protein 1
DDPI	Dipeptidyl peptidase I (or Cathepsin C)
DFCP1	Zinc-finger FYVE domain-containing protein 1
DGC	Degradative compartment
DTT	Dithiothreitol
DMEM	Dulbecco's Modified Eagle Medium
DMSO	Dimethyl sulfoxide
DNA	Deoxyribonucleic acid
dNTP	Deoxynucleoside triphosphate
DRiPs	Defective ribosomal products
DUB	Deubiquitinating enzyme
EBSS	Earle's Balanced Salt Solution
ECL	Enhanced chemiluminescence
E. coli	*Escherichia coli*
(e)GFP	(Enhanced) green fluorescent protein
e.g.	*Exempli gratia* ("for example")
EDTA	Ethylenediaminetetraacetic acid
EGFR	Epidermal growth factor receptor
EGTA	Ethylene glycol-bis(β-aminoethyl ether)-N,N,N',N'-tetraacetic acid
ELDR	Endo-lysosomal damage response
ER	Endoplasmic reticulum
ERK	Extracellular signal-regulated kinase
ESCRT	Endosomal sorting complex required for transport
et al.	*Et alii* ("and others")
FADD	FAS-associated death domain protein
FBS	Fetal bovine serum

FBXO	F-box only protein
FDA	Food and Drug Administration
FIP200	Focal adhesion kinase family-interacting protein of 200 kDa
FITC	Fluorescein isothiocyanate
for/fw	Forward
FOXO	Forkhead box O
G	Guanine
GABARAP	γ-aminobutyric acid receptor-associated protein
GBM	Glioblastoma multiforme
G3BP1	Ras GTPase-activating protein-binding protein 1
GSC	Glioblastoma stem cell
h	Hour
HBSS	Hanks' balanced salt solution
HCQ	Hydroxychloroquine
HD	Huntington disease
HDAC6	Histone deacetylase 6
HECT	Homologous to E6-associated protein (E6AP) C-terminus
HOIL-1	Heme-oxidized IRP2 Ubiquitin ligase 1 (or RBCK1)
HOIP	HOIL-1-interacting protein (or RNF31)
HOIPIN	HOIP inhibitor
HRP	Horseradish peroxidase
hsc70	Heat shock-cognate protein of 70 kDa
HSPA5	Heat shock protein family A member 5
HSPB8	Heat shock protein family B (small) member 8
HSP27	Heat shock protein 27
Htt	Huntingtin
IDH	Isocitrate dehydrogenase
i.e.	*Id est* ("that is")
IKK	Inhibitor of κB (IκB) kinase
IL-1βR	Interleukin-1β receptor
iPSC	Induced pluripotent stem cell
IRAK1	IL-1R-associated kinase 1
IRAK4	IL-1R-associated kinase 4
ISG15	Interferon-stimulated gene 15
JAMM	JAB1/MPN/MOV34 metalloprotease
kb	Kilobase (10^3 base pairs)
KBTBD7	Kelch repeat and BTB domain-containing protein 7
LAMP1	Lysosome-associated membrane protein 1

LAMP2A	Lysosomal-associated membrane protein type 2A
LDD	Linear Ubiquitin chain-determining domain
LIR	LC3-interacting region
LIMP2	Lysosome membrane protein 2
LFQ	Label-free quantification
LGALS	Galectin
LLOMe	L-Leucyl-L-Leucine methyl ester
LLPS	Liquid-liquid phase separation
LMP	Lysosomal membrane permeabilization
LOP	Loperamide hydrochloride
LRSAM1	Leucine rich repeat and sterile alpha motif containing 1
LSD	Lysosomal storage disease
LTM	LUBAC-tethering motif
LUBAC	Linear Ubiquitin chain assembly complex
LOF	Loss of function
3-MA	3-methyladenine
MAPK	Mitogen-activated protein kinase
MAP1LC3/LC3	Microtubule-associated proteins 1A/1B light chain 3
MEF	Mouse embryonic fibroblast
MINDY	Motif interacting with ubiquitin (MIU)-containing novel DUB family
MJD	Machado-Joseph Disease
MLKL	Mixed lineage kinase domain-like protein
mLST8	Mammalian lethal with SEC13 protein 8
MS	Mass spectrometry
mSIN1	Mammalian stress-activated map kinase-interacting protein 1
MST1	Mammalian ste20-like protein kinase 1
MTOC	Microtubule organizing centre
mTOR	Mammalian target of rapamycin
mTORC1	mTOR complex 1
mTORC2	mTOR complex 2
MyD88	Myeloid differentiation primary-response protein 88
N/A	Not available
NAP1	NAK-associated protein 1
NBR1	Next to BRCA1 gene 1
NEDD8	Neural precursor cell expressed developmentally down-regulated protein 8
NEMO	NF-κB essential modulator
ND	Neurodegenerative disease

NDP52	Nuclear dot protein 52
NF-κB	Nuclear factor-κB
NHT	Non-human target
NLR	NOD-like receptor
NLRP3	NACHT domain, leucine-rich repeat (LRR)-, and pyrin (N-terminal homology) domain (PYD)-containing protein 3
NOD2	Nucleotide-binding oligomerization domain-containing protein 2
NZF	Nuclear protein localization 4 zinc finger
OPTN	Optineurin
ORAS	OTULIN-related autoinflammatory syndrome
OTU	Ovarian tumor
OTULIN	OTU domain-containing DUB with linear linkage specificity
PAS	Phagophore assembly site
PB	Permeabilization buffer
PBS	Phosphate buffered saline
PBS-T	PBS-Tween
PB1	Phox and Bem1p
PCR	Polymerase chain reaction
PD	Parkinson disease
Pen/Strep	Penicillin-streptomycin
PE	Phosphatidylethanolamine
PH	Pleckstrin-homology
PI	Propidium iodide
PIC	Protease inhibitor cocktail
PIMO	Pimozide
PIM	PUB interaction motif
PINK1	PTEN-induced putative kinase 1
PI3P	Phosphatidylinositol-3-phosphate
PI3K	Phosphatidylinositol-3 kinase
PI3KC3-C1	Phosphatidylinositol-3-kinase catalytic subunit type 3 complex 1
PKC	Protein kinase C
PLAA	Phospholipase A-2-activating protein
polyQ-Htt	Poly-glutamine huntingtin
PRU	Pleckstrin-like receptor for ubiquitin
PTM	Post-translational modification
PTP4A2	Protein tyrosine phosphatase 4A2
PUB	Peptide N-glycosidase/UBA
qRT-PCR	Quantitative real-time PCR

Raptor	Regulatory-associated protein of mTOR
RB1CC1	RB1-inducible coiled-coil protein 1
RBR	RING-in-between-RING
RBCK1	RanBP-type and C3HC4-type zinc finger-containing protein 1
RETREG1	Reticulophagy regulator 1
rev/rv	Reverse
RFP	Red fluorescent protein
Rictor	Rapamycin-insensitive companion of mTOR
RIG-I	Retinoic acid-inducible gene 1 protein
RING	Really interesting new gene
RIPK1	Receptor-interacting protein kinase 1
RNF2	RING finger protein 2
RNF31	RING finger protein 31
ROS	Reactive oxygen species
rpm	Revolutions per minute
RSC	Receptor signaling complex
RT	Room temperature
SAR	Selective autophagy receptor
SCF	S-phase kinase-associated protein 1 (SKP1)-Cullin 1 (CUL1)-F-box protein
SDS	Sodium dodecyl sulfate
SDS-PAGE	SDS-polyacrylamide gel electrophoresis
Sharpin	Shank-associated RH domain-interacting protein
sHSP	Small heat shock protein
SKICH	Ski-interacting protein (SKIP) carboxyl homology
SNAP29	Synaptosomal-associated protein 29
SNARE	Soluble N-ethylmaleimide-sensitive factor attachment protein receptor
SNP	Single nucleotide polymorphism
SPATA2	Spermatogenesis-associated protein 2
Spi2A	Serine protease inhibitor 2A
SR-SIM	Super-resolution structured illumination microscopy
STAT1	Signal transducer and activator of transcription 1
STX17	Syntaxin 17
SUMO	Small ubiquitin-related modifier
T	Thymine
TANK	TRAF family member associated NF-κB activator
TAX1BP1	Tax1-binding protein 1

TBK1	TANK-binding kinase 1
TDP-43	TAR DNA-binding protein 43
TECPR1	Tectonin beta-propeller repeat-containing protein 1
TEMED	Tetramethylethylenediamine
TERT	Telomerase reverse transcriptase
TEX264	Testis expressed protein 264
TFEB	Transcription factor EB
TLR	Toll-like receptor
TNFα	Tumor necrosis factor alpha
TNFAIP3	Tumor necrosis factor alpha-induced protein 3
TNFR1	Tumor necrosis factor receptor 1
TMEM192	Transmembrane protein 192
TMZ	Temozolomide
TOLLIP	Toll-interacting protein
TOMM40	Mitochondrial import receptor subunit TOM40 homolog
TRAF6	TNF receptor-associated factor 6
TRiC	TCP-1 ring complex
TRIM16	Tripartite motif-containing protein 16
TSC2	Tuberous sclerosis 2 protein
TSG101	Tumor susceptibility gene 101
U	Enzyme unit
Ub	Ubiquitin
UBA	Ubiquitin-associated
UBAN	Ubiquitin-binding in A20-binding inhibitor of NF-κB (ABIN) and NF-κB essential modulator (NEMO)
UBD	Ubiquitin-binding domain
Ubl	Ubiquitin-like
UBXD1	UBX domain-containing protein 1
UB2QL1	Ubiquitin-conjugating enzyme E2Q-like protein 1
UBZ	Ubiquitin-binding zinc finger domain
UCH	Ubiquitin C-terminal hydrolases
UIM	Ubiquitin-interacting motif
ULK1	Unc-51-like kinase 1
UPS	Ubiquitin-proteasome system
USP	Ubiquitin-specific protease
UTR	Untranslated region
VAMP8	Vesicle-associated membrane protein 8
VCP	Valosin-containing protein (p97)

VPS4	Vacuolar protein sorting-associated protein 4
VPS15	Vacuolar protein sorting 15
VPS34	Vacuolar protein sorting 34
VPS37A	Vacuolar protein sorting-associated protein 37A
WCL	Whole cell lysate
WDFY1	WD repeat and FYVE domain-containing protein 1
WDR81	WD repeat-containing protein 81
WHO	World health organization
WIPI2	WD repeat domain phosphoinositide-interacting protein 2
WT	Wild-type
YOD1	Ubiquitin thioesterase OTU1
ZF	Zinc finger
ZUP1	Zinc finger-containing Ubiquitin peptidase 1

1 Abstract

Autophagy is an important degradation pathway mediating the engulfment of cellular material (cargo) into autophagosomes followed by degradation in autophagosomes. Different stress stimuli, e.g. nutrient deprivation, oxidative stress or organelle damage, engage autophagy to maintain cellular homeostasis, recycle nutrients or remove damaged cell organelles. Autophagy not only degrades bulk cytoplasmic material but also selective autophagic cargo, for example lysosomes (lysophagy), mitochondria (mitophagy), ER (ER-phagy), lipid droplets (lipophagy), protein aggregates (aggrephagy) or pathogens (xenophagy). Selective autophagy pathways are regulated by selective autophagy receptors which bind to ubiquitinated cargo proteins and link them to LC3 on the autophagosomal membrane.

Ubiquitination is an essential post-translational modification controlling different cellular processes such as proteasomal and lysosomal degradation or innate immune signaling. M1-linked (linear) poly-Ubiquitin (poly-Ub) chains are exclusively assembled by the E3 ligase linear ubiquitin chain assembly complex (LUBAC) and removed by the M1 poly-Ub-specific OTU domain-containing deubiquitinase with linear linkage specificity (OTULIN). In addition to key functions in innate immune signaling and nuclear factor-κB (NF-κB) activation, M1 ubiquitination is also implicated in the regulation of autophagy. LUBAC and OTULIN control autophagy initiation and maturation and the autophagic clearance of invading bacteria via xenophagy. However, additional functions of LUBAC- and OTULIN-regulated M1 ubiquitination in autophagy are largely unknown and it also remains unexplored if LUBAC and OTULIN control other selective autophagy pathways in addition to xenophagy. This study aimed to unravel the role of LUBAC- and OTULIN-controlled M1 ubiquitination in bulk and selective autophagy in more detail.

In this study, characterization of OTULIN-depleted MZ-54 glioblastoma (GBM) cells revealed that OTULIN deficiency results in enhanced LC3 lipidation in response to autophagy induction and upon blockade of late stage autophagy with Bafilomycin A1 (BafA1). Furthermore, electron microscopy analysis showed that OTULIN-deficient cells have an increased number of degradative compartments (DGCs), confirming enhanced autophagy activity upon loss of OTULIN. APEX2-based autophagosome content profiling identified various OTULIN-dependent autophagy cargo proteins. Among these were the autophagy receptor TAX1BP1 which regulates different forms of selective autophagy (e.g. lysophagy, aggrephagy) and the glycan-binding protein galectin-3 which serves key functions in lysophagy, suggesting a role of OTULIN and M1 poly-Ub in the regulation of aggrephagy and lysophagy.

To study aggrephagy, protein aggregation was induced with puromycin which causes premature termination of translation and accumulation of defective ribosomal products (DRiPs). Loss of OTULIN increased the number of M1 poly-Ub-positive foci and insoluble proteins and reduced the levels of soluble TAX1BP1 and p62 in response to puromycin-induced proteotoxic stress.

Intriguingly, upon induction of lysosomal membrane permeabilization (LMP) with the lysosomotropic drug L-Leucyl-L-Leucine methyl ester (LLOMe), M1 poly-Ub strongly accumulated at damaged lysosomes and colocalized with TAX1BP1- and galectin-3-positive puncta. M1 poly-Ub-modified lysosomes formed a platform for NF-κB essential modulator (NEMO) and inhibitor of κB (IκB) kinase (IKK) complex recruitment and local NF-κB activation in a K63 poly-Ub- and OTULIN-dependent manner. Furthermore, inhibition of lysosomal degradation enhanced LLOMe-induced cell death, suggesting pro-survival functions of lysophagy following LMP. Enrichment of M1 poly-Ub at damaged lysosomes was also observed in human dopaminergic neurons and in primary mouse embryonic cortical neurons, confirming the importance of M1 poly-Ub in the response to lysosomal damage.

Together, these results identify OTULIN as a negative regulator of autophagy induction and the autophagic flux and reveal OTULIN-dependent autophagy cargo proteins. Furthermore, this study uncovers novel and important roles of M1 poly-Ub in the response to lysosomal damage and local NF-κB activation at damaged lysosomes.

2 Introduction

2.1 Autophagy

Autophagy is a conserved catabolic pathway which can be engaged in response to different stress stimuli, such as oxidative stress, nutrient deprivation or DNA damage, and mediates the degradation of cytosolic components (cargo) in lysosomes [1]. Historically, the term ‘autophagy’ is derived from the Ancient Greek word for ‘self-eating’ and was established by Christian de Duve, the discoverer of lysosomes, in 1963 to describe the ability of lysosomes to digest portions of the cytoplasm [2]. However, the interest in autophagy research emerged after Yoshinori Ohsumi’s identification of 15 autophagy-related proteins (ATGs) in yeast which are required for the delivery of autophagic cargo to the vacuole [3]. In the following years, research in the autophagy field grew extensively and revealed the physiological importance of this process for cellular homeostasis as well as in health and disease [4]. Autophagy can be categorized into three major types: microautophagy [5], chaperone-mediated autophagy (CMA) [6] and macroautophagy. Microautophagy describes the direct engulfment of cytoplasmic components into lysosomes by membrane invagination and their degradation by lysosomal enzymes [5]. During CMA, the chaperone heat shock-cognate protein of 70 kDa (hsc70) selectively recognizes proteins with the motif KFERQ and targets them to the lysosomal membrane where they bind to monomers of the lysosomal membrane protein lysosomal-associated membrane protein type 2A (LAMP2A), thereby triggering formation of a multimeric LAMP2A translocation complex. After protein unfolding, the substrate proteins translocate into the lysosomal lumen with the help of a lysosomal form of hsc70 (lys-hsc70) and are degraded by lysosomal proteases [7]. Macroautophagy (hereafter referred to as ‘autophagy’) is the major type of autophagy and is characterized by the formation of double-membraned structures called autophagosomes which sequester cytoplasmic material. Upon fusion of autophagosomes with lysosomes to autolysosomes, the autophagic cargo is degraded by lysosomal hydrolases [8].

2.1.1 The autophagy pathway

Autophagy is a complex, multi-step process which requires the regulated action of five core ATG protein-containing complexes and can be divided into three steps: autophagy initiation and phagophore nucleation, phagophore expansion and maturation of the autophagosome [9].

2.1.1.1 Autophagy initiation and phagophore nucleation

Autophagy starts with nucleation of an isolation membrane to form the so-called phagophore, the autophagosome precursor, at the phagophore assembly site (PAS) on specific phosphatidylinositol-3-phosphate (PI3P)-rich endoplasmic reticulum (ER) sites called 'omegasomes' [10,11]. Different stress stimuli, including starvation, oxidative stress, protein misfolding or ER stress, initiate autophagy by inducing autophosphorylation and activation of the Unc-51-like kinase 1 (ULK1) complex composed of ULK1, autophagy-related protein 13 (ATG13), RB1-inducible coiled-coil protein 1 (RB1CC1, also called focal adhesion kinase family-interacting protein of 200 kDa (FIP200)) and autophagy-related protein 101 (ATG101) [1,12]. The ULK1 complex is recruited to the PAS and phosphorylates subunits of the class III phosphatidylinositol 3-kinase catalytic subunit type 3 (PI3KC3) complex 1 (PI3KC3-C1) which consists of vacuolar protein sorting 34 (VPS34), PI3-kinase p150 subunit, beclin-1 (BECN1) and autophagy-related protein 14 (ATG14) [13-15]. VPS34, the catalytic subunit of PI3KC3-C1, drives local production of PI3P at the omegasome, thereby enabling nucleation of the phagophore and recruitment of the PI3P-binding proteins WD repeat domain phosphoinositide-interacting protein 2 (WIPI2) and zinc-finger FYVE domain-containing protein 1 (DFCP1) [16,17]. Different membrane sources contribute to phagophore formation, including autophagy-related protein 9 (ATG9)-containing vesicles, the ER, the Golgi apparatus, the plasma membrane, the recycling endosome, lipid droplets or mitochondria [10,17-22].

2.1.1.2 Expansion of the phagophore

Expansion of the phagophore essentially relies on the action of two ubiquitin (Ub)-like conjugation complexes: The Ub-like ATG12~ATG5-ATG16L complex and the Ub-like ATG8 family proteins [23]. In humans, the ATG8 protein family is divided in the microtubule-associated proteins 1A/1B light chain 3 (MAP1LC3/LC3) subfamily with the members LC3A, LC3B, LC3B2, LC3C and the γ-aminobutyric acid receptor-associated protein (GABARAP) subfamily with the members GABARAP, GABARAPL1 and GABARAPL2 [24]. During phagophore expansion, ATG8 proteins are conjugated to the lipid phosphatidylethanolamine (PE) in autophagosomal membranes. ATG8 proteins are synthesized as a pro-form and cleaved by the cysteine protease ATG4, thereby exposing a C-terminal glycine residue [25]. Processed ATG8 proteins are then activated by the E1-like enzyme ATG7 and conjugated to PE by the E2-like enzyme ATG3 [26]. Lipidated LC3 and GABARAP proteins are designated as LC3- and GABARAP-II, respectively (in contrast to unlipidated LC3- and GABARAP-I) and serve as linkers between the autophagic cargo and autophagosomes [1,27,28]. In addition, ATG8 proteins support

elongation and closure of the phagophore [29]. Attachment of ATG8 proteins to PE is promoted by the E3-like ATG12~ATG5-ATG16L complex [30,31]. The ATG12~ATG5-ATG16L complex itself is also assembled in a Ub-like conjugation reaction: first, ATG12 is activated by the E1-like enzyme ATG7 and conjugated to ATG5 by the E2-like enzyme ATG10 [32]. The ATG12~ATG5 conjugate then forms a complex with ATG16L. Of note, WIPI2 which is bound to PI3P in the phagophore membrane also binds directly to ATG16L, thereby enabling recruitment of the dimeric ATG12~ATG5-ATG16L complex to the phagophore where it drives conjugation of ATG8 proteins to PE [33,34].

2.1.1.3 Maturation of the autophagosome

Phagophore expansion is followed by sealing of the phagophore to a double-membraned vesicle, the so-called autophagosome [1]. The mechanism of phagophore sealing is not fully understood so far, but it has been shown that it requires the endosomal sorting complex required for transport III (ESCRT-III) subunit charged multivesicular body protein 2a (CHMP2A), the ESCRT-I subunit vacuolar protein sorting-associated protein 37A (VPS37A) and the AAA-ATPase vacuolar protein sorting-associated protein 4 (VPS4) [35,36]. After phagophore sealing the autophagosome undergoes different maturation steps before fusion with the lysosome. Thus, ATG8 proteins on the outer autophagosomal membrane are delipidated via the activity of ATG4, thereby releasing them from the membrane [37,38]. Autophagosome maturation also involves recruitment of different tethering factors and fusion proteins. These include microtubule-based kinesin motor proteins which are responsible for the delivery of peripheral autophagosomes to lysosomes in the perinuclear area [39] and specific fusion proteins like the soluble N-ethylmaleimide-sensitive factor attachment protein receptor (SNARE) protein family members syntaxin 17 (STX17) [40], synaptosomal-associated protein 29 (SNAP29) [41] and vesicle-associated membrane protein 8 (VAMP8) [42]. STX17 and SNAP29 are recruited to the autophagosomal membrane and interact with VAMP8 on the lysosomal membrane to form the trans-SNARE complex [9]. The homotypic fusion and protein sorting (HOPS) complex which is recruited to the autophagosome by ATG8 proteins [43] acts as core tethering factor: by interacting with STX17, it supports assembly of the trans-SNARE complex, thereby enabling SNARE-mediated autophagosome-lysosome fusion [44]. The autolysosomal environment is then acidified through lysosomal proton pumps such as V-ATPase [45], followed by degradation of the inner autophagosomal membrane and the autophagic cargo by lysosomal enzymes [9]. Recycled nutrients are transported back to the cytosol and can serve as building blocks for cellular metabolism (**Figure 1**) [46].

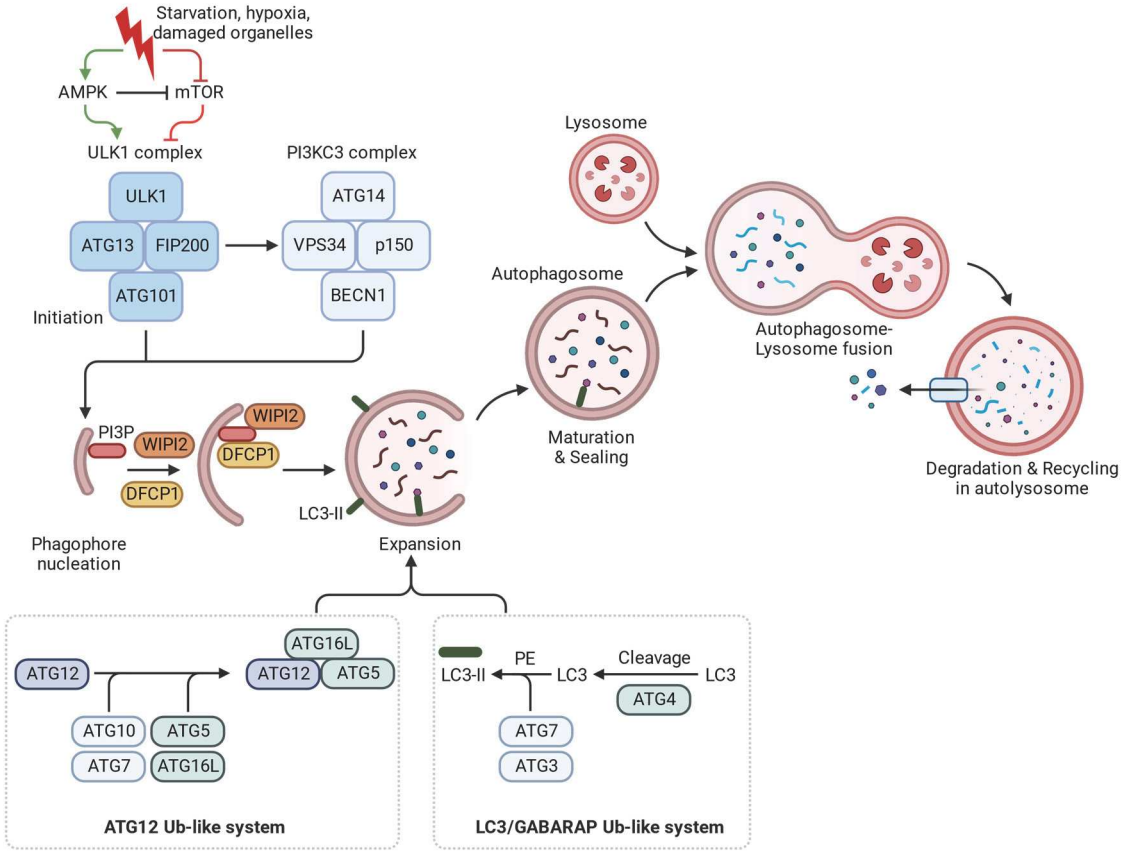

Figure 1. The autophagy pathway.

Different stress stimuli, including starvation, hypoxia or organelle damage, initiate phagophore nucleation by activating the ULK1 and PI3KC3 complex which drive PI3P production at specific ER sites called 'omegasomes'. WIPI2 and DFCP1 are recruited to the growing phagophore by binding to PI3P. Phagophore expansion requires the action of the ATG12 and LC3/GABARAP ubiquitin-like system. The ATG8 family proteins LC3 and GABARAP are processed by ATG4 and conjugated to PE in the phagophore membrane by ATG7 and ATG3. WIPI2 binds to ATG16L in the E3-like ATG12~ATG5-ATG16L complex, thereby recruiting the complex to the phagophore where it promotes conjugation of ATG8 proteins to PE. The phagophore is sealed to a double-membrane autophagosome and maturates through the action of different tethering and fusion factors. The mature autophagosome finally fuses with the lysosome to an autolysosome in which the autophagic cargo is degraded by acidic hydrolases. Recycled material is transported back to the cytosol and used for cellular metabolism. Adapted from [1] and created with BioRender.com.

2.1.2 Role of autophagy

Autophagy is an essential pathway for the maintenance of cellular homeostasis. There is always a basal rate of autophagy, however, in response to diverse stimuli including nutrient deprivation, oxidative stress, organelle damage, protein aggregation or pathogen infection, autophagy is increased [47,48]. Upregulation of autophagy serves cytoprotective functions, such as the recycling of nutrients for cellular metabolism or the clearance of damaged organelles and pathogens [49].

2.1.3 Regulation of autophagy

2.1.3.1 Post-translational regulation of autophagy

Due to its essential role in the response to stress and the maintenance of cellular homeostasis, autophagy is a tightly regulated process. Post-translational modifications (PTMs) including ubiquitination or phosphorylation serve key functions in the control of autophagy induction. One master negative regulator of autophagy is the serine/threonine kinase mammalian target of rapamycin (mTOR) which is found in two distinct complexes. mTOR complex 1 (mTORC1) contains the subunits mTOR, mammalian lethal with SEC13 protein 8 (mLST8) and regulatory-associated protein of mTOR (Raptor), and mTOR complex 2 (mTORC2) is composed of mTOR, mLST8, mammalian stress-activated map kinase-interacting protein 1 (mSIN1) and rapamycin-insensitive companion of mTOR (Rictor) [50]. Under nutrient-rich conditions, mTORC1 is active and inhibits autophagy initiation, nucleation and expansion by phosphorylating core autophagy proteins such as ULK1 [47,51], ATG13 [52], ATG14 [53], activating molecule in BECN1-regulated autophagy protein 1 (AMBRA1) [54], p300 [55] and WIPI2 [56]. mTORC1 activity is controlled by adenosine monophosphate (AMP)-activated protein kinase (AMPK). During starvation, decreased cellular energy levels result in changes of the adenosine triphosphate (ATP) to AMP ratio and this is sensed by AMPK [57]. AMPK phosphorylates raptor and tuberous sclerosis 2 protein (TSC2) [58-60], thereby negatively regulating mTORC1 and activating autophagy. Furthermore, AMPK can promote autophagy induction by directly phosphorylating and activating ULK1 and Beclin-1 [51,52,61]. Besides mTOR and AMPK, multiple other kinases such as mitogen-activated protein kinase (MAPK) or protein kinase C (PKC) are involved in the regulation of autophagy [62].

2.1.3.2 Transcriptional regulation of autophagy

In addition to regulation of key autophagy proteins by PTMs, autophagy is also controlled at the transcriptional level. Thus, the transcription factor EB (TFEB) critically regulates the expression of autophagy genes. Under basal conditions, TFEB is phosphorylated by mTORC1, which leads to sequestration of TFEB in the cytosol by binding to 14-3-3 proteins [63,64]. Nutrient deprivation or other stress stimuli such as lysosomal damage induce dephosphorylation of TFEB and release from 14-3-3 proteins, followed by translocation in the nucleus to induce the expression of genes involved in autophagy and lysosomal biogenesis [65]. Transcription factors of the forkhead box O (FOXO) family are also linked to transcriptional regulation of autophagy. Similar to TFEB, FOXOs are activated by phosphorylation and induce the expression of autophagy-related genes [66,67]. In contrast, autophagy is negatively regulated by the chromatin reader

bromodomain-containing protein 4 (BRD4) which acts together with the methyltransferase G9a to repress the expression of autophagy genes [68].

2.1.4 Selective autophagy pathways

Traditionally, autophagy was thought to be a non-selective process that degrades bulk cytoplasmic material. However, in the past years it was shown that autophagy can in fact be highly selective and specifically degrade cell organelles such as lysosomes (lysophagy) [69], mitochondria (mitophagy) [70], ER (ER-phagy) [71], ribosomes (ribophagy) [72] or peroxisomes (pexophagy) [73] as well as lipid droplets (lipophagy) [74], protein aggregates (aggrephagy) [75] and invading pathogens (xenophagy) [76]. By removing damaged cell organelles or potentially detrimental structures such as protein aggregates and pathogens, selective autophagy serves important functions for cellular homeostasis [77]. Recognition of the autophagic cargo usually requires its modification with degradation signals (in most cases Ub chains) [78,79]. These signals are recognized by selective autophagy receptors with LC3-interacting region (LIR) motifs that link the autophagic cargo to the growing autophagosomal membrane [80,81]. The autophagosome then encloses the receptor-bound cargo, followed by fusion with the lysosome and clearance of the cargo together with its receptor [28]. In the following, different forms of selective autophagy will be explained in more detail.

2.1.5 Selective autophagy of lysosomes (lysophagy)

Lysophagy describes the degradation of damaged lysosomes via autophagy. Lysosomes are single membrane cell organelles which mediate degradation of diverse cellular material from endocytic, phagocytic or autophagic pathways. Thereby, they serve essential functions for cellular homeostasis and the maintenance of lysosomal integrity is of great importance [82]. However, different stimuli and agents including oxidative stress, photodamage, silica crystals, pathogens, neurotoxic aggregates or lysosomotropic drugs can damage the lysosomal membrane and eventually lead to lysosomal membrane permeabilization (LMP) [69,83,84]. LMP can be harmful to the cell, since it causes the release of protons and reactive oxygen species (ROS) as well as leakage of lysosomal enzymes such as cathepsins in the cytosol which can trigger lysosomal cell death or pyroptosis through activation of the NACHT, LRR and PYD domains-containing protein 3 (NLRP3) inflammasome [85-87]. To maintain lysosomal integrity and cellular function, different mechanisms are engaged following LMP which are summarized under the term ‘endo-lysosomal damage response’ (ELDR) [88]. One part of the ELDR is the stabilization of damaged lysosomes by factors such as heat shock protein 70 (Hsp70) [89,90] and a second one is the activation of TFEB and transcriptional

upregulation of lysosomal genes for the biogenesis of new lysosomes [65,91]. In addition, an early response to lysosomal damage is activation of the ESCRT machinery [92]. LMP induces lysosomal calcium release which triggers recruitment of ESCRT-I, ESCRT-II and ESCRT-III components and the ESCRT-associated proteins VPS4 and ALG-2-interacting protein X (ALIX) to damaged lysosomes [93]. Importantly, recruitment of the ESCRT-III subunit charged multivesicular body protein 4b (CHMP4B) depends on the ESCRT-I tumor susceptibility gene 101 (TSG101) protein and ALIX [93]. The ability of CHMP4B to form filaments is thought to reseal ruptured membranes and restore membrane curvature, thus enabling repair of the lysosomal membrane [92]. In the case of severe lysosomal damage which cannot be repaired by the ESCRT machinery, the last element of the ELDR is activated, namely the clearance of defect lysosomes by lysophagy [94].

2.1.5.1 Sensing of lysosomal damage and ubiquitination in lysophagy

Lysophagy starts with the sensing of damaged lysosomes: rupture of the lysosomal membrane induces exposure of glycans (in most cases β-galactosides) which are located at the inner lysosomal membrane [82]. The galectins, a family of cytosolic, β-galactoside-binding proteins including galectin-1 (LGALS1), galectin-3 (LGALS3), galectin-8 (LGALS8) and galectin-9 (LGALS9), are recruited to damaged lysosomes, pass the permeabilized membrane and bind to glycans via their carbohydrate recognition domain (CRD) [95]. Importantly, galectins serve different functions in lysophagy. Galectin-3 triggers recruitment of the non-canonical E3 Ub ligase tripartite motif-containing protein 16 (TRIM16) which mediates ubiquitination of the damaged lysosome. In addition, galectin-3 and TRIM16 build a platform for components of the autophagy machinery, such as ULK1, ATG16L1 and Beclin-1, thereby promoting phagophore formation [96]. Galectin-8 directly binds to the autophagy receptor nuclear dot protein 52 (NDP52) in an Ub-independent manner and by interacting with LC3, NDP52 directs defect lysosomes to the phagophore membrane [97]. In addition, galectin-8 inhibits mTOR activity, thus inducing nuclear translocation of TFEB and expression of lysosomal genes [98]. Besides recognition of exposed glycans by galectins, glycans are also detected by proteins of the ubiquitination machinery. One E3 Ub ligase complex is the S-phase kinase-associated protein 1 (SKP1)-Cullin 1 (CUL1)-F-box protein (SCF) complex in which substrate specificity is determined by alternative F-box proteins [99]. Interestingly, the F-box proteins F-box only protein 2 (FBXO2), FBXO6 and FBXO27 directly bind to glycans, but FBXO27 can also get N-myristoylated. This allows membrane localization and recruitment of FBXO27 to defect lysosomes where it binds to lysosomal glycoproteins such as lysosomal-associated membrane protein 1 (LAMP1) and LAMP2 and promotes their ubiquitination (mainly with K48-linked Ub chains) [100].

SCF^{FBXO27}-mediated ubiquitination of lysosomal glycoproteins triggers recruitment of the autophagy machinery, including the autophagy receptor p62 and LC3 [100]. Importantly, SCF^{FBXO27} is not expressed in all cells and tissues and additional enzymes contribute to the ubiquitination of damaged lysosomes, underlining the complexity of Ub-mediated regulation of lysophagy. Thus, the cullin-4A (CUL4A)-DNA damage-binding protein 1 (DDB1)-WD repeat and FYVE domain-containing protein 1 (WDFY1) E3 Ub ligase complex is ubiquitously expressed and following LMP, CUL4A-DDB1-WDFY1 drives K48-linked poly-ubiquitination of LAMP2, thereby initiating lysophagy [101]. In addition, the E3 Ub ligase Leucine rich repeat and sterile alpha motif containing 1 (LRSAM1) participates in the clearance of damaged lysosomes during *Salmonella typhimurium* infection [102]. Another regulator of lysophagy is the Ub-directed ATPase Associated with diverse cellular Activities (AAA+)-type ATPase p97 (or valosin-containing protein (VCP)) [103]. In response to lysosomal damage, p97 localizes to lysosomes and acts together with the cofactors UBX domain-containing protein 1 (UBXD1), phospholipase A-2-activating protein (PLAA) and the deubiquitinating enzyme ubiquitin thioesterase OTU1 (YOD1) to extract K48-linked proteins on a subset from K63-modified lysosomes. This is thought to enable binding of autophagy receptors and to drive clearance of damaged lysosomes by lysophagy [103]. Of note, the mechanism of p97-driven removal of ubiquitinated proteins from the lysosomal membrane is not fully understood so far and its targets proteins remain to be identified. However, the ubiquitin-conjugating enzyme E2Q-like protein 1 (UBE2QL1) was shown to regulate p97 recruitment to damaged lysosomes [104]. UBE2QL1 is targeted to permeabilized lysosomes and required for modification of proteins with K48 Ub chains which are subsequently extracted from the membrane by p97. So far, it is not known how UBE2QL1 is recruited to damaged lysosomes and which E3 Ub ligase associates with UBE2QL1 [104]. Furthermore, it was shown recently that protein tyrosine phosphatase 4A2 (PTP4A2) dephosphorylates p97 at Y805, thereby facilitating interaction of p97 with UBXD1 and PLAA and promoting autophagosome formation and clearance of damaged lysosomes via lysophagy [105]. As already described above, different types of Ub chains are involved in lysophagy. Very early after lysosomal damage (~ 30 min), K63-linked Ub chains are detected on damaged lysosomes and mediate recruitment of autophagy receptors such as p62 and the core autophagy machinery [82]. K48 Ub chains appear with some delay on lysosomes (~ 2 h after LMP) and are largely regulated by UBE2QL1 [104]. In general, the ubiquitination machinery involved in lysophagy as well as the substrate proteins are largely unknown. Thus, it is very likely that future research will reveal additional E2 and E3 enzymes which participate in lysophagy and identify more of their target proteins.

2.1.5.2 Autophagy receptors in lysophagy

Lysophagy is mediated by different selective autophagy receptors. Usually, these autophagy receptors bind to ubiquitinated lysosomes via their ubiquitin-binding domain (UBD) and to LC3 on the phagophore membrane via a LIR motif, thereby linking the autophagic cargo to the growing phagophore. However, there are also ubiquitin-independent mechanisms for receptor recruitment, as in the case of NDP52 which directly binds to galectin-8 on damaged *Salmonella*-containing vesicles [97]. To date, different lysophagy receptors have been identified, including p62 [106], optineurin (OPTN) [107], Tax1-binding protein 1 (TAX1BP1) [108], lysosome membrane protein 2 (LIMP2) [109] and NDP52 [97]. Some of these receptors are also involved in other forms of selective autophagy such as mitophagy, xenophagy or aggrephagy [110-114]. Even though multiple lysophagy receptors are recruited to damaged lysosomes, it is not fully understood which of them are essential for the lysophagic flux or if they have redundant functions. However, there is evidence that the requirement of specific autophagy receptors for lysophagy might be context- or cell type-dependent. Thus, depletion of TAX1BP1 greatly reduced the lysophagic flux in HeLa cells and iNeurons, indicating an essential, non-redundant function for TAX1BP1 in this context. Of note, TAX1BP1-mediated lysophagy requires its ski-interacting protein (SKIP) carboxyl homology (SKICH) domain which binds to TANK-binding kinase 1 (TBK1) and FIP200 [108]. p62 also has an important role in lysophagy. In response to lysosomal damage in HeLa cells and neurons, p62 oligomerizes and forms condensates on damaged lysosomes by liquid-liquid phase separation (LLPS) which likely serve as platforms for autophagosome formation. Oligomerization of p62 is mediated by its N-terminal Phox and Bem1p (PB1) domain which is bound by the heat shock protein 27 (HSP27). HSP27 regulates the liquidity of p62 condensates and is necessary for efficient clearance of damaged lysosomes [106]. Of note, a similar role of p62 condensates is also described in other forms of selective autophagy, such as aggrephagy [115].

2.1.5.3 Regulation of lysophagy

So far, the mechanisms regulating lysophagy and the function of lysophagy receptors are largely unknown. However, it was shown that phosphorylation of TBK1 on serine 172 which activates its kinase activity occurs in response to lysosomal damage. Furthermore, pTBK1 localizes to galectin-3-positive puncta and TBK1 inhibition decreases the lysophagic flux, suggesting an important role of TBK1 in the regulation of lysophagy [108]. In mitophagy and xenophagy, TBK1 is recruited as well and mediates phosphorylation of autophagy receptors such as p62, OPTN and NDP52, thereby promoting their association with ubiquitin [116-119]. Even though the targets of TBK1 in

lysophagy have not been identified yet, it is very likely that the clearance of damaged lysosomes is also regulated by TBK1-driven phosphorylation of lysophagy receptors. In addition, it was shown recently that Tectonin beta-propeller repeat-containing protein 1 (TECPR1) is recruited to damaged lysosomes and forms an E3-like complex with ATG12~ATG5 to drive ATG16L1-independent LC3 lipidation. Localization of TECPR1 to damaged lysosomes occurs within minutes after lysosomal damage and precedes glycan exposure and galectin recruitment. ATG12~ATG5-TECPR1-mediated LC3 lipidation of damaged lysosomal membranes is thought to support membrane repair and lysosomal recovery after damage [120].

2.1.6 Selective autophagy of protein aggregates (aggrephagy)

Various neurodegenerative diseases (NDs), including Alzheimer disease (AD), Parkinson disease (PD) or Huntington disease (HD), are characterized by the accumulation of protein aggregates [121-123]. Protein misfolding and aggregation can be very harmful to the cell, so different quality control pathways exist to regulate protein homeostasis (proteostasis) and to remove toxic protein aggregates. So-called chaperones, which are in many cases small heat shock proteins (sHSPs), are responsible for protein folding or refolding [124]. If repair fails, misfolded proteins are eliminated via the ubiquitin-proteasome system (UPS) or the autophagy-lysosomal system. The UPS mediates degradation of small, soluble proteins which are marked with Ub [125]. In contrast, large insoluble protein aggregates are degraded by a selective form of autophagy, referred to as aggrephagy [126].

2.1.6.1 Autophagy receptors in aggrephagy

Similar to other forms of selective autophagy, aggrephagy requires the action of soluble selective autophagy receptors (SARs) which usually bind to polyubiquitinated cargo proteins (e.g. K63 Ub) via their UBD and to LC3 on autophagosomal membranes via their LIR motif [127,128]. Autophagy receptors mediating aggrephagy include p62, TAX1BP1, NBR1, OPTN, Toll-interacting protein (TOLLIP) and chaperonin-containing TCP-1 subunit 2 (CCT2) [113,129-132]. It has been shown that aggregation-prone proteins (e.g. tau protein in AD) assemble into condensates by LLPS before forming solid protein aggregates [133-135]. Importantly, formation and autophagic clearance of these liquid phase-separated condensates is regulated by p62, NBR1 and TAX1BP1 [136]. As described above (see 2.1.5.2), p62 oligomerizes through its PB1 domain and p62 oligomers bind to ubiquitinated protein aggregates, thereby forming larger condensates which are referred to as p62 bodies. NBR1 also contains a PB1 domain which directly associates with the PB1 domain of p62 and enhances the formation of phase-separated

condensates [137]. Furthermore, TAX1BP1 binds to NBR1 and promotes autophagosome formation and autophagic degradation of condensates by recruitment of FIP200 via its SKICH domain [136,138,139]. In contrast to p62, NBR1 and TAX1BP1, the aggrephagy receptor CCT2 mediates clearance of solid protein aggregates [140]. CCT2 is one of eight subunits of the eukaryotic chaperonin TCP-1 ring complex (TRiC) which functions in folding of cytosolic proteins [141] and was shown to prevent protein aggregation [142,143]. Importantly, CCT2-driven aggrephagy is independent of Ub. CCT2 contains two non-classical VLIR (VIL and VLL) motifs which enable interaction of CCT2 with ATG8 proteins on autophagosomal membranes and aggregation-prone proteins. Under basal conditions, these VLIR motifs are masked in the TRiC complex. However, excessive accumulation of protein aggregates induces a partial switch of CCT2 into a monomeric formation, thereby exposing the VLIR motifs to associate with ATG8 proteins and to promote autophagic degradation of solid protein aggregates [140]. In addition to CCT2, OPTN was also shown to drive clearance of protein aggregates in a Ub-independent manner [130].

2.1.6.2 Regulation of aggrephagy

Aggrephagy is a complex process which is tightly regulated at different levels to ensure efficient and selective targeting of cargo proteins. PTMs (e.g. ubiquitination, phosphorylation etc.) of aggrephagy receptors and substrate proteins have an important role in the regulation of aggrephagy. As described above, most of the aggrephagy receptors recognize polyubiquitinated cargo proteins, however, their binding affinity to Ub is variable. For example, p62 has a relative low affinity for Ub and requires oligomerization for efficient cargo binding [144]. In contrast, NBR1 has an increased affinity for Ub indicating that it binds ubiquitinated substrates more efficiently than p62 [145]. Furthermore, the type of poly-Ub chain linkage might also influence protein degradation. K48-linked poly-Ub is considered to mainly target substrate proteins for proteasomal degradation [146], whereas K63-linked poly-Ub is associated with clearance via the autophagy-lysosomal system [147,148] and some autophagy receptors are reported to bind preferentially to K63 poly-Ub [129,149]. Another important PTM regulating aggrephagy is phosphorylation. ULK1 and TBK1 mediate phosphorylation of p62, thereby increasing its binding to ubiquitin and enabling efficient degradation of protein aggregates [150,151]. In addition to PTMs, several adaptor proteins are also involved in the regulation of aggrephagy. Autophagy-linked FYVE protein (ALFY or WD repeat and FYVE domain-containing protein 3 (WDFY3)) is a large protein harbouring different domains such as a Beige and Chendiak-Higashi (BEACH) domain, an ATG5 interacting WD40 repeat region and a PI3P-binding FYVE domain [152,153]. ALFY binds to p62 and NBR1 and is recruited to ubiquitinated protein aggregates such as α-synuclein

or poly-glutamine huntingtin (polyQ-Htt) [154,155]. Furthermore, interaction of ALFY with ATG5 enables local autophagosome formation and links protein aggregates with the autophagy machinery, thereby driving their efficient autophagic clearance [152]. Other regulatory proteins in aggrephagy are WD repeat-containing protein 81 (WDR81) which increases p62 clustering to promote aggrephagy [156], or TECPR1 which binds to LC3C, thus linking aggregates to the autophagosome [157].

2.1.6.3 Chaperone-assisted selective autophagy (CASA)

Chaperone-assisted selective autophagy (CASA) is a specific form of aggrephagy mediating the degradation of so-called aggresomes [158]. Aggresomes are formed following proteasomal inhibition or overexpression of aggregation prone proteins. They are localized at the microtubule organizing centre (MTOC) and contain ubiquitinated protein aggregates enveloped by intermediate filaments like vimentin or keratin [159,160]. In CASA, ubiquitination of protein aggregates is regulated by HSP70 family and heat shock protein family B (small) member 8 (HSPB8) chaperones together with the E3 Ub ligase Carboxy terminus of Hsp70-interacting protein (CHIP) [161]. In addition, Bcl-2 associated athanogene (BAG) family molecular chaperone regulator 3 (BAG3) has a crucial role in aggresome formation. BAG3 binds to dynein and mediates the transport of protein aggregates along microtubules to the MTOC with the help of histone deacetylase 6 (HDAC6) [160,162,163].

2.1.7 Glioblastoma multiforme (GBM)

Gliomas represent primary brain tumors originating from neuroglial stem or progenitor cells [164,165]. The world health organization (WHO) grade IV glioma glioblastoma multiforme (GBM) is the most malignant primary brain tumor with an incidence of around 3-4 cases per 100,000 persons per year [166-168]. Even though all age groups are affected, the number of patients diagnosed with GBM increases with age [169]. According to the fifth edition of the WHO Classification of Tumors of the CNS, GBM is characterized as a diffuse, astrocytic glioma in adults with the expression of wild-type (WT) isocitrate dehydrogenase (IDH), telomerase reverse transcriptase (TERT) promoter mutation or epidermal growth factor receptor (EGFR) gene amplification or combined gain of entire chromosome 7 and loss of entire chromosome 10 [+7/−10] [170]. The current standard therapy of GBM combines surgery, radiotherapy and chemotherapy with the alkylating agent temozolomide (TMZ). However, the median overall survival is only 15 months and there is no cure for GBM so far, highlighting the importance to identify new treatment strategies for GBM [169].

2.1.7.1 Role of autophagy in GBM

In general, autophagy is known to have a dual role in cancer. On the one hand, autophagy can be tumor-protective by supplying the cell with nutrients in stressful situations such as starvation, hypoxia or oxidative stress [171]. On the other hand, hyperactivation of autophagy can also induce an alternative form of cell death, referred to as autophagy-dependent cell death (ADCD) [172-174]. Due to its essential function in cancer, autophagy is investigated as a potential new treatment strategy. In GBM, autophagy is often upregulated due to the rapid tumor growth which leads to hypoxia and insufficient nutrient supply [175]. Therefore, inhibition of autophagy is investigated in the treatment of GBM. In one study, combination of the proteasome inhibitor bortezomib with the autophagy inhibitor 3-methyladenine (3-MA) increased caspase-3 activation and apoptosis induction in GBM cells [176]. There is also evidence that autophagy-suppressing micro ribonucleic acid (miRNA) can have beneficial effects. Thus, the autophagy inhibitor miR-30e enhanced proanthocyanidin-mediated cell death in human glioblastoma stem cells (GSCs) and the glioblastoma cell line SNB19 [177]. In addition to these examples of autophagy inhibitors as candidates for the treatment of GBM, the potential of activating ADCD in GBM cells is also investigated. This is of particular interest since GBM cells often become resistant to standard, apoptosis-inducing therapies [178]. Our group could show that the compounds loperamide hydrochloride (LOP, see also 2.1.9.1), pimozide (PIMO) and STF-26647 induce ADCD in glioblastoma cells [172,179]. In addition, the mTOR inhibitor RAD001 in combination with TMZ and γ-radiation increased cell death in a GBM cell line and this cell death was largely autophagy-dependent [180]. Despite these promising examples addressing the potential of autophagy inhibition or activation in GBM therapy *in vitro*, very few clinical trials have been conducted so far. The autophagy inhibitor hydroxychloroquine (HCQ) was tested in a phase I/II clinical trial in GBM patients in combination with TMZ and radiotherapy. However, high doses of HCQ caused severe side effects and HCQ was not able to consistently inhibit autophagy in lower concentrations which were tolerated by the patients [181]. So, there is a high need of identifying less toxic autophagy inhibitors to further investigate the therapeutic potential of autophagy inhibition in clinical trials with GBM patients. Similarly, due to a lack of clinically approved autophagy activators, no clinical trials have addressed the benefit of autophagy activation in GBM so far [182].

2.1.8 Role of autophagy in neurodegenerative diseases

Many NDs, including AD, PD or amyotrophic lateral sclerosis (ALS), are characterized by the accumulation of toxic protein aggregates [122,123,183]. Protein aggregates are usually cleared via autophagy (see also 2.1.6), but NDs are often associated with defects

in autophagy, for example p62 mutations in ALS [184] or PTEN-induced putative kinase 1 (PINK1) and parkin mutations in PD [185]. Therefore, the therapeutic benefit of enhancing autophagy in NDs is investigated and several studies testing the effect of autophagy-activating compounds in NDs have been conducted. For example, the mTOR inhibitor rapamycin was shown to reduce amyloid-β levels in a mouse model of AD [186] and beclin-1 overexpression reduced α-synuclein accumulation in a model of PD [187]. However, only few clinical trials tested the potential of autophagy activators in NDs so far, and some of them showed no beneficial effects [188,189]. Thus, it needs further investigation to address if activation of autophagy could be a useful therapeutic strategy for NDs.

2.1.9 Autophagy-inducing drugs

2.1.9.1 Loperamide hydrochloride (LOP)

The piperidine derivate LOP is approved by the Food and Drug Administration (FDA) for the treatment of diarrhoea. Pharmacologically, it is directly absorbed into the gut and acts as an μ-opioid agonist in nanomolar concentrations, thereby decreasing gut motility [190]. At higher concentrations, LOP inhibits calmodulin activity and voltage-gated Ca^{2+} channels [191,192]. Since LOP is metabolized in the liver by cytochrome P450 3A4 (CYP3A4), it has very little systemic effects and acts largely gut-specific [190]. As a substrate of the efflux membrane transporter P-glycoprotein, LOP is not able to pass the blood-brain barrier and is excluded from the central nervous system (CNS) [190,193]. Interestingly, LOP was shown to induce autophagy in a high-throughput screen in the glioblastoma cell line H4 [194]. Consistent with this, our group demonstrated that LOP induces autophagy and ADCD in glioblastoma cells [172]. Mechanistically, activating transcription factor 4 (ATF4) and other proteins such as chaperone heat shock protein family A member 5 (HSPA5) are upregulated following LOP treatment, indicating the induction of ER stress. In addition, LOP specifically triggers autophagic clearance of ER fragments (ER-phagy) and LOP-induced cell death partially depends on the ER-phagy receptors reticulophagy regulator 1 (RETREG1 or FAM134B) and testis expressed protein 264 (TEX264) [179].

2.1.9.2 L-Leucyl-L-Leucine methyl ester (LLOMe)

The lysosomotropic drug L-Leucyl-L-Leucine methyl ester (LLOMe) is transported into lysosomes through receptor-mediated endocytosis and converted by dipeptidyl peptidase I (DPPI or Cathepsin C (CTSC)) into the membranolytic, polymeric condensation product $(LL)_n$-OMe which induces DNA fragmentation and LMP [195,196]. The effects of LLOMe on lysosomal integrity are dose-dependent: At low concentrations

and short treatment time points, LLOMe induces minor lysosomal damage which can be repaired by the ESCRT machinery [197]. In contrast, severe LMP caused by higher LLOMe concentrations or prolonged administration triggers activation of lysophagy and cell death induction [69,198].

2.2 The ubiquitin code

2.2.1 Ubiquitination

The attachment of Ub to substrate proteins, referred to as ubiquitination, is one of the most common PTMs and regulates diverse cellular processes, such as proteasomal and lysosomal degradation [78,199], cell cycle [200,201], trafficking [202] or nuclear factor-κB (NF-κB) and innate immune signaling [203,204]. Ub is a ubiquitously expressed protein which is highly conserved from yeast to man. It has a molecular weight of about 8.5 kDa (76 amino acids) and a compact β-grasp fold structure with a flexible C-terminal tail [205]. Different hydrophobic surfaces of Ub, including the I44 patch [206], the I36 patch [207,208] and the F4 patch [209,210], are responsible for the recognition of Ub by UBDs. Ubiquitination is an ATP-dependent enzymatic cascade including E1 Ub-activating enzymes [211], E2 Ub-conjugating enzymes [212] and E3 Ub ligases [213]. First, the E1 enzyme activates Ub under ATP consumption by catalyzing the formation of a thioester bond between the C-terminus of Ub and a cysteine residue in the E1. Ub is then directly transferred to the active site cysteine of the E2 enzyme. In the final step, an E3 Ub ligase catalyzes the formation of an isopeptide bond between the C-terminus of Ub and a lysine residue of the substrate protein [214]. E3 ligases are divided into three groups and use different mechanisms for ligation of Ub to the substrate protein. The really interesting new gene (RING)-type E3 ligases have a scaffolding function: they bring the Ub-conjugated E2 enzyme in close proximity to the substrate protein, thereby facilitating direct Ub transfer from the E2 to the target protein. In the case of the homologous to E6-associated protein (E6AP) C-terminus (HECT)-type and RING-in-between-RING (RBR)-type E3 ligases, Ub attachment is a two-step reaction. First, Ub is transferred from the E2 to a catalytic cysteine of the E3, followed by transfer to the substrate protein (**Figure 2A**) [213,215]. Ubiquitination is a PTM with a high complexity. The simplest form of ubiquitination is monoubiquitination, the modification of a substrate protein with one single Ub molecule. If one Ub molecule is attached to multiple lysine residues of a protein, this is a referred to a multi-monoubiquitination [216]. In addition, proteins can be modified with poly-Ub chains. In this case, additional Ub monomers are ligated to one of seven lysine residues (K6, K11, K27, K29, K33, K48 and K63) or the N-terminal methionine residue (M1) of the first Ub molecule. Polyubiquitination can be

homotypic (one linkage type) or heterotypic. Heterotypic poly-Ub chains either comprise different linkage types in one Ub chain (mixed type) or one Ub molecule is ubiquitinated at different lysine residues forming branched chains [217,218]. In addition, Ub can be modified by other PTMs, including phosphorylation [219] and acetylation [220] or form hybrid chains by interaction with Ub-like (Ubl) proteins such as small ubiquitin-related modifier (SUMO) [221], neural precursor cell expressed developmentally down-regulated protein 8 (NEDD8) [222] or interferon-stimulated gene 15 (ISG15) (**Figure 2B**) [223]. The highly complex process of ubiquitination encodes information to regulate a variety of cellular functions. Effector proteins non-covalently bind to Ub via their UBDs and serve to propagate the information of the Ub code. UBDs are divided into different subfamilies, such as the single or multiple α-helices (e.g. Ub-associated (UBA) domain, Ub-interacting motif (UIM), Ub-binding in A20-binding inhibitor of NF-κB (ABIN) and NF-κB essential modulator (NEMO) (UBAN)), zing fingers (ZFs) (e.g. nuclear protein localization 4 zinc finger (NZF), zinc finger in A20 protein (ZnF A20)) or pleckstrin-homology (PH) folds (e.g. pleckstrin-like receptor for ubiquitin (PRU)) [206,224]. Some Ub linkage types are associated to specific cellular functions. For example, K48-linked Ub is the major signal for proteasomal degradation [199] and K63-linked and M1 Ub regulate NF-κB and innate immune signaling [203,204].

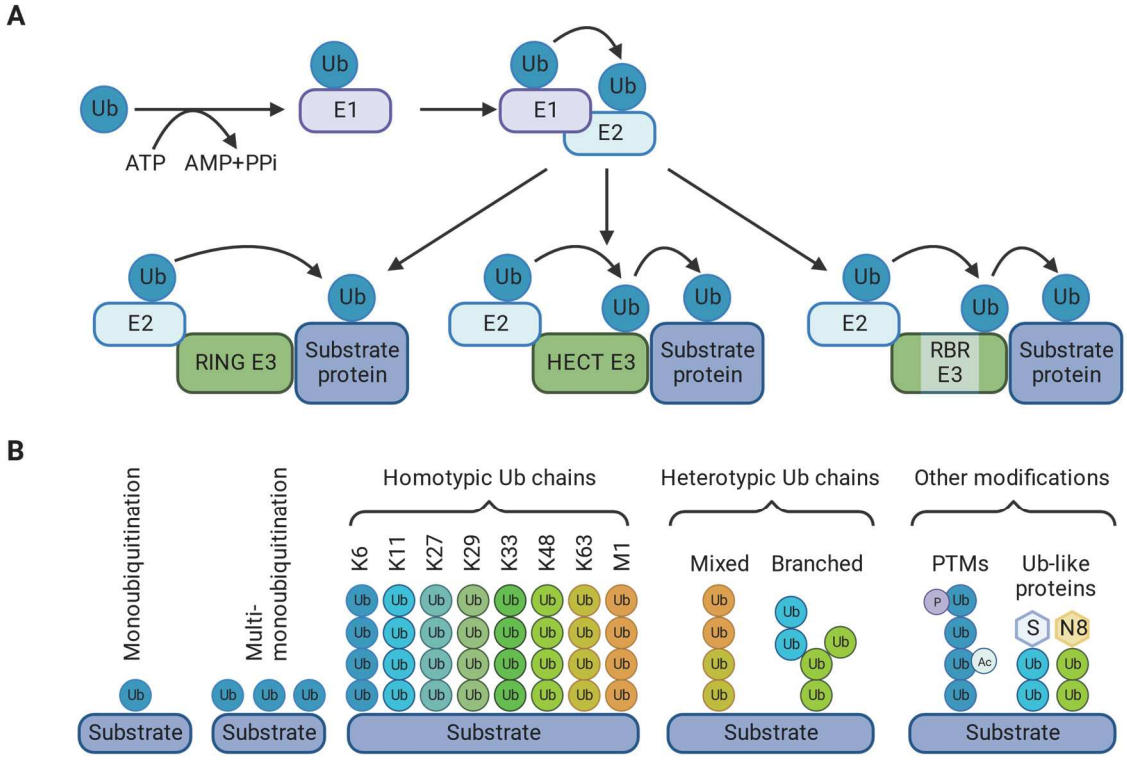

Figure 2. The ubiquitin code.

Figure 2. Continued.
A. The ubiquitination cascade starts with ATP-dependent ubiquitin (Ub) activation by the E1 activating enzyme, followed by direct transfer to the E2 conjugating enzyme. E3 Ub ligases are divided in three groups which use different mechanisms for ligation of Ub to the substrate protein. The really interesting new gene (RING)-type E3 ligases catalyze Ub transfer by bringing the Ub-conjugated E2 enzyme in close proximity to the substrate protein. The homologous to E6-associated protein (E6AP) C-terminus (HECT)-type and RING-in-between-RING (RBR)-type E3 ligases attach Ub in a two-step reaction. First, Ub is transferred to a catalytic cysteine in the E3 and then to the target protein. **B.** Diverse forms of ubiquitination exist, including monoubiquitination, multi-monoubiquitination, homotypic poly-Ub chains and mixed or branched heterotypic poly-Ub chains. Ub chains can also be modified with other post-translational modifications (PTMs) or form hybrid chains with Ub-like proteins like small ubiquitin-related modifier (SUMO, S) or neural precursor cell expressed developmentally down-regulated protein 8 (NEDD8, N8). Adapted from [225,226] and created with BioRender.com.

2.2.2 Deubiquitinating enzymes

Ubiquitination is reversed by deubiquitinating enzymes (DUBs) which are divided into 7 subfamilies, namely the Ub-specific proteases (USPs), the Ub C-terminal hydrolases (UCHs), the ovarian tumor (OTU) proteases, the Machado-Joseph Disease (MJD) DUBs, the motif interacting with Ub (MIU)-containing novel DUB family (MINDY), the zinc finger-containing Ub peptidase 1 (ZUP1) and the JAB1/MPN/MOV34 metalloprotease (JAMM) DUBs [227-229]. Apart from the JAMM family which are zinc-dependent metalloproteinases, all other DUB are cysteine proteases [230]. A common feature shared by all DUBs is the presence of at least one Ub-binding site, the so-called S1 site, which is required for mediating deubiquitination. The S1 site binds to Ub and directs the modified residue of the substrate protein into the active catalytic center, thereby enabling hydrolysis of the peptide bond between the substrate and the Ub C-terminus [231]. The active site of cysteine proteases contains a catalytic triad formed by a cysteine, a histidine and an acidic residue, whereas the catalytic center of JAMM DUBs contains a zinc atom which is regulated by surrounding conserved catalytic residues and a water molecule [231]. DUBs can act in a substrate-specific manner or show specificity for particular Ub linkage types. Thus, most USP family members do not prefer a specific Ub linkage type, but their selectivity relies on interaction with specific protein domains [230,232]. In contrast, linkage-specific DUBs target selected Ub chain types, thereby regulating overall abundance of specific linkage types. Examples of linkage-specific DUBs include OTU domain-containing DUB with linear linkage specificity (OTULIN or Gumby, FAM105B) (M1 Ub) [233], Cezanne (K11 Ub) [234,235] or USP30 (K6 Ub) [236-238]. In addition, there are other variables which determine DUB specificity. Thus, DUBs can have a preference for a particular chain length [229], they can process the Ub chain from the distal end (exo-DUB activity) [239], cleave within the Ub chain (endo-DUB activity) [240], remove an intact Ub chain (en bloc cleavage) [241] or mono-Ub [242]. By

counteracting E3 Ub ligase-mediated ubiquitination, DUBs regulate diverse cellular processes, such as protein degradation [241], DNA repair [243], cell cycle [201,244], immune signaling [245,246] and cell death [247,248]. Different mechanisms exist to tightly regulate DUB abundance, localization and activity, including the use of PTMs like phosphorylation [249], posttranslational proteolytic processing [250] or stimulus-dependent regulation of DUB abundance [251].

2.3 M1-linked (linear) ubiquitination

2.3.1 Linear ubiquitin chain assembly complex (LUBAC)

M1-linked ubiquitination is an atypical form of poly-ubiquitination in which the C-terminal carboxyl group of a donor Ub forms a peptide bond with the α-amino group of the N-terminal methionine of an acceptor Ub [252]. The only E3 ligase identified so far which catalyzes M1-linked ubiquitination is the linear Ub chain assembly complex (LUBAC). LUBAC consists of the subunits heme-oxidized IRP2 Ub ligase 1 (HOIL-1, or RanBP-type and C3HC4-type zinc finger-containing protein 1 (RBCK1)) [253], HOIL-1-interacting protein (HOIP or RING finger protein 31 (RNF31)) [252] and shank-associated RH domain-interacting protein (Sharpin) [204,254]. HOIP has two UBA domains, UBA1 and UBA2, which associate with the Ubl domains of Sharpin and HOIL-1, respectively [255]. Furthermore, HOIP contains a peptide N-glycosidase/UBA (PUB) domain at the N-terminus which interacts with the M1 Ub-cleaving DUBs OTULIN [256,257] and cylindromatosis (CYLD) (indirect binding via the CYLD-spermatogenesis-associated protein 2 (SPATA2) complex) [258,259] and with the AAA-ATPase p97 [260]. Sharpin and HOIL-1 dimerize through their LUBAC-tethering motif (LTM), thereby stabilizing the trimeric LUBAC complex [261]. All LUBAC subunits contain UBDs, such as ZF and NZF domains, which mediate binding to poly-Ub chains (**Figure 3**) [262,263]. HOIP and HOIL-1 are both RBR-type E3 ligases, but the catalytic center for M1 poly-ubiquitination is localized in the C-terminal RBR of HOIP [252]. HOIP-mediated poly-ubiquitination is a RING-HECT hybrid reaction. First, the RING1 domain of HOIP interacts with the E2-bound donor Ub, followed by transfer of Ub to the C885 residue in RING2. Then, the donor Ub is ligated to the N-terminal methionine of the acceptor Ub, which is facilitated by the linear Ub chain-determining domain (LDD) of HOIP [264,265]. LUBAC function is tightly regulated. The HOIL-1 RBR catalyzes mono-ubiquitination of all LUBAC subunits to initiate HOIP-mediated auto-ubiquitination of LUBAC itself which decreases LUBAC activity [266]. OTULIN counteracts LUBAC auto-ubiquitination, thereby maintaining LUBAC function [248]. Loss of any LUBAC component impairs LUBAC activity [267,268] and PTMs can also regulate LUBAC function, as in the case of mammalian ste20-like

protein kinase 1 (MST1)-mediated inhibitory phosphorylation of HOIP [269]. Pharmacologically, LUBAC activity can be inhibited with different small molecule inhibitors, including BAY11-7082 [270], gliotoxin [271], bendamustine [272] or the HOIP inhibitors (HOIPINs) [273,274]. However, BAY11-7082, gliotoxin and bendamustine only show little inhibitory effect and selectivity in non-toxic concentrations. HOIPIN-8 inhibits the *in vitro* M1 ubiquitination activity of LUBAC in nanomolar concentrations and is the most potent LUBAC inhibitor described so far [275]. Mechanistically, HOIPINs are conjugated to C885 in the RING2 domain of HOIP and block the RING-HECT hybrid reaction in HOIP. Furthermore, HOIPIN-8 interacts with R935 and D936 in the LDD, thereby masking these residues for binding of the acceptor Ub [275].

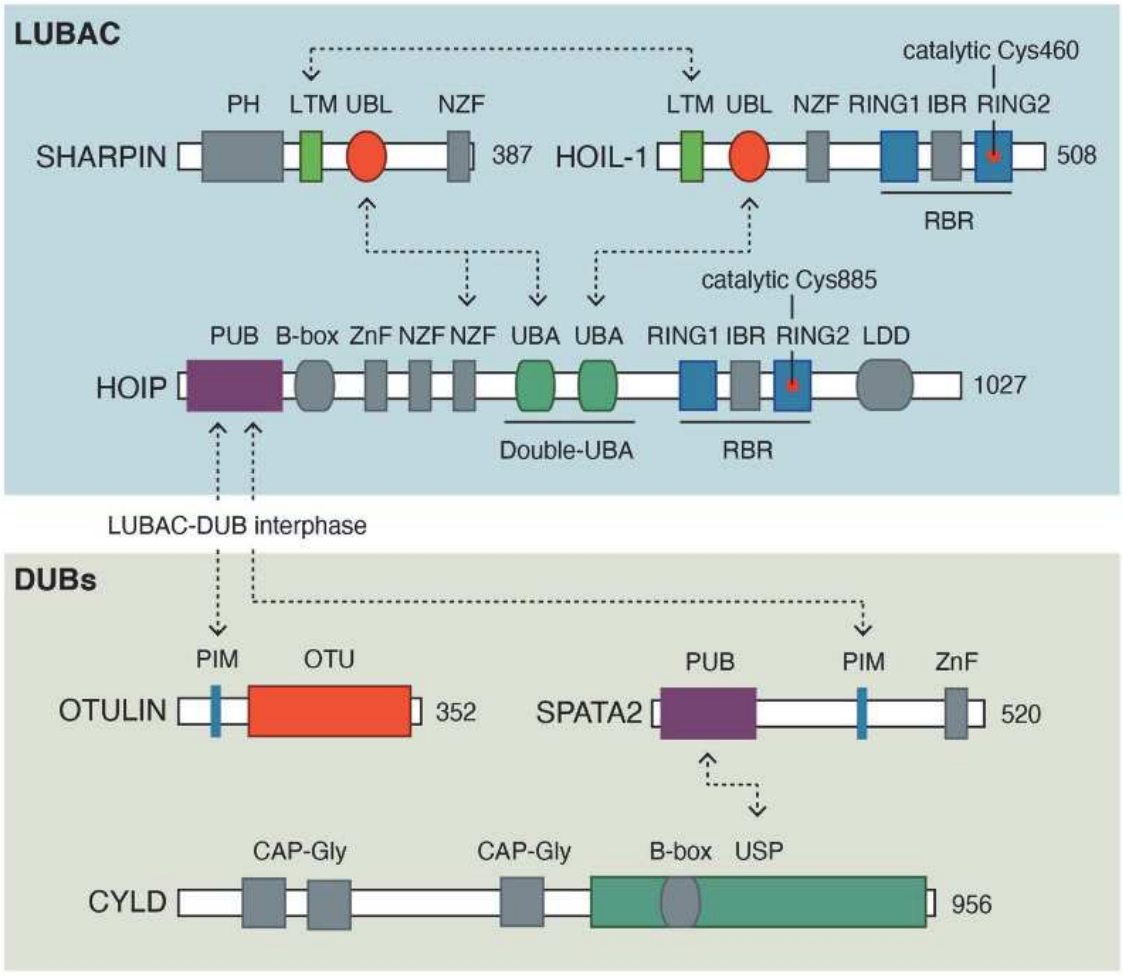

Figure 3. Structure of LUBAC subunits and the DUBs OTULIN and CYLD.

LUBAC is composed of the subunits HOIP, HOIL-1 and Sharpin. HOIP is a RING-in-between-RING (RBR)-type E3 ligase and contains an N-terminal peptide N-glycosidase/UBA (PUB) domain, one zinc finger (ZnF) domain, two nuclear protein localization 4 zinc finger (NZF) domains, two ubiquitin-associated (UBA) domains, two really interesting new gene (RING) domains with the active site C885 in RING2 and a C-terminal linear Ub chain-determining domain (LDD). The PUB domain interacts with OTULIN and SPATA2-CYLD, whereas the two UBA domains associate with the Ub-like domains (UBLs) of Sharpin and HOIL-1. Dimerization between Sharpin and HOIL-1 is mediated through their LUBAC-tethering motif (LTM).

Figure 3. Continued.
CAP-Gly, cytoskeleton-associated protein-glycine rich; IBR, in-between RING; OTU; ovarian tumor; PH, Pleckstrin-homology; PIM, PUB interaction motif; USP, ubiquitin-specific protease. From [276].

2.3.2 M1 Ub-specific DUBs

M1-linked ubiquitination is reversed by the DUBs OTULIN and CYLD. OTULIN is specific for M1 Ub, whereas CYLD cleaves both M1 and K63 poly-Ub [233,277]. Both DUBs have essential roles in NF-κB and innate immune signaling [278]. The DUB A20 (or tumor necrosis factor alpha-induced protein 3 (TNFAIP3)) also regulates NF-κB signaling by binding to M1 Ub via its ZF7 domain, but possesses no catalytic activity towards M1 Ub [279,280].

2.3.2.1 OTULIN

OTULIN is the only DUB identified so far which exclusively cleaves M1 Ub. OTULIN contains an N-terminal PUB interaction motif (PIM) which interacts with the PUB domain of HOIP, and this association is inhibited by phosphorylation of Y56 in the PIM [256,257]. Interaction of OTULIN with the HOIP PUB domain promotes LUBAC function by preventing LUBAC auto-ubiquitination [248]. Furthermore, OTULIN deficiency causes cell-type specific decreases in the abundance of LUBAC subunits [281-283]. The high specificity of OTULIN for M1 poly-Ub relies on its Ub binding site which has a high affinity for M1 poly-Ub but not the topologically similar K63 Ub, and a process referred to as Ub-assisted catalysis [233]. The catalytic triad of OTULIN is composed of C129, H339 and N341. When the proximal Ub binds to OTULIN, the Ub E16 residue is directly inserted into the active site of OTULIN where it organizes the catalytic triad by displacing the inhibitory D336 and bringing H339 into an active conformation, enabling deprotonation of C129 and coordinating N341. Thus, the bound di-Ub regulates the catalytic activity of OTULIN and contributes to its own cleavage [233,284]. OTULIN has key functions in NF-κB activation, innate immune signaling and cell death. It was shown that OTULIN antagonizes LUBAC-mediated M1 poly-ubiquitination and NF-κB activation [233,245,285], and loss of OTULIN or overexpression of catalytically inactive variants greatly increases total cellular M1 Ub levels [245,283,286]. However, the role of OTULIN in NF-κB signaling is complex and cell type-dependent and it has also been demonstrated that NF-κB activation is reduced in mouse embryonic fibroblasts (MEFs) overexpressing catalytically inactive OTULIN [248]. OTULIN regulates different immune receptor signaling pathways, including tumor necrosis factor receptor 1 (TNFR1) and nucleotide-binding oligomerization domain-containing protein 2 (NOD2) signaling [233,245,256]. In addition, OTULIN has key functions in cell death control. Thus, OTULIN deficiency sensitizes cells towards tumor necrosis factor alpha (TNFα)-induced

apoptosis and TNFα/cycloheximide (CHX)/zVAD-induced necroptosis [281,287]. Similarly, OTULIN-depleted mouse hepatocytes show increased apoptosis [282,288]. In addition to OTULIN-mediated regulation of immune signaling and cell death, OTULIN functions in other cellular processes. Thus, OTULIN was shown to regulate the autophagic clearance of bacteria (xenophagy) during infection [111,289], mTOR signaling [282], endosomal trafficking [290] as well as antiviral interferon signaling through M1 ubiquitination of signal transducer and activator of transcription 1 (STAT1) [291].

2.3.2.2 CYLD

In contrast to OTULIN, CYLD is not specific for M1 Ub, but cleaves M1 and K63 Ub with similar activity [277]. CYLD is a USP DUB and requires SPATA2 for interaction with HOIP. The USP domain of CYLD binds to the PUB domain of SPATA2 and SPATA2 associates with the HOIP PUB domain through a conserved PIM [258,259,292]. Due to this binding mode, interaction of OTULIN and CYLD/SPATA2 with HOIP is mutually exclusive [247]. CYLD inhibits NF-κB activation and in contrast to OTULIN, CYLD expression is induced by NF-κB to limit NF-κB signaling in a negative feedback loop [293]. CYLD is recruited to receptor signaling complexes (RSCs) such as TNFR1 and NOD2 where it cleaves M1 and K63 Ub chains. In this way, CYLD restricts NOD2 signaling and cytokine production [246] and at TNFR1 complex, CYLD inhibits gene activation and increases TNFα-induced cell death [247].

2.3.3 Roles of M1 poly-Ub

M1 Ub is involved in different cellular functions, three of which are discussed in more detail below.

2.3.3.1 Immune receptor-mediated NF-κB activation

M1 poly-Ub has a key role in immune receptor-mediated activation of canonical NF-κB signaling. Ligand binding to different immune receptors, including TNFR1, NOD-like receptors (NLRs), Toll-like receptors (TLRs) or interleukin-1β receptor (IL-1βR), induces the formation of RSCs, consisting of the receptor itself as well as multiple adapter proteins which are usually modified with Ub chains [276,294]. In the case of TNFR1 signaling, K63 Ub chains are attached to receptor-interacting protein kinase 1 (RIPK1) by the E3 ligases cellular inhibitor of apoptosis 1 and 2 (cIAP1/2), thus inducing recruitment of LUBAC to the TNFR1 signaling complex (complex I). LUBAC then conjugates M1 Ub to RIPK1, FAS-associated death domain protein (FADD) and NEMO which forms the inhibitor of κB (IκB) kinase (IKK) complex together with IKK1 (IKKα) and

IKK2 (IKKβ) [203,295,296]. Due to the high binding affinity of the NEMO UBAN domain for M1 Ub, NEMO of another IKK complex is recruited to M1-ubiquitinated NEMO, thereby inducing activation of IKK2 through dimerization and trans-autophosphorylation. IKK2 in turn mediates phosphorylation of IκB which results in NF-κB activation and transcription of NF-κB target genes [263]. LUBAC also targets proteins of other immune signaling pathways, for example RIPK2 during NOD2 signaling [297,298] or myeloid differentiation primary-response protein 88 (MyD88) and IL-1R-associated kinase 1 (IRAK1) and 4 (IRAK4) during IL-1βR and TLR signaling [299-302].

2.3.3.2 Cell death

M1 Ub has an important role in the regulation of cell fate. Apart from activating NF-κB, TNFR1 signaling also induces apoptosis and necroptosis by conversion of complex I to death-inducible complex II or necrosome activation, respectively [303]. Inhibition of complex II formation requires LUBAC-mediated ubiquitination of different proteins (e.g. RIPK1) in complex I [304]. Thus, mutations or deficiency in LUBAC components were shown to sensitize mice towards cell death which could be blocked by deletion of *Tnfr1*, *Caspase-8* and *Ripk3* [305-307]. In addition, homozygous genetic deletion of HOIP and HOIL-1 in mice results in embryonic lethality via TNFR1-mediated cell death [267,308], and cell death of HOIL-1-deficient mice can be rescued by deletion of *Caspase-8*, *Ripk3* and mixed lineage kinase domain-like protein (*Mlkl*) [308]. Importantly, the effects of LUBAC deficiency can also be mimicked pharmacologically with LUBAC inhibitors. Thus, HOIPIN-1 and HOIPIN-8 were shown to increase TNFα- and CHX-induced cell death in human A549 cells and in Sharpin-deficient (*cpdm*) MEFs [275].

2.3.3.3 Autophagy

Another function of M1 Ub is the regulation of autophagy. During *Salmonella typhimurium* infection, the surface of cytosolic bacteria is modified with M1 poly-Ub and the M1 Ub coat recruits autophagy receptors such as p62 and OPTN, thereby driving autophagic clearance of bacteria via xenophagy. M1 poly-Ub chains on bacteria also serve as a platform to recruit NEMO and locally activate NF-κB which leads to an increase in the secretion of pro-inflammatory cytokines and restricts bacterial proliferation [111,289]. In addition, LUBAC was shown to control autophagy initiation and maturation by mediating M1 ubiquitination and stabilization of ATG13 [309].

2.3.3.4 Other roles of M1 poly-Ub

Other reported roles of M1 poly-Ub include the regulation of interferon (IFN) signaling and retinoic acid-inducible gene 1 protein (RIG-I)-mediated IFN production [310,311] as

well as activation of the NLRP3 inflammasome [312]. It also very likely that future research will unravel yet unknown cellular functions of M1 poly-Ub.

2.3.4 M1 poly-Ub in human diseases

Due to the role of M1 poly-Ub in crucial cellular processes, dysfunction of M1 ubiquitination is associated with different disorders. In mice, deficiency in LUBAC components mainly results in autoinflammatory diseases with defects in NF-κB signaling and increased cell death [203,267]. Mice with mutations in Sharpin (*cpdm* mice) develop chronic proliferative dermatitis with severe skin inflammation and defects in secondary lymphoid organ development, caused by dysregulated TNFR1-dependent cell death and keratinocyte apoptosis [305,306,313]. Complete genetic depletion of *Hoip* or *Hoil-1* in mouse models causes disrupted vascularization in the yolk sac and cardiovascular failure eventually leading to embryonic lethality at mid-gestation [267,308]. In humans, cases of patients with homozygous loss of function (LOF) mutations in LUBAC components are very rare. The first patient described with a homozygous LOF variant of sharpin suffered from severe joint inflammation caused by decreased LUBAC expression and attenuated NF-κB activation, but did not show dermatologic features [314]. Complete deficiency of HOIL-1 in patients is associated with chronic autoinflammation, infections, glycogen storage disease (amylopectinosis), muscular weakness and cardiomyopathy [268,315,316]. These clinical features are very similar in patients with genetic HOIP deficiency [317]. In addition, two single nucleotide polymorphisms (SNPs) of *HOIP* are enriched in the activated B cell-like subtype of diffuse large B-cell lymphoma (ABC-DLBCL) and cause increased HOIP-HOIL1 association, LUBAC enzymatic activity and NF-κB activation. Of note, peptide-mediated inhibition of HOIP-HOIL1 interaction was shown to attenuate NF-κB activation and decrease cell survival of ABC-DLBCL lines [318]. LOF mutations in OTULIN are causative for the TNFα-driven autoinflammatory disease OTULIN-related autoinflammatory syndrome (ORAS, or otulipenia) which is characterized by systemic inflammation, fever, panniculitis, diarrhea and arthritis [281,283,286]. OTULIN deficiency leads to cell-type specific effects on LUBAC expression, TNFα signaling and NF-κB activation. While OTULIN-deficient monocytes show stable LUBAC expression and increased TNFα signaling and NF-κB activation, LUBAC expression is reduced in OTULIN-deficient fibroblasts and causes impaired TNFα signaling [281]. LUBAC and OTULIN are also implicated in the development of NDs as they regulate M1 ubiquitination of neural protein aggregates, such as tau aggregates in AD [319] or TAR DNA-binding protein 43 (TDP-43) aggregates in ALS [320], to mark them for degradation [260].

3 Aim of the study

Autophagy is a conserved catabolic process which mediates engulfment of cellular material in autophagosomes and subsequent degradation in autolysosomes [1]. Thereby, autophagy serves key functions in the response to stress stimuli and the maintenance of cellular homeostasis. Furthermore, dysfunction or dysregulation of autophagy is associated with different diseases, such as cancer [175,321,322], NDs [184,185] or lysosomal storage diseases (LSDs) [323,324]. Autophagy is a highly complex pathway which is tightly controlled at different levels, including transcriptional regulation of autophagy [63,66] or regulation by PTMs such as phosphorylation or ubiquitination [47,51,325]. The E3 ligase LUBAC and the DUB OTULIN catalyse M1 ubiquitination and deubiquitination of substrate proteins and were shown to regulate autophagic turnover of invading bacteria via xenophagy [111] and autophagy initiation and maturation by controlling M1 ubiquitination and protein stability of ATG13 [309].

The aim of this study was to further characterize the role of LUBAC- and OTULIN-regulated M1 ubiquitination in bulk and selective autophagy. MZ-54 GBM cells with a genetic knockout of OTULIN were generated using clustered regularly interspaced short palindromic repeats (CRISPR)/Cas9 and used to study the effect of OTULIN deficiency on autophagy induction, the autophagic flux and to characterize morphological hallmarks of these cells in relation to autophagy.

Furthermore, autophagosome content profiling was performed to identify OTULIN-dependent autophagic cargo and revealed enrichment of the proteins TAX1BP1 and galectin-3 in the autophagosomes of OTULIN-depleted cells. Since TAX1BP1 and galectin-3 are known to act in lysophagy and aggrephagy [82,108,113], the role of OTULIN and M1 poly-Ub in these two selective autophagy pathways was investigated as well. In this context, it was of particular interest to address if the function of OTULIN and M1 poly-Ub in aggrephagy and lysophagy shares similarities to that in xenophagy [111,289].

4 Materials and methods

4.1 Materials

4.1.1 Cell lines

Table 1. Human cell lines

Cell line	Source	Identifier
MZ-54	Prof. Dr. Kögel	N/A
MZ-54 CRISPR/Cas9 control (Non-human target (NHT))	Zielke, Kardo, Zein *et al.* [179]	N/A
MZ-54 *OTULIN* KO	This study	N/A
MZ-54 NHT myc-APEX2-LC3B	This study	N/A
MZ-54 *OTULIN* KO myc-APEX2-LC3B	This study	N/A
HEK293T	ATCC	RRID:CVCL_0063
HeLa	ATCC	RRID:CVCL_0030
HeLa CRISPR/Cas9 control (NHT)	Nadine Weinelt	N/A
HeLa *OTULIN* KO	Nadine Weinelt	N/A
HeLa Penta KO	Gift from Richard Youle [114]	N/A
DA-iPSn A53T	Gift from Friederike Zunke	N/A
DA-iPSn A53T corr. (isogenic control)	Gift from Friederike Zunke	N/A
Primary mouse cortical neurons	Gift from Konstanze Winklhofer	N/A

4.1.2 Cell culture reagents

Table 2. Media, supplements and additional cell culture reagents

Reagent	Source	Identifier
Biotin Tyramide	Iris Biotech	Product code #LS-3500
Blasticidin S hydrochloride	Carl Roth	Cat#CP14.4
Doxycycline hydrochloride	Sigma-Aldrich	Cat#D3447
Dulbecco's Modified Eagle medium (DMEM) GlutaMAX™	Thermo Fisher Scientific	Cat#32430-100
Dulbeccos's Phosphate Buffer Saline (DBPS)	Thermo Fisher Scientific	Cat#14190169
Earle's Balanced Salt Solution (EBSS) with calcium and magnesium	Thermo Fisher Scientific	Cat#24010043

Reagent	Source	Identifier
Fetal bovine serum (FBS)	Thermo Fisher Scientific	Cat#10270-106
FuGENE HD Transfection Reagent	Promega	Cat#E2311
Geneticin™ Selective Antibiotic (G418 Sulfate)	Thermo Fisher Scientific	Cat#10131035
Lipofectamine™ 2000 Transfection Reagent	Thermo Fisher Scientific	Cat#11668027
Lipofectamine™ RNAiMAX Transfection Reagent	Thermo Fisher Scientific	Cat#13778030
Opti-MEM™ I Reduced Serum Medium	Thermo Fisher Scientific	Cat#31985062
Penicillin/streptomycin	Thermo Fisher Scientific	Cat#15140-122
Polybrene	Merck Sigma	Cat#TR-1003
Puromycin dihydrochloride	Thermo Fisher Scientific	Cat#A1113803
Trypan Blue Solution, 0.4%	Thermo Fisher Scientific	Cat#15250061
Trypsin-EDTA (0.05%), phenol red	Thermo Fisher Scientific	Cat#25200056

4.1.3 Drugs and inhibitors

Table 3. Drugs and inhibitors

Reagent	Source	Identifier
Bafilomycin A1 (BafA1)	Selleckchem	Cat#S1413
Cycloheximide	Sigma-Aldrich	Cat#C7698
DMSO	Sigma-Aldrich	Cat#20-139
HOIPIN-8	Axon Medchem	Cat#2972
L-leucyl-L-leucine methyl ester (LLOMe)	Cayman Chemical	Cat#16008
Loperamide hydrochloride	Enzo Life Sciences	Cat#ALX-550-253
MG132	Millipore Sigma	Cat#474791
NSC697923	Selleckchem	Cat#S7142
Pimozide	Sigma-Aldrich	Cat#P1793
Torin 1	Selleckchem	Cat#S2827
TPCA-1	Selleckchem	Cat#S2824
zVAD.fmk	Bachem	Cat#4027403

4.1.4 Chemicals and reagents

Table 4. Chemicals and reagents

Reagent	Source	Identifier
cOmplete™ Protease Inhibitor Cocktail	Roche/Merck Sigma	Cat#04693116001
Disodium phosphate (Na_2HPO_4)	Carl Roth	Cat#P030.3
Ethylene glycol-bis(β-aminoethyl ether)-N,N,N′,N′-tetraacetic acid (EGTA)	Sigma-Aldrich	Cat#E3889
Ethylenediaminetetraacetic acid (EDTA)	Fluka	Cat#03680
HEPES	Thermo Fisher Scientific	Cat#15630080
IGEPAL CA-630/NP-40	Sigma-Aldrich	Cat#56741
N-Ethylmaleimide (NEM)	Sigma-Aldrich	Cat#E3876
PageRuler™ Plus Prestained Protein Ladder	Thermo Fisher Scientific	Cat#26619
Pierce Universal Nuclease	Thermo Fisher Scientific	Cat#88701
Pierce™ 16% Formaldehyde	Thermo Fisher Scientific	Cat#28908
Pierce™ ECL Western Blotting-Substrate	Thermo Fisher Scientific	Cat#32106
Ponceau S	Merck Sigma	Cat#P7170
Potassium chloride (KCl)	Carl Roth	Cat#6781.1
Potassium dihydrogen phosphate (KH_2PO_4)	Carl Roth	Cat#3904.3
Proteinase K Solution	PanReac AppliChem	Cat#A4392.0001
ROTIPHORESE® Gel 30 (37.5:1)	Carl Roth	Cat#3029.1
Saponin	Sigma-Aldrich	Cat#84510
Sodium chloride (NaCl)	Carl Roth	Cat#HN00.3
Sucrose	Sigma-Aldrich	Cat#S0389
SYBR™ Green PCR Master Mix	Thermo Fisher Scientific	Cat#4312704
Tetramethylethylenediamine (TEMED)	Carl Roth	Cat#2367.1
Tris Base	Carl Roth	Cat#4855.1
Tris HCl	Carl Roth	Cat#9090.3
Triton X-100	Carl Roth	Cat#3051.2

Reagent	Source	Identifier
Trolox	Sigma-Aldrich	Cat#238813

All other chemicals and reagents were purchased from Carl Roth and Merck Sigma.

4.1.5 Fluorescent dyes

Table 5. Fluorescent dyes

Reagent	Source	Identifier
4′,6-diamidino-2-phenylindole (DAPI)	Sigma-Aldrich	Cat#D8417
Hoechst33342	Thermo Fisher Scientific	Cat#H1399

4.1.6 Buffers and solutions

Table 6. Buffers and solutions

Buffer	Composition
RIPA Lysis buffer	50 mM Tris-HCl pH 8, 150 mM NaCl, 1% NP-40, 2 mM $MgCl_2$, 0.5% sodium deoxycholate
1% NP-40 lysis buffer	20 mM Tris-HCl pH 7.5, 50 mM NaCl, 5 mM EDTA, 10% glycerol, 1% NP-40
Isolation buffer for nuclear fractionation	250 mM sucrose, 20 mM HEPES, 5 mM $MgCl_2$, 10 mM KCl, 0.025 % digitonin, pH 7.4
6x SDS loading buffer	350 mM Tris Base pH 6.8, 38% glycerol, 10% SDS, 93 mg/ml dithiothreitol (DTT), 120 mg/mL bromophenol blue
5x SDS-PAGE running buffer	30.2 g Tris-HCl, 188 g glycine, 100 mL 10% SDS, filled up to 2 L of ddH_2O
1x Blotting buffer	11.6 g Tris-HCl, 5.8 g glycine, 7.5 mL 10% SDS, 400 mL methanol, filled up to 2 L of ddH_2O
Blocking buffer	5% milk powder in PBS-Tween (PBS-T)
Stripping buffer	0.4 M NaOH
Separating gel 13.5%	13.5% polyacrylamide, 375 mM Tris/HCl pH 8.8, 0.1% SDS, 0.1% APS, 0.04% TEMED
Stacking gel 5%	5% polyacrylamide, 125 mM Tris/HCl pH 6.8, 0.1% SDS, 0.1% APS, 0.1% TEMED
BSA solution	2% BSA, 0.1% ProClin™ 150 in 0.1% PBS-T
TBS-T	20 mM Tris, 150 mM NaCl, 0.1% Tween 20, pH 8.0
PBS-T	0.1% Tween 20 in PBS
PMS buffer (for IF AB dilution)	5mM $MgCl_2$, 0.1% Saponin in PBS

Buffer	Composition
Quencher Solution	10 mM Sodium azide, 10 mM Sodium ascorbate, 5 mM Trolox in PBS
Homogenization Solution I	10 mM KCl, 1.5 mM $MgCl_2$, 10 mM HEPES-KOH, 1 mM DTT, pH 7.5
Homogenization Solution II	375 mM KCl, 22.5 mM $MgCl_2$, 220 mM HEPES-KOH, 0.5 mM DTT, pH 7.5

4.1.7 Antibodies

Table 7. Primary antibodies

Antibody	Dilution	Source	Identifier
mouse anti-GAPDH	1:5000	Hytest	Cat#5G4cc-6C5cc; RRID: AB_2858176
mouse anti-Vinculin	1:2000	Sigma-Aldrich	Cat#V9131; RRID: AB_477629
mouse anti-β-actin	1:10,000	Sigma-Aldrich	Cat#A5441; RRID: AB_476744
human anti-linear poly-Ub (1F11/3F5/Y102L)	1:1000 1:2000 IF	Genentech	N/A
rabbit anti-Ub K63-specific, clone Apu3	1:100 IF	Millipore	Cat#05-1308; RRID:AB_1587580
rabbit anti-RNF31/HOIP	1:1000 1:100 IF	Abcam	Cat#ab46322; RRID: AB_945269
mouse anti-HOIL-1 clone 2E2	1:1000	Merck Millipore	Cat#MABC576; RRID: AB_2737058
rabbit anti-Sharpin (D4P5B)	1:1000	Cell Signaling Technology	Cat#12541; RRID: AB_2797949
rabbit anti-OTULIN	1:1000	Cell Signaling Technology	Cat# 14127; RRID:AB_2576213
rabbit anti-LC3B	1:2000	Thermo Fisher Scientific	Cat#PA1-16930, RRID:AB_2281384
mouse anti-LC3 Clone 4E12	1:100	MBL International	Cat# M152-3, RRID:AB_1279144
rabbit anti-TAX1BP1 (D1D5)	1:1000 1:100 IF	Cell Signaling Technology	Cat# 5105; RRID:AB_11178939
rabbit anti-p62	1:5000 1:500 IF	MBL International	Cat#PM045; RRID:AB_1279301
mouse anti-Galectin 3	1:1000	Thermo Fisher Scientific	Cat#MA1-940; RRID:AB_2136775

Antibody	Dilution	Source	Identifier
rabbit anti-TOMM40 [EPR6932(2)]	1:1000	Abcam	Cat#ab185543
rabbit anti-NAK (phospho S172)	1:1000 1:100 IF	Abcam	Cat#ab109272; RRID:AB_10862438
rabbit anti-IKBKG	1:100 IF	Sigma-Aldrich	Cat#HPA000426; RRID:AB_1851572
rabbit anti-phospho-IKKα/β (Ser176/180) (16A6)	1:100 IF	Cell Signaling Technology	Cat#2697; RRID:AB_2079382
rabbit anti-TBK1	1:1000	Cell Signaling Technology	Cat#38066; RRID:AB_2827657
rabbit anti-Cathepsin D (E179)	1:1000	Cell Signaling Technology	Cat#69854
rabbit anti-LAMP1 (D2D11) XP	1:1000	Cell Signaling Technology	Cat#9091; RRID:AB_2687579
rabbit anti-LAMP1	1:250	Abcam	Cat#ab24170, RRID:AB_775978
mouse anti-LAMP1	1:200 IF	DSHB	Cat# H4A3; RRID:AB_2296838
rat anti-mouse/human Galectin 3	1:100 IF	BioLegend	Cat#125402; RRID:AB_1134238
rat anti-mouse/human Galectin 3	1:250 IF	Thermo Fisher Scientific	Cat#14-5301-82, RRID:AB_837132
goat anti-Biotin	1:10,000	Thermo Fisher Scientific	Cat#31852; RRID:AB_228243
rabbit anti-KBTBD7	1:1000	Novus Biologicals	Cat#NBP1-92040; RRID:AB_11024468
goat anti-Myc Tag	1:1000	Bethyl Laboratories	Cat#A190-104A, RRID:AB_66864
rabbit anti-Histone H3	1:1000	Abcam	Cat#ab1791; RRID:AB_302613
mouse anti-Puromycin	1:1000 1:500 IF	Millipore	Cat#MABE343; RRID:AB_2566826
rabbit anti-TFEB	1:1000	Cell Signaling Technology	Cat#37785, RRID:AB_2799119

All primary antibodies for Western blotting were diluted in PBS-Tween (0.1%) with 2% BSA, except for anti-LC3B which was diluted in PBS-Tween (0.1%) supplemented with 5% milk powder. All primary antibodies for immunofluorescence of MZ-54 and HeLa cells were diluted in PMS buffer (composition see table 6) with 5% FBS. Antibodies for primary

mouse cortical neurons were diluted in 0.1% Triton X-100, 5% goat serum and 1% BSA in PBS.

Table 8. Secondary antibodies for Western Blotting

Antibody	Dilution	Source	Identifier
HRP-conjugated polyclonal goat anti-mouse IgG H&L	1:10,000	Abcam	Cat#ab6789; RRID: AB_955439
HRP-conjugated polyclonal goat anti-rabbit IgG H&L	1:10,000	Abcam	Cat#ab6721; RRID: AB_955447
HRP-conjugated goat anti-human IgG	1:10,000	Merck Millipore	Cat#AP309P; RRID: AB_92684
HRP-conjugated donkey anti-goat IgG	1:10,000	Santa Cruz	Cat#sc-2020 RRID: AB_631728

Secondary antibodies for Western blotting were diluted in PBS-Tween (0.1%) supplemented with 5% milk powder.

Table 9. Secondary antibodies and other reagents for immunofluorescence

Antibody	Dilution	Source	Identifier
goat anti-mouse IgG (H+L) Alexa Fluor™ 555	1:500	Thermo Fisher Scientific	Cat#A-21422; RRID:AB_2535844
goat anti-rabbit IgG (H+L) Alexa Fluor™ 555	1:500	Thermo Fisher Scientific	Cat#A-21428; RRID:AB_2535849
goat anti-mouse IgG (H+L) Alexa Fluor™ 647	1:500	Thermo Fisher Scientific	Cat#A-21235; RRID:AB_2535804
goat anti-rabbit IgG (H+L) Alexa Fluor™ 647	1:500	Thermo Fisher Scientific	Cat#A-21244; RRID:AB_2535812
goat anti-human IgG (H+L) Alexa Fluor™ 647	1:500	Thermo Fisher Scientific	Cat#A-21445; RRID:AB_2535862
donkey anti-rat IgG (H+L) Alexa Fluor™ 488	1:500	Thermo Fisher Scientific	Cat#A-21208; RRID:AB_2535794
ProLong™ Diamond Antifade Mountant with DAPI	dropwise	Thermo Fisher Scientific	Cat#P36966
ProLong™ Gold Antifade Mountant	dropwise	Thermo Fisher Scientific	Cat#P36930
EverBrite™ Hardset Mounting medium	dropwise	Biotium	Cat#23003
Type F Immersion Liquid	dropwise	Thorlabs	Cat#11513859

All secondary antibodies for immunofluorescence of MZ-54 and HeLa and DA-iPSn were diluted in PMS buffer (composition see table 6) with 5% FBS. Antibodies for primary

mouse cortical neurons were diluted in 0.1% Triton X-100, 5% goat serum and 1% BSA in PBS.

4.1.8 qPCR primer

Table 10. qPCR primer

Target	Sequence (5'-3')
hIL-6 forward	GATGAGTACAAAAGTCCTGATCCA
hIL-6 reverse	CTGCAGCCACTGGTTCTGT
hIL-8 forward	CTCTTGGCAGCCTTCCTGATT
hIL-8 reverse	TATGCACTGACATCTAAGTTCTTTAGCA
hTNFA forward	ACAACCCTCAGACGCCACAT
hTNFA reverse	TCCTTTCCAGGGGAGAGAGG
hRPII forward	GCACCACGTCCAATGACAT
hRPII reverse	GTGCGGCTGCTTCCATAA

4.1.9 siRNA

Table 11. siRNA

siRNA	Source	Identifier
Silencer™ Select Negative Control No. 1 siRNA	Thermo Fisher Scientific	Cat#4390843
Silencer™ Select OTULIN siRNA#1 s40306	Thermo Fisher Scientific	Cat#4392420
Silencer™ Select OTULIN siRNA#2 s40307	Thermo Fisher Scientific	Cat#4392420
Silencer™ Select OTULIN siRNA#3 s40308	Thermo Fisher Scientific	Cat#4392420

4.1.10 Guide RNA sequences for CRISPR/Cas9

Table 12. Guide RNA sequences for CRISPR/Cas9

guide RNA	Source	Identifier
eGFP#1 (NHT): GGAGCGCACCATCTTCTTCA	from Brunello library Doench et al. [326]	RRID:Addgene_73178
eGFP#2 (NHT): GGCCACAAGTTCAGCGTGTC	from Brunello library Doench et al. [326]	RRID:Addgene_73178
eGFP#3 (NHT): GGGCGAGGAGCTGTTCACCG	from Brunello library Doench et al. [326]	RRID:Addgene_73178

guide RNA	Source	Identifier
human OTULIN#1: ACCACGGACTCGCCGTATGG	from Brunello library Doench et al. [326]	RRID:Addgene_73178
human OTULIN#2: ATTGCTTATACATGAAAGAG	from Brunello library Doench et al. [326]	RRID:Addgene_73178
human OTULIN#3: TGAACTATTCACAAATGAGG	from Brunello library Doench et al. [326]	RRID:Addgene_73178

4.1.11 Plasmids

Table 13. Plasmids

Plasmid	Source	Identifier
pMD2.G	Addgene	RRID:Addgene_12259
psPAX2	Addgene	RRID:Addgene_12260
lentiCRISPRv2 puro	Addgene	RRID:Addgene_98290
pHAGE-myc-APEX2-LC3B	Gift from Christian Behrends [327]	N/A
pHDM-VSV-G	Addgene	RRID:Addgene_164440
pHDM-Tat1b	Addgene	RRID:Addgene_164442
pHDM-Hgpm2	Addgene	RRID:Addgene_164441
pRC-CMV-Rev1b	Addgene	RRID:Addgene_164443

4.1.12 Kits and cloning reagents

Table 14. Kits and cloning reagents

Assay/Kit	Source	Identifier
Ampicillin sodium salt	Carl Roth	Cat#K029.1
GeneJET plasmid Miniprep Kit	Thermo Fisher Scientific	Cat#K0502
Kanamycin sulfate	Thermo Fisher Scientific	Cat#11815024
LB medium (Lennox)	Carl Roth	Cat#X964.2
peqGOLD total RNA isolation kit	VWR Life Science	Cat#13-6834-02
Pierce™ BCA Protein Assay Kit	Thermo Fisher Scientific	Cat#23227
PureLinkTM HiPure Plasmid filter Maxiprep Kit	Thermo Fisher Scientific	Cat#K210006
RevertAid H Minus First Strand cDNA Synthesis Kit	Thermo Fisher Scientific	Cat#K1632

4.1.13 Plastic ware and consumables

Table 15. Plastic ware and consumables

Plastic ware/Consumables	Source
15 ml and 50 ml conical tubes, polypropylene	Greiner Bio-One
Amersham Hyperfilm™ (High performance chemiluminescence film)	GE Healthcare
Amersham™ Protran™ 0.2 µm Nitrocellulose Membrane	GE Healthcare
Cell culture dishes 100 mm	Greiner Bio-One
Cell culture dishes 145 mm	Greiner Bio-One
Cell culture dishes 60 mm	Greiner Bio-One
CELLSTAR® 12-well tissue culture plates	Greiner Bio-One
CELLSTAR® 6-well tissue culture plates	Greiner Bio-One
CELLSTAR® 96-well tissue culture plates	Greiner Bio-One
Cellstar® cell culture flasks T-25, T-75, T-175	Greiner Bio-One
Combitips advanced (0.5 ml, 1 ml, 2.5 ml, 5 ml, 10 ml)	Eppendorf
Cryogenic vials (1.8 ml)	Starlab
Disposal bags	Carl Roth
Filter paper	Carl Roth
Filter tips (10 µl, 200 µl, 1000 µl)	Starlab
Marienfeld Superior™ Microscope Cover Glasses, 18 mm Ø, thickness Nr. 1 (0,13-0,16 mm)	Marienfeld Laboratory Glassware
MicroAmp™ Optical 384-Well Reaction Plate	Thermo Fisher Scientific
Microcentrifuge tubes (0.5 ml, 1.5 ml, 2 ml)	Starlab
Millex-HA Filter, 0.45 µm	Merck
Nitril gloves, sterile, powder-free	Kimberly-Clark
Nitril gloves, sterile, powder-free	Starlab

Plastic ware/Consumables	Source
Parafilm	VWR
Pasteur pipettes (15 cm/30 cm)	Carl Roth
Scalpel	B. Braun
Sterile pipettes (2 ml, 5 ml, 10 ml, 25 ml, 50 ml)	Greiner Bio-One
Surgipath X-tra Adhesive Slides	Leica Biosystems
Syringes (5 ml)	B. Braun
TipOne Graduated Tip (10 µl, 200 µl, 1000 µl)	Starlab
Trans-Blot SD semi-dry transfer cell	Bio-Rad

4.1.14 Equipment and instruments

Table 16. Equipment and instruments

Equipment/Instruments	Source
ARE heating magnetic stirrer	VELP Scientifica
Autoclave Systec V150	Systec
Balance 440-47N	Kern
BioRAD Mini Protean® Tetra Cell	BioRAD Laboratories
BioRAD Power-Pac HC	BioRAD Laboratories
BioRAD Trans-Blot SD Semi-Dry Transfer Cell	BioRAD Laboratories
Biowizard biosafety cabinet	Kojair
CASY® cell counter	OMNI Life Science
Centrifuge MIKRO 200 R	Hettich
Centrifuge ROTANTA 460 R	Hettich
Centrifuge ROTIXA 50 RS	Hettich
Easypet© 3	Eppendorf
Electronic analytical balance EW	Kern
Electronic precision balance 770	Kern
Freezer (-20°C)	EWALD Innovationstechnik
Freezer (-80°C)	Sanyo Electric Co. Ltd.
Fridge (4°C)	EWALD Innovationstechnik

Equipment/Instruments	Source
HERAsafe class II biological safety cabinet	Kendro
ImageXpress Micro XLS Imaging System	Molecular Devices
inCUsafe CO_2 incubator model: MCO-20AIC	Sanyo Electric Co. Ltd.
Infinite M200 microplate reader	Tecan
Leica SP8 laser-scanning microscope (LSM)	Leica Microsystems
Mastercycler® pro S Thermal Cycler	Eppendorf
Micro Centrifuge SD	Carl Roth
MM-Separator M12+12, MD90001	MagnaMedics
Multipette® M4	Eppendorf
NanoDrop 1000	PeqLab
Odyssey® Imaging System	LI-COR Biosciences
Olympus CKX41 Microscope	Olympus
Peqlab PerfectBlue™ Vertical Double Gel System	VWR Life Science
Pipettes Research Plus (2.5 µl, 10 µl, 20 µl, 100 µl, 200 µl, 1000 µl)	Eppendorf
QuantStudio™ 7 Flex Real-Time PCR System	Applied Biosystems
Rocking shaker	MS-L GmbH
Roller mixer	Ratek
Rotating wheel	Stuart, Staffordshire, UK
Rotator	MS-L GmbH
Steam pressure autoclave Systec VX-150	Systec GmbH
ThermoMixer® comfort	Eppendorf
Vacuum Pump HLC	Ditabis
Vapo.Protect Mastercycler® Pro	Eppendorf
Vortex (ZX classic, wizard X)	VELP Scientifica
Water bath SWB20	Medingen
Zeiss AxioObserver Z1	Carl Zeiss Microscopy GmbH

Equipment/Instruments	Source
Zeiss LSM 780	Carl Zeiss Microscopy GmbH
Zeiss Elyra7 Structured Illumination Microscope (SIM)	Carl Zeiss Microscopy GmbH

4.1.15 Software and algorithms

Table 17. Software and algorithms

Software/Algorithm	Version	Source
Endnote™	20	Clarivate
ImageJ	1.53u	National Institute of Health
(Fiji Is Just) ImageJ	2.14.0/1.54f	National Institute of Health
GraphPad Prism	9.3.1(471)	GraphPad Software
i-control	1.10	Tecan Life Sciences
Leica Application Suite X	2019.01.30	Leica Microsystems
Magellan™ Data Analysis	7.2	Tecan Life Sciences
MetaXpress® 6.7.2	6.7.1.157	Molecular Devices
MS Office	2019	Microsoft
NanoDrop 1000 Software	3.8.1	PEQLAB
Zeiss blue software	ZEN lite 2012	Carl Zeiss Microscopy GmbH
ZEN image acquisition software (SIM2 upgrade)	N/A	Carl Zeiss Microscopy GmbH
Imaris image analysis software	10.0.1	Bitplane

4.2 Methods

4.2.1 Cell culture

All cell culture works were done under biological safety cabinets and autoclaved, or sterile packed materials were used to avoid contamination. Absence of mycoplasma contamination was regularly controlled by PCR.

4.2.1.1 Culturing conditions of cell lines

All cell lines were cultured at 37°C in incubators with 5% CO_2 and a relative humidity of 95%. MZ-54 and HeLa cells were grown in Dulbecco's Modified Eagle Medium (DMEM) GlutaMAX™ supplemented with 10% FBS and 1% Penicillin-Streptomycin (Pen/Strep) and passaged two to three times per week. For passaging, medium was aspirated and cells were washed with pre-warmed PBS, followed by the addition of 0.05% trypsin-

EDTA and incubation at 37°C, 5% CO_2 for 4 to 5 min to detach cells. Trypsin activity was stopped by addition of fresh culture medium and the appropriate number of cells was transferred to a new cell culture flask with fresh medium. The ratios for passaging were between 1:4 to 1:10. Cell culture was terminated if cells reached a number of 25 to 30 passages.

4.2.1.2 Freezing and thawing of cell lines

Freezing:

For freezing, cells were centrifuged at 1800 rpm for 5 min at RT and cell pellets were resuspended in freezing medium composed of 50% FBS, 40% culture medium and 10% DMSO. Cell suspension was aliquoted in cryogenic vials and frozen in a Mr. Frosty™ Freezing Container at -80°C overnight. For long-term storage, cells were transferred to a liquid nitrogen tank.

Thawing:

Cells were quickly thawed at RT and added dropwise to 5 ml culture medium. After centrifugation at 1800 rpm for 5 min at RT, cells were resuspended in culture medium, transferred to a cell culture flask and cultured as described above.

4.2.1.3 Cell counting

For cell counting, cells were thoroughly resuspended and 100 µl cell suspension was diluted in 10 ml CasyTon. The cell number was measured with the CASY cell counter according to the manufacturer's instructions. Alternatively, a Neubauer counting chamber was used to determine the cell number. Therefore, the cell suspension was diluted with the Trypan Blue and 10 µl of the cell dilution was applied onto the Neubauer counting chamber. The cells in the four large squares of the chamber were counted using a light microscope and the average cell number was determined. The cell number per ml was calculated with the formula:

Cell number per ml = Average cell number per square x 10^4 x (Dilution factor)

4.2.1.4 Seeding and treatment of cells

For seeding, cells were prepared in fresh culture medium at the desired density depending on the type of plate/dish and experiment (see table 18). 24 h after seeding, treatment compounds were diluted in fresh culture medium and applied on the cells after removing of the old medium. Experimental details about treatment concentrations and time points are described in the figure legends.

Table 18. Cell numbers for seeding

Experiment	Plate/dish (Surface)	Cell number
Western Blot	60 mm dish (21 cm^2)	MZ-54: 300,000 cells in 4 ml HeLa: 800,000 cells in 4 ml
	100 mm dish (58 cm^2)	MZ-54: 850,000 cells in 8 ml
	145 mm dish (143 cm^2)	MZ-54: $3x10^6$ in 12 ml
Immunofluorescence	12-well (3.9 cm^2)	MZ-54: 30,000 cells in 1 ml HeLa: 70,000 cells in 1 ml
qRT-PCR	6-well (9.6 cm^2)	MZ-54: 100,000 cells in 2 ml
Cell death	96-well (0.28 cm2)	MZ-54: 4,000 cells in 100 µl HeLa: 10,000 cells in 100 µl

4.2.2 iPSC culture and neuronal differentiation

Culturing of induced pluripotent stem cells (iPSCs) was performed by Denise Balta and Julia Vandrey (Department of Molecular Neurology, University Hospital Erlangen, Friedrich-Alexander-University Erlangen-Nürnberg, Germany). Isogenic controls of Parkinson disease patient-derived human iPSCs, carrying a triplication in the alpha-synuclein gene, were generated via CRISPR/Cas9 gene editing and previously characterized by Stojkovska *et al.* [328,329]. iPSCs were cultivated in mTeSR1 plus media on matrigel-coated 6-well plates and differentiated into dopaminergic neurons (DA-iPSn) using an established protocol [330] at a constant of 37°C and 5% CO_2. Between day 25-30 of differentiation, neurons were seeded on poly-D-lysine and LAM/Laminin coated 24-well plates at a number of $3x10^5$ per well on 12-mm cover glasses for immunofluorescence. Neurons were maintained in Neurobasal media containing NeuroCult SM1 Neuronal Supplement and 1% Pen/Strep. Around day 90, neurons were used for treatment.

4.2.3 Culture of primary mouse cortical neurons

Culturing of primary mouse cortical neurons was performed by Verian Bader and Konstanze Winklhofer (Department of Molecular Cell Biology, Institute of Biochemistry and Pathobiochemistry, Ruhr University Bochum, Germany). Mouse cortices from embryonic day 18 (E18) embryos were dissected into ice-cold Hanks' balanced salt solution (HBSS) and dissociated in acetylated trypsin for 20 min at 37°C. Subsequently, tissues were rinsed with HBSS and treated with DNase I to break down DNA and triturated with a cell strainer. For immunocytochemistry, the cell suspension was resuspended in Neurobasal medium and plated in 24-well plates on coverslips coated with poly-L-lysine and laminin at a concentration of 50,000 neurons per well. Medium

was replaced after 45 min. Primary neurons were cultured in Neurobasal medium with B27 and glutamine in a humidified incubator at 37°C and 5% CO_2. At day 7 in vitro, LLOMe treatment was performed, followed by fixation of cortical neurons in 4% paraformaldehyde in PBS for 15 min and washing with PBS. Protocols were performed in compliance with institutional and governmental regulations.

4.2.4 Generation of CRISPR/Cas9-derived *OTULIN* KO cells

To generate CRISPR/Cas9-mediated genetic knockout of OTULIN in MZ-54 cells, guideRNAs from the Brunello library [326] against human OTULIN or eGFP as non-human target (NHT) control were cloned into pLenti-CRISPRv2 using standard cloning procedures with *BsmBI* restriction sites. All plasmids were verified by Sanger sequencing.

4.2.4.1 Viral particle production and target cell transduction

Knockout of target genes was done by lentiviral transduction. For the production of viral particles HEK293T cells were co-transfected with 1.65 µg of the gRNA-encoding pLenti-CRISPRv2 plasmids and 2.7 µg packaging plasmid psPAX2 and 1 µg pMD2.G. Transfection was done using FuGENE® HD Transfection Reagent at a ratio of 1:3 (µg DNA/µl FuGENE) according to the manufacturer's protocol in Pen/Strep-free medium. 24 h later, the medium was replaced with fresh culture medium and the virus containing supernatant was harvested 48 and 72 h after transfection, pooled, sterile filtered through a 0.45 µm filter and frozen at -80°C for long-term storage. Target cell transduction was done with 0.5 ml of viral supernatant in 3 ml of total medium supplemented with 8 µg/ml polybrene. 2 to 4 days post transduction, cells were reseeded in medium supplemented with 1 µg/ml puromycin to select cells with successful knockout. Knockout efficiency of the bulk culture was verified by western blotting.

4.2.5 Generation of myc-APEX2-LC3B expressing MZ-54 cells

Stable expression of myc-APEX2-LC3B in MZ-54 cells was achieved by lentiviral transduction. One day before transfection HEK293T cells were seeded with a density of $1x10^6$ cells per 6-well. For transfection, 2 µg of the pHAGE-myc-APEX2-LC3B expression plasmid and the packaging plasmids pHDM-VSV-G, pHDM-Tat1b, pHDM-Hgpm2 and pRC-CMV-Rev1b (0.5 µg each) were mixed with OptiMEM transfection medium, followed by addition of Lipofectamine 2000. After incubation for 15 to 20 min at RT the transfection mix was added on top of HEK293T cells in Pen/Strep-free medium. 24 h and 48 h after transfection the viral particle containing medium was harvested, pooled and sterile filtered through a 0.45 µm filter. Transduction of MZ-54 cells was

performed with 3 ml of viral supernatant supplemented with 8 µg/ml polybrene. 2 days after transduction, cells were reseeded and selection with 1 µg/ml puromycin was started. Successful overexpression of myc-APEX2-LC3B was confirmed by western blotting.

4.2.6 Quantification of cell death

For cell death analysis, cells were seeded in 96-well plates (density see table 18) and at the end of treatment, Hoechst 33342 and propidium iodide was diluted in PBS and added 1:100 to the cells (Working concentration: 10 mg/ml Hoe and 1 µg/ml PI), followed by incubation for 10 min at 37 °C. Cell death was determined by fluorescence-based measurement of the ratio of non-viable (PI positive) cells compared to the total number of cells (Hoechst-positive cells) using the ImageXpress Micro XLS Widefield High-Content Analysis Sytem and MetaXpress Software.

4.2.7 RNAi-mediated silencing of protein expression

RNAi-mediated silencing of protein expression was performed by reverse transfection of the desired siRNAs (see table 11) with Lipofectamine™ RNAiMAX Transfection Reagent. To prepare siRNA-lipid complexes for reverse transfection, siRNA was diluted in OptiMEM transfection medium and added to a Lipofectamine-OptiMEM mix (final siRNA concentration=20 nM), followed by incubation at RT for 5 min. The transfection mix was then distributed dropwise in cell culture plates and the cells were seeded on top in Pen/Strep-free medium. 24 h after transfection, medium was replaced with fresh medium. Reseeding and treatment of knockdown cells for experiments was done 48 h and 72 h after transfection, respectively. Knockdown efficiency was confirmed by western blotting.

4.2.8 Immunofluorescence analysis (confocal microscope)

For immunofluorescence staining, cells were seeded on microscope coverslips into Greiner 12-well plates (cell density see table 18). At the end of treatment, cells were carefully washed with PBS and fixed by adding 4% formaldehyde for 5 min at RT. Fixation was followed by blocking and permeabilization of the cells in permeabilization buffer (PB) (0.1% Saponin and 5 mM $MgCl_2$ in PBS) supplemented with 10% FBS for 1 h at RT. Primary antibody incubation was done overnight at 4°C in PB with 5% FBS. After 3 washing steps with PB for 5 min at RT, cells were incubated with secondary antibodies diluted 1:500 in PB with 5% FBS for 2 h at RT. After two washing steps with PB coverslips were rinsed in ddH_2O and placed on glass slides with ProLong™ Diamond Antifade Mountant with DAPI. Images were acquired with the Leica SP8 laser-scanning

microscope using 63x magnification and Type F Immersion Oil. Immunofluorescence of DA-iPSn was performed as for MZ-54 and HeLa cells, except for the following steps: After removal of the secondary antibodies, cells were stained with DAPI diluted 1:10,000 in PBS for 10 min at RT. After two washing steps with PBS and one washing step with ddH_2O, DA-iPSn were mounted on glass slides with ProLong™ Gold Antifade Mountant and image acquisition was performed with a Zeiss LSM 780 (Carl Zeiss Microscopy GmbH) and the Zeiss blue software (ZEN lite 2012). For immunofluorescence of primary mouse neurons, neurons were permeabilized and blocked in 0.1% Triton X-100, 5% goat serum, 1% BSA in PBS for 1 h. Staining with primary antibodies diluted in 0.1% Triton X-100, 5% goat serum, 1% BSA in PBS was performed at 4°C overnight, followed by washing three times with PBS, and incubation with fluorescent dye-conjugated secondary antibodies at a dilution of 1:1000 for 1 h at RT. After 3 washing steps in PBS, cells were incubated with DAPI and mounted in EverBrite™ Hardset Mounting medium. Super-resolution structured illumination microscopy (SR-SIM) was performed using a Zeiss Elyra7 equipped with an 63x NA 1.4 OIL objective and the ZEN image acquisition software including the SIM2 upgrade. 3D image reconstruction was performed using the surface function of the Imaris 10.0.1 image analysis software. All other images were processed and analyzed with FIJI and ImageJ. Quantification of puncta was done manually or using the FIJI plugin Aggrecount (v1.13) with at least three independent microscopic views. Pearson's correlation coefficient was calculated with the FIJI plugin Coloc2.

4.2.9 Electron microscopy

Conventional transmission electron microscopy was performed in collaboration with Muriel Mari (Department of Biomedicine, Aarhus University, Denmark). After treatment of MZ-54 NHT and *OTULIN* KO cells with 17.5 µM LOP for 16 h, cells were prepared for electron microscopy as previously described [172]. Cell sections were analyzed using a Talos™ F200i TEM (Thermo Fisher Scientific, Eindhoven, The Netherlands). The average number of autophagosomes and degradative compartments (amphisomes, lysosomes and autolysosomes) per cell section was determined by counting these compartments through 120 cell sections per condition, randomly selected from three independent grids.

4.2.10 Western blot analysis

4.2.10.1 Cell lysis and Bicinchoninic acid assay (BCA)

All steps for cell lysis were performed on ice to avoid protein degradation. Cells were seeded in 60 mm, 100 mm or 145 mm cell culture dishes depending on the experimental setup (cell density see table 18). After treatment, cells were harvested with a cell scraper, washed with PBS and lysed in RIPA lysis buffer (supplemented with protease inhibitor complex (PIC), 1 mM sodium orthovanadate, 5 mM sodium fluoride, 2 mM DTT, 1 mM phenylmethylsulfonyl fluoride and Pierce™ Universal Nuclease) or 1% NP-40 lysis buffer (supplemented with PIC, 1 mM sodium orthovanadate, 5 mM sodium fluoride, 25 mM NEM and Pierce™ Universal Nuclease). Cell lysates were incubated for 20-25 min on ice, followed by centrifugation at 18,000xg and 4°C for 25 min. The supernatant was collected in a new tube and protein concentration was determined with the Pierce™ BCA Protein Assay kit (Thermo Scientific) according to the manufacturer's protocol by measuring absorbance of the samples at 550 nm with a Tecan Sunrise microplate reader and comparing it with a BSA standard curve.

4.2.10.2 SDS-polyacrylamide gel electrophoresis (SDS-PAGE)

To prepare samples for SDS-polyacrylamide gel electrophoresis (SDS-PAGE), a defined amount of protein (25-50 µg) was mixed with 6x SDS loading buffer (1x final concentration) and ddH_2O and boiled at 96°C for 5 min. For storage, protein lysates were frozen at -20°C or directly loaded on self-cast polyacrylamide gels (Gel percentage depending on the proteins of interest, composition of stacking and separating gel see table 6) together with PageRuler™ Plus Prestained Protein Ladder as size standard. Gel electrophoresis was performed in 1x SDS-PAGE running buffer (composition see table 6) and started at 80 V. When samples had passed the stacking gel voltage was increased to 120 V and gel electrophoresis was stopped when the desired protein separation was reached.

4.2.10.3 Western Blotting

Transfer of proteins on a nitrocellulose membrane was performed with a semi-dry blotting system (BioRad). The separating gel, a nitrocellulose membrane and four Whatman filter papers were soaked into 1x blotting buffer (composition see table 6). To assemble the transfer sandwich, two Whatman papers were placed on the anode of the blotting chamber, the membrane with the gel on top of it and covered again with two Whatman papers. Protein transfer was performed with a current of 1-1.25 mA/cm^2 of nitrocellulose membrane for 90 min.

4.2.10.4 Protein detection by enhanced chemiluminescence (ECL)

To prevent unspecific antibody binding the membrane was blocked with 5% milk powder in PBS-T for 1 h, followed by three washing steps with PBS-T. Incubation of the membrane with first antibodies was usually done overnight at 4°C, only the anti-M1 Ub antibody was incubated for 1 h at RT (for antibody dilutions see table 7). On the next day, membranes were washed three times for 7-10 min, followed by incubation with species-specific horseradish peroxidase (HRP)-conjugated secondary antibodies for 1 h at RT. After three washing steps with PBS-T proteins were detected on X-ray films in a dark room using Pierce™ ECL Western Blotting Substrate according to the manufacturer's instructions. If incubation of the membrane with additional antibodies was required, first antibodies were stripped off the membrane with 0.4 M NaOH for 5 min at RT, followed by three washing steps with PBS-T and blocking with 5% milk powder in PBS-T for 1 h. Incubation with the new primary antibodies and protein detection was performed as described above. Proteins were usually detected with multiple exposure times and X-ray films were scanned for further analysis. Representative blots of at least two independent experiments are shown in the Results section unless stated otherwise.

4.2.11 NP-40-soluble and NP-40-insoluble cell fractionation

NP-40-soluble and NP-40-insoluble cell fractionation was performed for the detection of intracellular protein aggregates. Cells were lysed with 1% NP-40 lysis buffer plus supplements as described above (see 4.2.10.1). After centrifugation and transfer of the supernatant (NP40-soluble fraction) in a new tube, the remaining pellet containing NP-40-insoluble cell organelles and large protein aggregates was washed two times with 200 µl NP-40 lysis buffer and centrifuged at 18,000xg for 5 min between the washing steps. Then, 40-100 µl NP-40 lysis buffer plus 1% SDS was added to the pellet. Samples were resuspended and briefly sonicated, followed by incubation at 96°C for 30 min. Finally, samples were centrifuged and the supernatant (NP-40-insoluble/SDS-soluble fraction) was collected. Protein concentration of the NP-40-soluble and NP-40-insoluble fraction was determined using BCA as described above (see 4.2.10.1). Western blot analysis of the different cell fractions was performed as described above with GAPDH as loading control for the NP-40-soluble fraction and histone H3 for the NP-40-insoluble fraction.

4.2.12 Organelle (nuclear) fractionation

For isolation of the cytosolic and organelle (nuclear) fraction, cells were seeded in 145 mm dishes (cell density see table 18). At the end of treatment, cells were washed with PBS, harvested with a cell scraper and centrifuged at 1800 rpm for 5 min at 4°C. Cell

pellets were resuspended in 100-200 µl isolation buffer with 0.025% digitonin and incubated on ice for 10 min. After centrifugation at 16,000xg and 4°C for 3 min the supernatant (cytosolic fraction) was transferred in a new tube. The pellet (organelle fraction containing nuclei and mitochondria) was resuspended in 50-100 µl RIPA lysis buffer and cell lysis and measurement of protein concentration using BCA was performed as described above (see 4.2.10.1).

4.2.13 Quantitative real-time PCR (qRT-PCR)

4.2.13.1 RNA isolation and cDNA synthesis

Quantitative real-time PCR was used to analyze relative mRNA expression levels. This technique requires RNA isolation from cells (or tissue), reverse transcription of RNA into complementary DNA (cDNA) and SYBR Green-based fluorescent analysis of relative mRNA expression levels. For RNA isolation, cells were seeded in 6-well plates (cell density see table 18) one day before treatment. At the end of treatment, medium was aspirated and total RNA was isolated using the peqGOLD Total RNA Kit according to the manufacturer's instructions. RNA concentration of the samples was measured with a NanoDrop 1000 spectrophotometer and 1 µg RNA was used for cDNA synthesis with the RevertAid H Minus First Strand cDNA Synthesis Kit (Thermo Scientific) according to the manufacturer's protocol and with the program shown in table 19. After cDNA synthesis, cDNA was diluted 1:10 with nuclease-free water and used for qRT-PCR.

Table 19. Program for cDNA synthesis

Step	Temperature	Time
Start	25°C	5 min
Synthesis	42°C	60 min
Stop	70°C	5 min
Hold cooling	4°C	Infinite

4.2.13.2 qRT-PCR

SYBR Green-based qRT-PCR was performed with the QuantStudio™ 7 Flex Real-Time PCR System. Per reaction, 10 µl PCR master mix (composition see table 20) and 1 µl diluted cDNA were added to a MicroAmp™ Optical 384-Well-Reaction plate. The program for qRT-PCR is shown in table 21. At least three independent experiments were performed in technical triplicates and the specificity of the qRT-PCR products was controlled with melting curves. Data analysis was done using the $2^{-\Delta\Delta Ct}$ method [331] and relative mRNA expression levels of the target transcripts were normalized to the housekeeping gene *RPII*.

Table 20. qRT-PCR Master Mix

Component	Volume
SYBR™ Green PCR Master Mix	5 µl
Forward primer 10 µM	0.25 µl
Reverse primer 10 µM	0.25 µl
ddH_2O	4.5 µl

Table 21. qRT-PCR program

Step	Temperature	Time	
Annealing	50°C	2 min	
Polymerase activation	95°C	10 min	
Denaturation	95°C	15 sec	40 cycles
Annealing and Elongation	60°C	1 min	

4.2.14 APEX2-based autophagosome content profiling

APEX2-based autophagosome-content profiling was described by Zellner *et al.* [327] and combines APEX2-mediated proximity labeling and proteinase K protection with quantitative proteomics of enriched autophagosomes to identify autophagy cargo.

4.2.14.1 Proximity labeling

For proximity labeling with biotin-phenol, myc-APEX2-LC3B expressing MZ-54 NHT and *OTULIN* KO cells were seeded in 145 mm dishes with a density of $1.5x10^6$ cells per dish. The next day, cells were treated with 17.5 µM LOP for 16 h or 200 nM BafA1 for 2 h alone or in combination. Treatment with BafA1 was always performed in the last 2 h of the LOP treatment. At the end of treatment, 500 µM biotin-phenol diluted in DMSO was added to the cells for 30 min at 37°C, followed by addition of 1 mM H_2O_2 for 1 min at RT. The biotinylation reaction was immediately quenched by washing the cells three times with quencher solution (see table 6), then three washing steps with PBS were performed and cells were scraped and pelleted by centrifugation at 500xg for 5 min at 4°C. Cell pellets were frozen at -80°C and sent to Munich for further processing and mass spectrometry (MS) analysis of the autophagosome content.

4.2.14.2 Proteinase K digest

Unless stated otherwise, all steps for proteinase K digest were performed on ice or at 4°C. Cell pellets were washed with homogenization solution I, centrifuged at 500xg for 5 min and resuspended in homogenization solution I. After incubation for 20 min on a rotating wheel, samples were centrifuged at 500xg for 3 min. The cell pellet was

resuspended in the supernatant and homogenized in a Dounce homogenizer with a set of 70 strokes. Homogenization solution II (see table 6) was added to the samples at a ratio of 1:5 (homogenization solution I:II), followed by centrifugation at 600xg for 10 min to clear lysates. For western blotting, each sample was distributed equally in 4 tubes and the reactions for the proteinase K protection assay were prepared as shown in table 22.

Table 22. Reactions for proteinase K protection assay

Water control	Proteinase K only	TX-100 control	Proteinase K+TX-100
~ 25 µl lysate ddH_2O ad 30 µl	~ 25 µl lysate 30 µg/ml Proteinase K ddH_2O ad 30 µl	~ 25 µl lysate 0.2% TX-100 1x PIC ddH_2O ad 30 µl	~ 25 µl lysate 30 µg/ml Proteinase K 0.2% TX-100 ddH_2O ad 30 µl

Proteinase K digest was performed for 30 min and stopped by addition of 10 mM PMSF. After addition of 6x SDS loading buffer (1x final concentration) samples were incubated at 96°C for 5 min and submitted to SDS-PAGE and western blot analysis.

For MS, samples were treated with 100 µg/ml Proteinase K for 1 h at 37°C or 0.1% RAPIGest™ in addition to Proteinase K for the control samples. This was followed by centrifugation at 17,000xg for 15 min to separate digested from membrane-protected material.

4.2.14.3 Streptavidin pulldown

Streptavidin pulldown was performed as described previously [327]. In brief, biotin-labeled pellets with or without proteinase K digestion were resuspended in RIPA buffer with quenching components (50 mM Tris, 150 mM NaCl, 0.1% SDS, 0.5% sodium deoxycholate, 1% Triton X-100, 1x protease inhibitors (Roche), 1x PhosStop (Roche), 1 mM sodium azide, 10 mM sodium ascorbate and 1 mM Trolox), sonicated and centrifuged at 10,000xg. The supernatants were applied on pre-equilibrated Streptavidin-Agarose resins and incubated overnight. Next, samples were washed 3x in RIPA buffer with quenching components and 3x in 3 M Urea buffer (in 50 mM NH_4HCO_3) before incubation with 5 mM TCEP for 30 minutes at 55°C and shaking. To alkylate samples, 10 mM IAA was added for 20 minutes at room temperature and quenched by addition of 20 mM DTT. After two washing steps with 2 M Urea buffer (in 50 mM NH_4HCO_3) overnight trypsin digestion was performed with 1 µg trypsin per 20 µl beads at 37°C. Supernatants were collected from the resin, washed two times with 2 M Urea buffer and acidified with 1% trifluoroacetic acid. The sample volume was then decreased by vacuum

centrifugation and digested peptides were desalted on custom-made C18 stage tips. Finally, samples were reconstituted with 0.5% acetic acid for MS analysis.

4.2.15 Mass spectrometry (MS) data collection and analysis

MS data collection and analysis was performed as described previously [327]. Samples were loaded onto 75 µm x 15 cm fused silica capillaries (custom-made) packed with C18AQ resin (Reprosil-Pur 120, 1.9 µm, Dr. Maisch HPLC) using an Easy-nLC1200 liquid chromatography. Peptide mixtures were separated at a 400 nl/min flow rate using a 35 min ACN gradient in 0.5% acetic acid (5–38% ACN gradient for 23 min followed by 38-60% ACN gradient for 3 min and 60-95% ACN gradient for 2 min plus another 3 min at 95% CAN prior to 95-5% gradient for 2 min and another 2 min at 5% ACN) and detected on an Q Exactive HF mass spectrometer. Dynamic exclusion was enabled for 20 s and singly charged species, charge states above 8 or species for which a charge could not be assigned were rejected. MS raw data was analyzed using MaxQuant (version 1.6.0.1) [332] and a human Uniprot FASTA reference proteome (UP000005640) in reverted decoy mode with the following allowance: methionine oxidation and protein N-terminus acetylation as variable modifications, cysteine carbamidomethylation as fixed modifications, 2 missed cleavages and 5 modifications per peptide, minimum peptide length of 7 amino acids, first search peptide tolerance of ±20 ppm, main search peptide tolerance of ±4.5, match between runs, label-free quantification (LFQ), as well as protein, peptide and site level false discovery rates of 0.01. For further processing, MaxQuant output files (protein groups) were loaded into Perseus (version 1.6.5.0) [333] where matches to common contaminants, reverse identifications, identifications based only on site-specific modifications and with less than 2 peptides and MS/MS counts were removed. Identifications from the RAPIGest™ and proteinase K treated controls were subtracted from proteinase K treated APEX2-LC3B samples. Only proteins with LFQ intensities in 2 out of 3 biological replicates in at least one experimental group were kept for the subsequent label-free quantification (LFQ). LFQ intensities were $\log_2$ transformed and missing values were replaced with random numbers drawn from a normal distribution. Student t-tests were used to determine the statistical significance of the abundance alterations of proteins identified in the proximity of APEX2-LC3B between experimental conditions. Proteins with p-values ≤ 0.05 and t-test differences ≥ 1 or ≤ -1 were defined as significantly up- and downregulated cargo candidates.

Proteinase K digest for MS, streptavidin pulldown as well as MS data collection and analysis were performed by Susanne Zellner and Christian Behrends (Munich Cluster for Systems Neurology (SyNergy), Ludwig-Maximilians-University (LMU) Munich, Germany).

4.2.16 Statistical analysis

Results are shown as mean ± SEM. Statistical analysis was done with GraphPad Prism 9, using student's t-test and 2-way ANOVA, followed by Tukey's test for multiple comparisons. p-values <0.05 were interpreted as significant and are shown as follows: p≤ 0.05: *, p≤ 0.01: **, p≤ 0.001: ***, p≤ 0.0001: ****, ns: not significant.

5 Results

Parts of this work are described in the manuscript “Linear ubiquitination at damaged lysosomes induces local NF-κB activation and controls cell survival” (bioRxiv 2023.10.06.560832; doi: https://doi.org/10.1101/2023.10.06.560832) [334]. Electron microscopy was performed by Muriel Mari of the Department of Biomedicine (Aarhus University, Denmark). Proteinase K digest, streptavidin pulldown as well as MS data collection and analysis for the APEX2-based autophagosome content profiling was performed by Susanne Zellner and Christian Behrends at the Munich Cluster for Systems Neurology (SyNergy) (Ludwig-Maximilians-University, Munich, Germany). Denise Balta, Julia Vandrey and Friederike Zunke provided support with culturing of iPSCs, differentiation to DA-iPSn and immunofluorescence staining and imaging of DA-iPSn (Department of Molecular Neurology, University Hospital Erlangen, Friedrich-Alexander-University Erlangen-Nürnberg, Germany). Verian Bader and Konstanze Winklhofer performed culturing, immunofluorescence staining and SR-SIM of primary mouse cortical neurons (Department of Molecular Cell Biology, Institute of Biochemistry and Pathobiochemistry, Ruhr University Bochum, Germany). Marvin Dietrich (MD student, Institute for Experimental Pediatric Hematology and Oncology, Goethe University Frankfurt) participated in this project and performed a part of the experiments (indicated in the figure legends).

5.1 Characterization of the function of OTULIN and LUBAC in autophagy

5.1.1 Loss of OTULIN leads to enhanced autophagy induction and increases the autophagic flux

LUBAC and OTULIN are known to be involved in the regulation of autophagy initiation and selective autophagy. During *Salmonella typhimurium* infection, M1 poly-Ub chains are formed at the surface of invading bacteria and recruit the autophagy receptors p62 and OPTN to promote degradation of bacteria via xenophagy [111]. In addition, LUBAC and OTULIN function in autophagy initiation and maturation by controlling M1 ubiquitination and stabilization of ATG13 [309]. Based on this, the aim of this work was to further characterize the role of OTULIN and LUBAC in the regulation of bulk and selective autophagy. Therefore, OTULIN-deficient and NHT control MZ-54 GBM cells were generated using CRISPR/Cas9. Since GBM cells have high levels of basal autophagy activity, they are good models to investigate autophagy pathways [179,335,336]. Depletion of OTULIN strongly increased M1 poly-Ub levels, whereas expression of the LUBAC subunits HOIP and HOIL-1 was slightly reduced (**Figure 4A**).

The increase in M1 poly-Ub corresponds with previous findings describing higher M1 poly-Ub expression upon loss of OTULIN [281,286]. It is also reported that the expression of LUBAC subunits is affected by depletion of OTULIN. However, this relationship seems to be cell and tissue type-specific: in fibroblasts, B- and T-cells, OTULIN deficiency correlates with decreased levels of LUBAC subunits, whereas there are no changes in OTULIN-deficient myeloid cells [281,283,286]. To address how autophagy is affected by the loss of OTULIN, autophagy was induced with the mTORC1 inhibitor torin 1 and the autophagy-activating compound LOP. LC3 lipidation in response to torin and LOP treatment was higher in *OTULIN* KO cells compared to control (NHT) cells (**Figure 4B and 4C**). Since higher amounts of lipidated LC3 can either result from an increased autophagic flux or a block in autophagosome degradation, the vacuolar H^+-ATPase inhibitor BafA1, which blocks lysosomal acidification and autophagosome degradation, was applied to *OTULIN* KO and control cells. Increased LC3-II levels upon BafA1 addition reflect enhanced autophagy activity and a higher autophagic flux [337]. BafA1 treatment caused enhanced LC3-II accumulation in OTULIN-depleted cells (**Figure 4D**), suggesting that loss of OTULIN increases the autophagic flux.

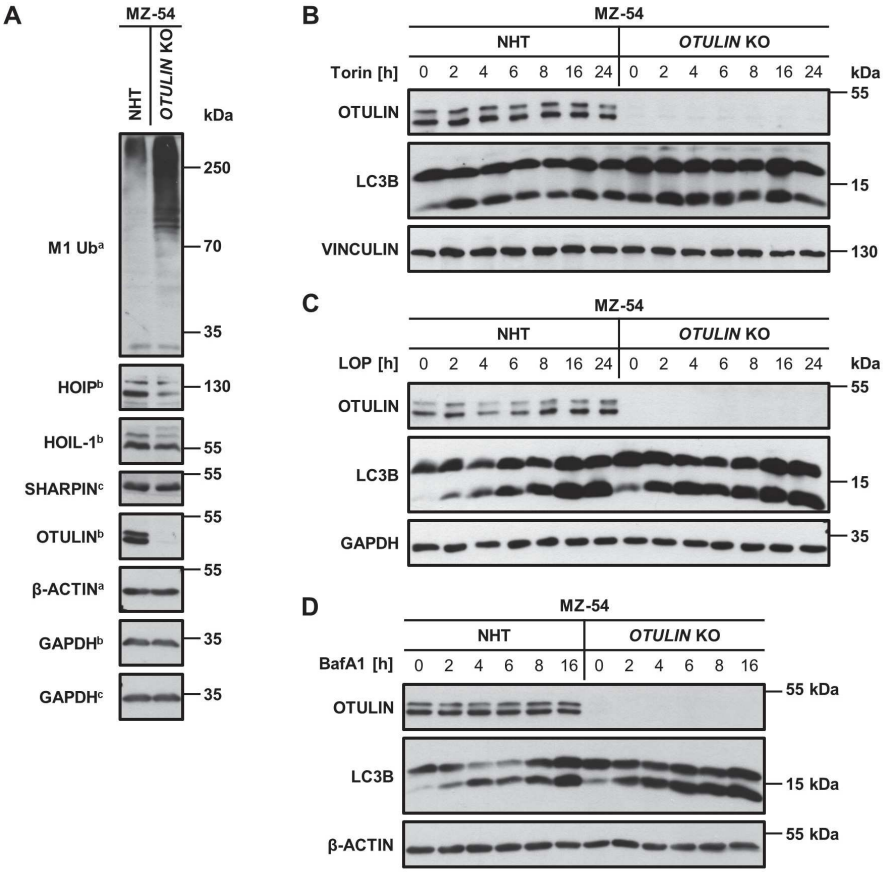

Figure 4. Loss of OTULIN enhances LC3 lipidation in response to autophagy induction and increases the autophagic flux.

Figure 4. Continued.

A. Western blot analysis of total M1 poly-Ub, HOIP, HOIL-1 and Sharpin expression in MZ-54 non-human target (NHT) and *OTULIN* KO GBM cells. GAPDH and β-Actin were used as loading controls. Representative blots of two independent experiments are shown. **B.** Western blot analysis of LC3B lipidation in MZ-54 NHT and *OTULIN* KO GBM cells, treated with Torin-1 (0.25 µM) for the indicated time points. Vinculin was used as loading control. Representative blots of two independent experiments are shown. **C.** Idem as B, but cells were treated with loperamide (LOP, 17.5 µM). GAPDH was used as loading control. Representative blots of two independent experiments are shown. **D.** Idem as B, but cells were treated with Bafilomycin A1 (BafA1, 200 nM) for the indicated time points. β-actin was used as loading control. Representative blots of two independent experiments are shown.

Lipidated LC3 proteins localize to autophagosomal membranes and form punctate structures in response to autophagy induction which can be monitored by immunofluorescence staining [337]. Endogenous staining of LC3 after LOP treatment showed that the number of LC3 puncta was enhanced in *OTULIN* KO cells (**Figure 5A**). In addition, LOP treatment also increased the formation of M1 poly-Ub-positive puncta in OTULIN-deficient cells (**Figure 5B**).

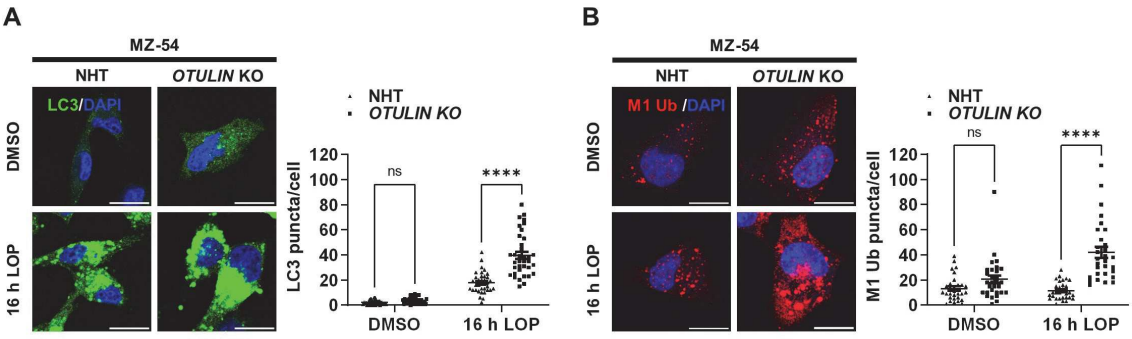

Figure 5. OTULIN depletion enhances LOP-induced formation of LC3 and M1 poly-Ub puncta.

A. Representative immunofluorescence staining of LC3 in MZ-54 NHT and *OTULIN* KO GBM cells, treated with LOP (17.5 µM) for 16 h. Scale bar: 15 µm. Right panel: Quantification of LC3 puncta. Mean and SEM of 36 cells from three independent experiments are shown. **** $p < 0.0001$, ns: not significant. **B.** Idem as A, but MZ-54 NHT and *OTULIN* KO GBM cells treated with LOP (17.5 µM) for 16 h were stained for M1 poly-Ub. Scale bar: 15 µm. Right panel: Quantification of M1 poly-Ub puncta. Mean and SEM of 30 cells from three independent experiments are shown. **** $p < 0.0001$, ns: not significant. Statistical significance was determined with two-way ANOVA followed by Tukey's multiple comparisons tests.

5.1.2 OTULIN depletion triggers ultrastructural increases in degradative compartments and autophagosomes

To characterize autophagic changes upon loss of OTULIN in more detail, an ultrastructural electron microscopy analysis was performed in LOP-treated *OTULIN* KO and control MZ-54 cells. Loss of OTULIN significantly increased the number of basal and LOP-induced degradative compartments (DGCs), which comprise lysosomes,

amphisomes (i.e. hybrid organelles of autophagosomes fused with endosomes) and autolysosomes. In addition, the number of autophagosomes under basal conditions was also enhanced in OTULIN-deficient cells (**Figure 6A and 6B**).

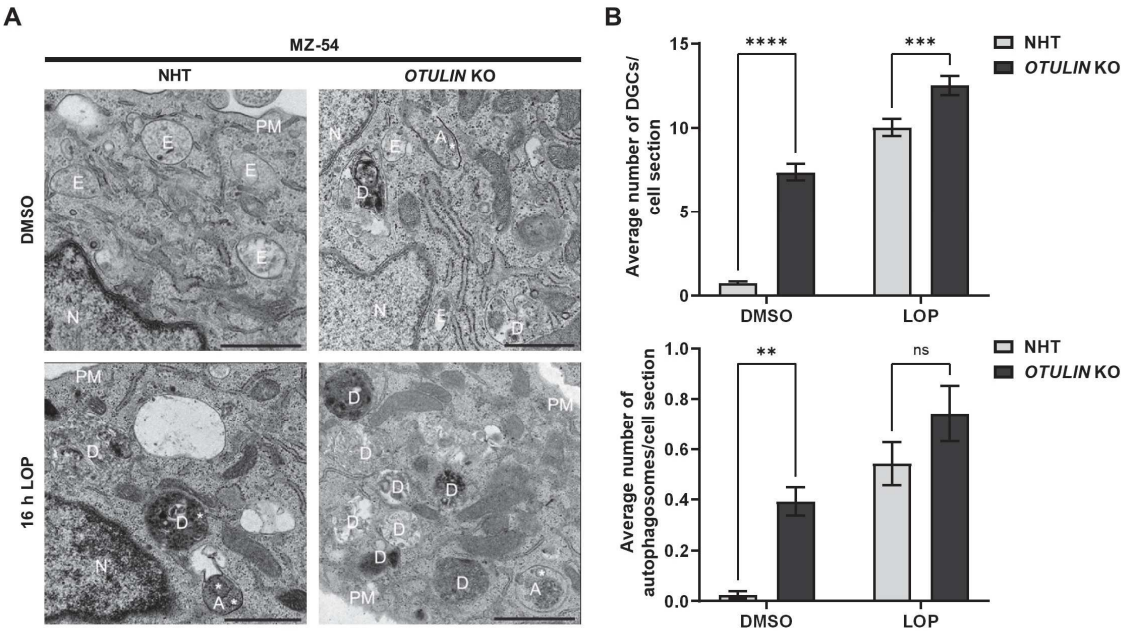

Figure 6. Loss of OTULIN enhances the formation of degradative compartments and autophagosomes.

A. Representative electron microscopy images of MZ-54 NHT and *OTULIN* KO cells treated with LOP (17.5 µM) for 16 h. A, autophagosome; D, degradative compartment; M, mitochondria; N, nucleus; PM, plasma membrane; asterisk, rough-ER fragment. Scale bar: 1 µm. **B.** Quantification of the average number of degradative compartments (DGCs) and autophagosomes per cell section. Mean and SEM are shown. ** $p < 0.01$, *** $p < 0.001$, **** $p < 0.0001$, ns: not significant. Statistical significance was determined with two-way ANOVA followed by Tukey's multiple comparisons tests.

5.1.3 Autophagosome content profiling reveals OTULIN-dependent autophagy cargo proteins

To identify OTULIN-dependent autophagy cargo proteins, an APEX2-based autophagosome content profiling was performed. This technique was developed by Zellner *et al*. [327] and combines APEX2 proximity labeling and autophagosome enrichment with proteomics to identify autophagy cargo proteins. Cells expressing LC3 (or another autophagy-related protein like p62, TAX1BP1 etc.) fused to the peroxidase APEX2 are treated with biotin-phenol and pulsed with H_2O_2 to trigger biotinylation of proteins in proximity to APEX2 fusions. This is followed by proteinase K treatment which digests all proteins that are not protected by intact membranes and streptavidin pulldown to enrich biotinylated proteins in autophagosomes. These enriched proteins can then be analyzed by quantitative proteomics or other approaches such as Western blot analysis, immunofluorescence or electron microscopy [327]. First, myc-APEX2-LC3B-expressing *OTULIN* KO and control MZ-54 cells were generated and successful myc-APEX2-LC3B

overexpression was verified (**Figure 7A**). Treatment of these cells with proteinase K confirmed partial protection of biotinylated proteins, myc-APEX2-LC3B and endogenous p62 from degradation, whereas addition of the membrane-lysing agent Triton X-100 resulted in almost complete clearance of these proteins (**Figure 7B**). The ATG8-interacting protein Kelch repeat and BTB domain-containing protein 7 (KBTBD7) was used as negative control and degraded in the presence of proteinase K only (**Figure 7B**), as described earlier [338]. Furthermore, LOP-induced autophagy decreased the levels of biotinylated proteins (**Figure 7C**), whereas autophagy inhibition with BafA1 increased the levels of biotinylated proteins (**Figure 7D**).

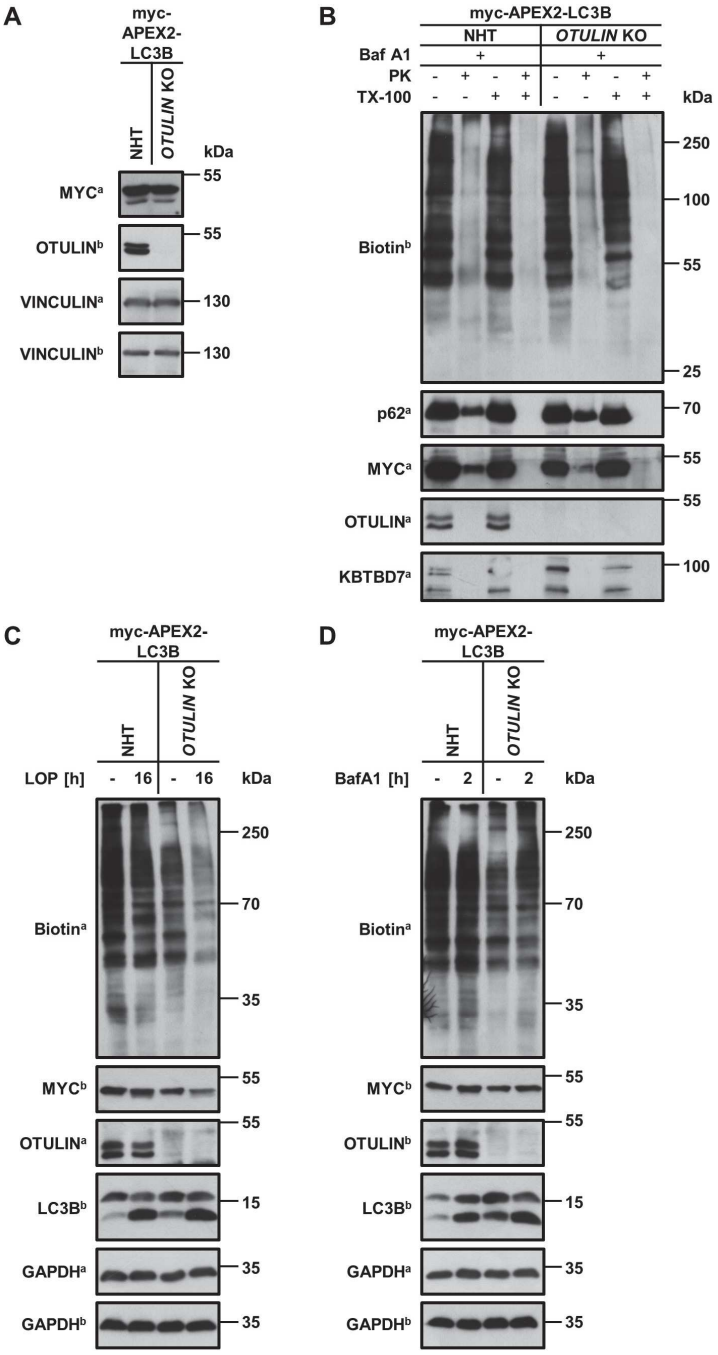

Figure 7. Generation and validation of myc-APEX2-LC3B-expressing MZ-54 cells.

Figure 7. Continued.

A. Western blot analysis of MYC and OTULIN expression in myc-APEX2-LC3B-expressing MZ-54 NHT and *OTULIN* KO GBM cells. Vinculin was used as loading control. Representative blots of two independent experiments are shown. **B.** Western blot analysis of Biotin, p62, MYC, OTULIN and KBTBD7 expression in myc-APEX2-LC3B-expressing MZ-54 NHT and *OTULIN* KO GBM cells, treated with BafA1 (200 nM) for 2 h, homogenized and incubated with Proteinase K (PK), Triton X-100 (TX-100) or both. KBTBD7 was used as negative control. Representative blots of two independent experiments are shown. **C.** Western blot analysis of Biotin, MYC, OTULIN and LC3B expression in myc-APEX2-LC3B-expressing MZ-54 NHT and *OTULIN* KO GBM cells, treated with LOP (17.5 µM) for 16 h. GAPDH was used as loading control. Representative blots of at least two independent experiments are shown. **D.** Idem as C, but myc-APEX2-LC3B-expressing MZ-54 NHT and *OTULIN* KO GBM cells were treated with BafA1 (200 nM) for 2 h. GAPDH was used as loading control. Representative blots of at least two independent experiments are shown.

After validation of the myc-APEX2-LC3B-expressing cells, biotinylated protein fractions from BafA1- and LOP-treated *OTULIN* KO and control cells were analyzed by MS (**Figure 8A and 8B**). This revealed striking differences in the autophagic cargo candidates upon loss of OTULIN. Of note, among the significantly up- and downregulated proteins in the autophagosomes of *OTULIN* KO cells were several proteins which are known to regulate autophagy (e.g. TAX1BP1, galectin-3), but also organelle-specific (e.g. TOMM40, VDAC3) and endosomal and lysosomal (e.g. RAB11A) proteins were identified (**Figure 8A and 8B**).

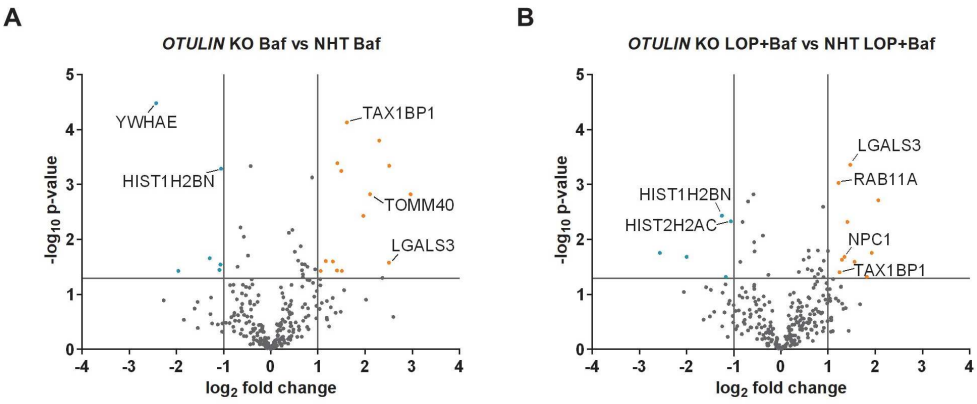

Figure 8. APEX2-based autophagosome content profiling identifies OTULIN-dependent autophagy cargo candidates.

A. Volcano plot of significantly up- and downregulated (orange and blue, respectively) autophagosome enriched cargo candidates from myc-APEX2-LC3B-expressing MZ-54 NHT and *OTULIN* KO cells treated with BafA1 (200 nM) for 2 h, followed by biotinylation, proteinase K digest, streptavidin pulldown and mass spectrometry. Data are derived from four replicates. $p \leq 0.05$. **B.** Idem as A, but myc-APEX2-LC3B-expressing MZ-54 NHT and *OTULIN* KO cells were treated with LOP (17.5 µM) for 16 h plus BafA1 (200 nM) for the last 2 h. Statistical significance was determined with student's t-test.

To validate the MS results, the cargo candidates TAX1BP1, TOMM40 and galectin-3 were selected and proteinase K protection assays verified that these proteins are partly

protected from digestion (**Figure 9A**). Furthermore, abundance changes of these cargo candidates after BafA1 treatment were investigated. The BafA1-mediated increase in TAX1BP1 expression was higher upon loss of OTULIN compared to control cells (**Figure 9B**). However, despite being membrane-protected, TOMM40 and galectin-3 did not substantially accumulate in *OTULIN* KO after BafA1 treatment (**Figure 9B**). One possible explanation for this could be that slower translation or transcription rates of these proteins prevent significant increases in response to BafA1 treatment.

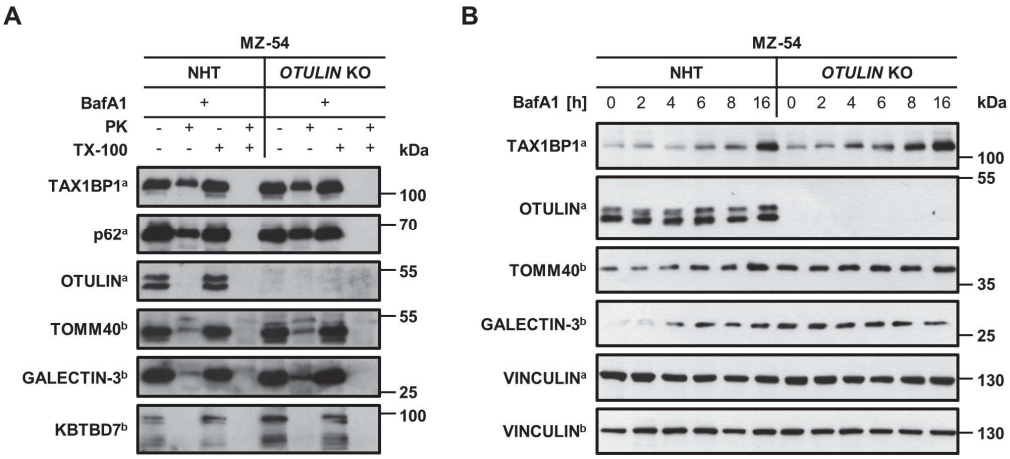

Figure 9. Validation of selected cargo candidates.

A. Western blot analysis of TAX1BP1, p62, OTULIN, TOMM40 and galectin-3 expression in MZ-54 NHT and *OTULIN* KO GBM cells, treated with BafA1 (200 nM) for 2 h, homogenized and incubated with Proteinase K (PK), Triton X-100 (TX-100) or both. KBTBD7 was used as negative and p62 as positive control. Representative blots of two independent experiments are shown. **B.** Western blot analysis of TAX1BP1, OTULIN, TOMM40 and galectin-3 expression in MZ-54 NHT and *OTULIN* KO GBM cells, treated with BafA1 (200 nM) for the indicated time points. Vinculin was used as loading control. Representative blots of two independent experiments are shown.

TAX1BP1 is an autophagy receptor which is involved in different forms of selective autophagy such as xenophagy, aggrephagy, mitophagy and lysophagy [108,113,114,339]. The enhanced BafA1-mediated accumulation of TAX1BP1 in OTULIN-deficient cells indicates that autophagic degradation of TAX1BP1 is regulated in an OTULIN-dependent manner. To address this, translation was blocked with cycloheximide (CHX) and TAX1BP1 protein stability was followed over time in *OTULIN* KO and control cells. The decrease in TAX1BP1 protein levels was faster in OTULIN-depleted cells (**Figure 10A**) and this could be partially rescued with BafA1 (**Figure 10B**), suggesting that turnover of TAX1BP1 via autophagy depends on OTULIN.

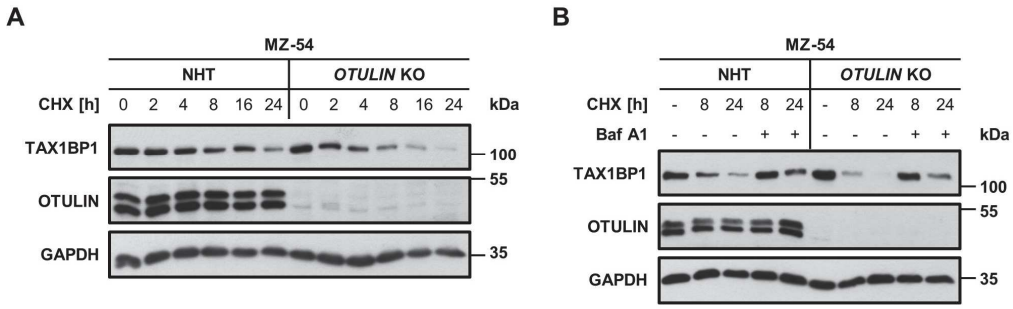

Figure 10. TAX1BP1 degradation is regulated in an OTULIN-dependent manner.

A. Western blot analysis of TAX1BP1 and OTULIN expression in MZ-54 NHT and *OTULIN* KO GBM cells, treated with cycloheximide (CHX, 10 µg/ml) for the indicated time points. GAPDH was used as loading control. Representative blots of two independent experiments are shown. **B.** Idem as A, but MZ-54 NHT and *OTULIN* KO GBM cells were pre-treated with BafA1 (200 nM) for 30 min before addition of CHX (10 µg/ml) for 8 and 24 h. GAPDH was used as loading control. Representative blots of two independent experiments are shown.

5.2 Role of OTULIN and M1 poly-Ub in aggrephagy

5.2.1 Loss of OTULIN enhances the formation of M1 poly-Ub-positive protein aggregates in response to proteotoxic stress

In addition to its role in different forms of selective autophagy (e.g. lysophagy, aggrephagy, mitophagy) [108,113,114] the autophagy receptor TAX1BP1 was recently shown to bind M1 poly-Ub chains in dependence of its Ub-binding zinc finger domains 1 and 2 (UBZ1/2), thereby recruiting the autophagy machinery and promoting lysosomal turnover of M1 ubiquitinated proteins [340]. The autophagosome content profiling revealed an enrichment of TAX1BP1 in the autophagosomes of OTULIN-deficient cells (**Figure 8**) and follow-up experiments indicated an OTULIN-dependent regulation of TAX1BP1 degradation via autophagy (**Figure 10**). This raises the possibility that in addition to their function in xenophagy [111], OTULIN and M1 poly-Ub might also affect other selective autophagy pathways. Since LUBAC is known to assemble M1 poly-Ub at misfolded proteins [260], a potential role of OTULIN and M1 poly-Ub in the regulation of aggrephagy was investigated. Protein aggregation was induced with the translation inhibitor puromycin which leads to premature release of the nascent peptide chain from the ribosome and accumulation of misfolded proteins, referred to as defective ribosomal products (DRiPs) [113,126]. Formation of M1 poly-Ub- and K63 poly-Ub-labeled puncta in response to puromycin treatment was greatly enhanced upon loss of OTULIN (**Figure 11A and 11B**). Almost all of the M1 poly-Ub puncta were cleared 16 h after puromycin washout, but this could be partially blocked by addition of BafA1 (**Figure 11C**), indicating that degradation of M1 poly-Ub-labeled puncta is mediated via autophagy.

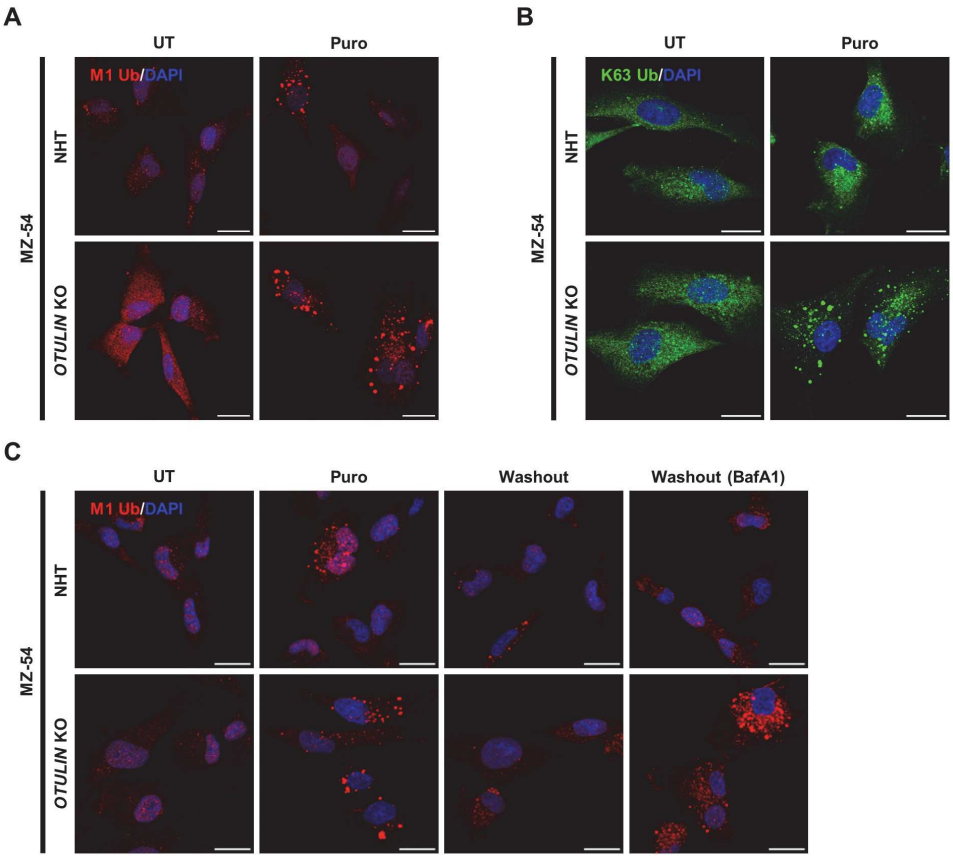

Figure 11. Puromycin-induced formation of M1 poly-Ub- and K63 poly-Ub-positive puncta is enhanced in OTULIN-deficient cells.

A. Representative immunofluorescence staining of M1 poly-Ub in MZ-54 NHT and *OTULIN* KO GBM cells, treated with puromycin (Puro, 10 µg/ml) for 4 h. Scale bar: 20 µm. **B.** Idem as A, but cells were stained for K63 poly-Ub. Scale bar: 20 µm. **C.** Idem as A, but treatment with puro (10 µg/ml) for 6 h was followed by puro washout for 16 h with or without BafA1 (200 nM). Scale bar: 20 µm.

Western blot analysis of puromycin-treated cells also revealed an accumulation of M1 poly-Ub-modified proteins in the NP40-insoluble fraction of *OTULIN* KO cells and clearance of these insoluble proteins was prevented by BafA1 or the proteasome inhibitor MG132 (**Figure 12**). Furthermore, puromycin treatment resulted in a substantial reduction of soluble TAX1BP1 and p62 in OTULIN-deficient cells, with a concomitant increase of p62 in the insoluble fraction. Puromycin washout decreased the levels of insoluble p62 and this was blocked by BafA1 and MG132 (**Figure 12**).

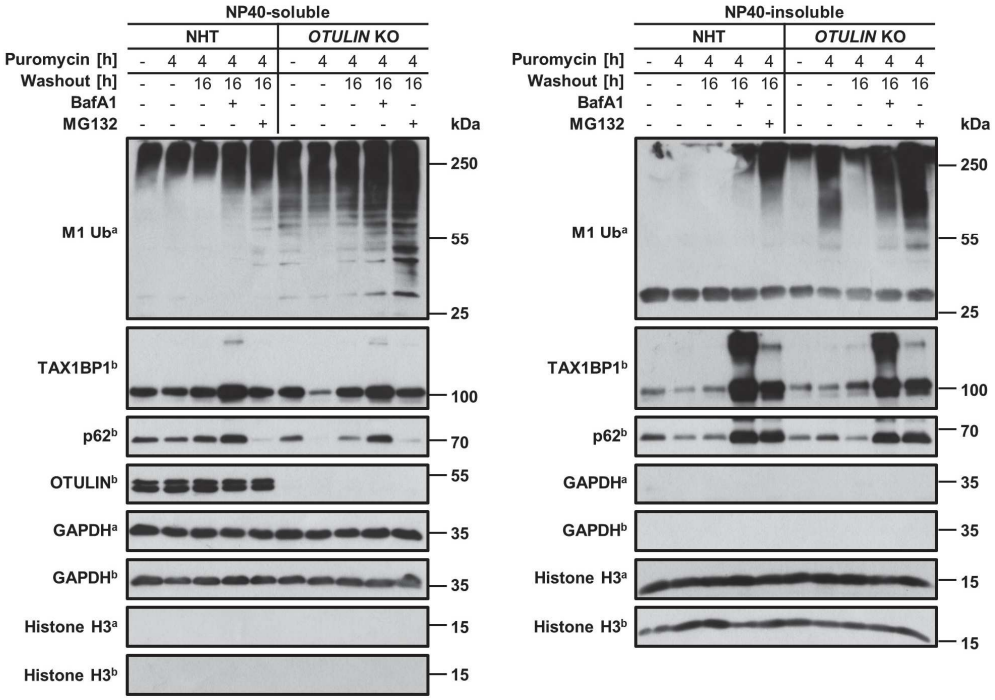

Figure 12. Puromycin induces accumulation of insoluble M1 poly-Ub-modified proteins upon loss of OTULIN.

Western blot analysis of M1 poly-Ub, TAX1BP1, p62 and OTULIN expression in the NP40-soluble and NP40-insoluble fractions of MZ-54 NHT and *OTULIN* KO GBM cells, treated with puromycin (10 µg/ml) for 4 h, followed by puromycin washout for 16 h with or without BafA1 (200 nM) and MG132 (1 µM) as indicated. GAPDH and histone H3 were used as loading controls for the NP40-soluble and -insoluble fractions, respectively. Representative blots of two independent experiments are shown.

Since aggrephagy receptors are known to bind to ubiquitinated protein aggregates [126], localization of p62 and TAX1BP1 after puromycin treatment was investigated. Both p62 and TAX1BP1 formed puncta in response to puromycin treatment which colocalized with M1 poly-Ub foci (**Figure 13A and 13B**). Formation of p62/M1 poly-Ub- or TAX1BP1/M1 poly-Ub-positive puncta was enhanced upon loss of OTULIN, but 16 h after puromycin washout, almost all of these puncta were effectively cleared (**Figure 13A and 13B**). Together, these results suggest that p62 and TAX1BP1 are recruited to M1 poly-Ub-positive structures in response to puromycin-induced proteotoxic stress in an OTULIN-dependent manner.

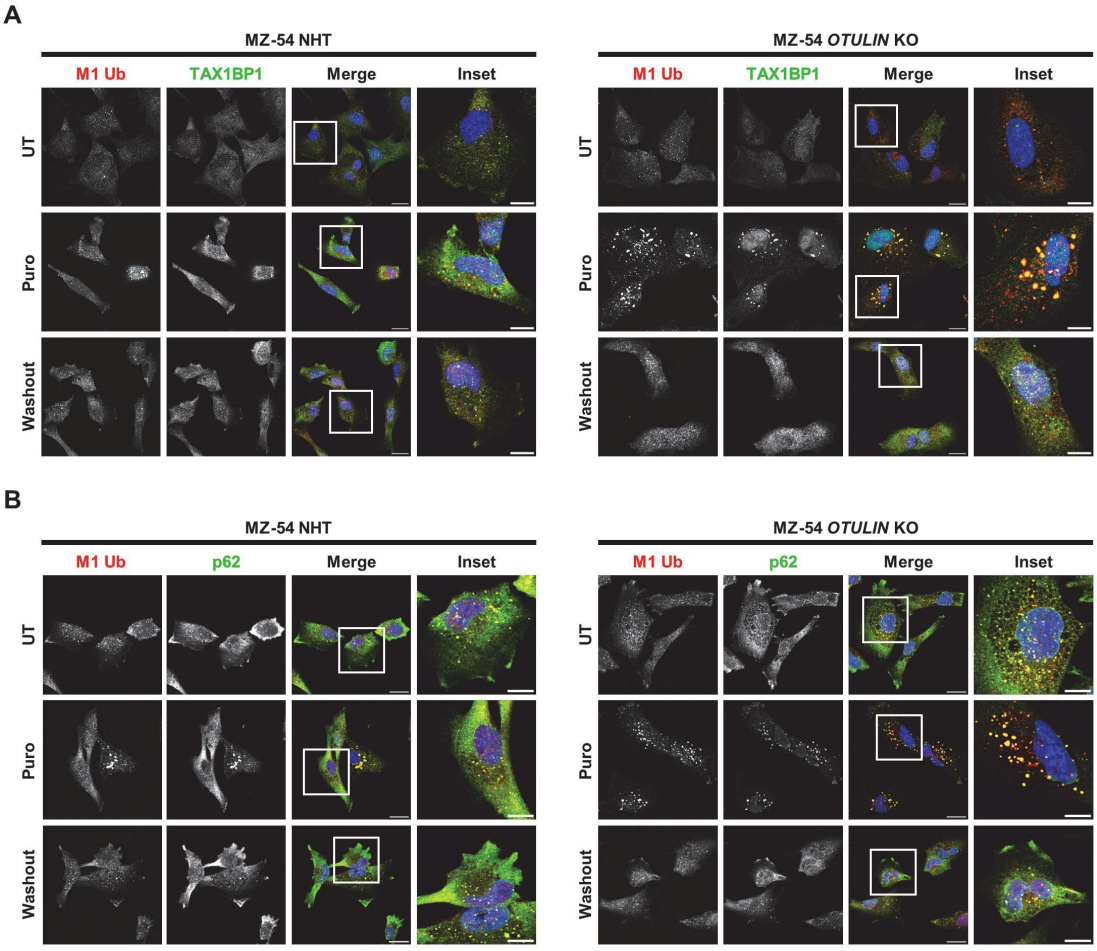

Figure 13. TAX1BP1 and p62 colocalize with M1 Ub-labeled puncta in response to puromycin-induced proteotoxic stress.

A. Representative immunofluorescence staining of M1 poly-Ub and TAX1BP1 in MZ-54 NHT and *OTULIN* KO GBM cells, treated with puro (10 µg/ml) for 4 h, followed by puro washout for 16 h. Scale bar: 20 µm (10 µm for insets). **B.** Idem as A, but after treatment with puro (10 µg/ml) for 4 h and puro washout for 16 h, MZ-54 NHT and *OTULIN* KO GBM cells were stained for M1 poly-Ub and p62. Scale bar: 20 µm (10 µm for insets).

5.2.2 Formation and clearance of puromycin-labeled peptides is regulated in an OTULIN-dependent manner

To further address a potential role of OTULIN on the formation and turnover of protein aggregates, cells were exposed to puromycin with or without cycloheximide to inhibit synthesis of new proteins, followed by puromycin washout to assess loss of protein aggregates over time. The formation of puromycin-labeled peptides was greatly enhanced upon loss of OTULIN compared to control cells (**Figure 14**). Furthermore, the level of puromycin-labeled peptides after 22 h puromycin washout were higher in OTULIN-deficient cells (**Figure 14**). One explanation for this could be the overall higher amounts of puromycin-labeled peptides in *OTULIN* KO cells, but it might also reflect delayed clearance of protein aggregates after puromycin treatment.

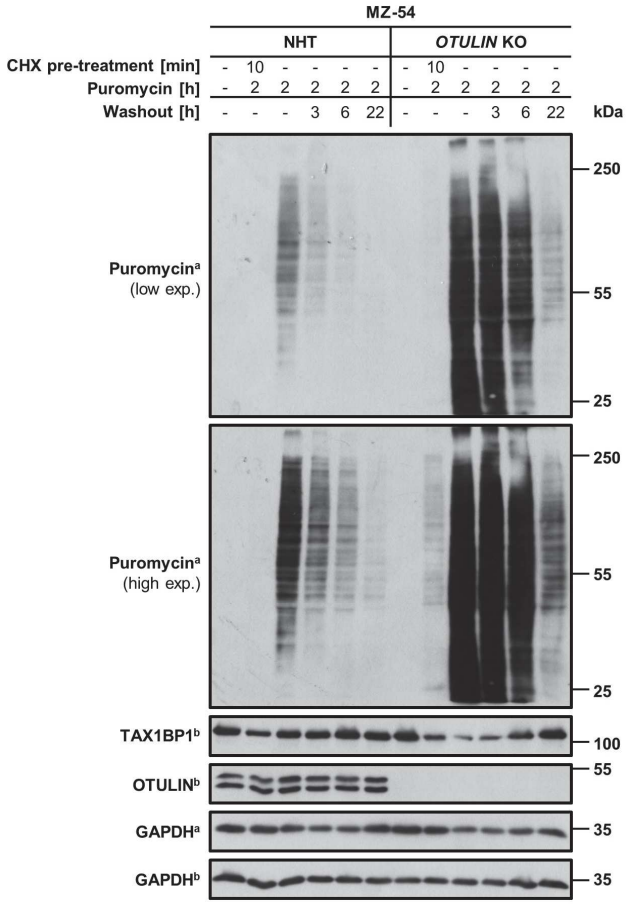

Figure 14. Loss of OTULIN delays clearance of puromycin-labeled peptides.
Western blot analysis of puromycin, TAX1BP1 and OTULIN expression in MZ-54 NHT and *OTULIN* KO GBM cells, pre-treated with cycloheximide (CHX, 10 µg/ml) as indicated, followed by treatment with puromycin (10 µg/ml) for 2 h and puromycin washout for the indicated time points. GAPDH was used as loading control. Representative blots of two independent experiments are shown.

Since ubiquitination is known to mark protein aggregates for lysosomal degradation [126], ubiquitination was inhibited with TAK-243, a small molecule inhibitor of the E1 Ub activating enzyme [341]. While TAK-243 had no effect on the formation of puromycin-labeled peptides, it effectively blocked the clearance of the insoluble peptides after puromycin washout and this effect was more prominent in OTULIN-deficient cells (**Figure 15**). In addition, TAK-243 also increased the amount of insoluble TAX1BP1 after puromycin washout in *OTULIN* KO cells and, to a lesser extent, in control cells (**Figure 15**). Together, these results confirm that the clearance of puromycin-labeled protein aggregates and the autophagy receptor TAX1BP1 is Ub-dependent.

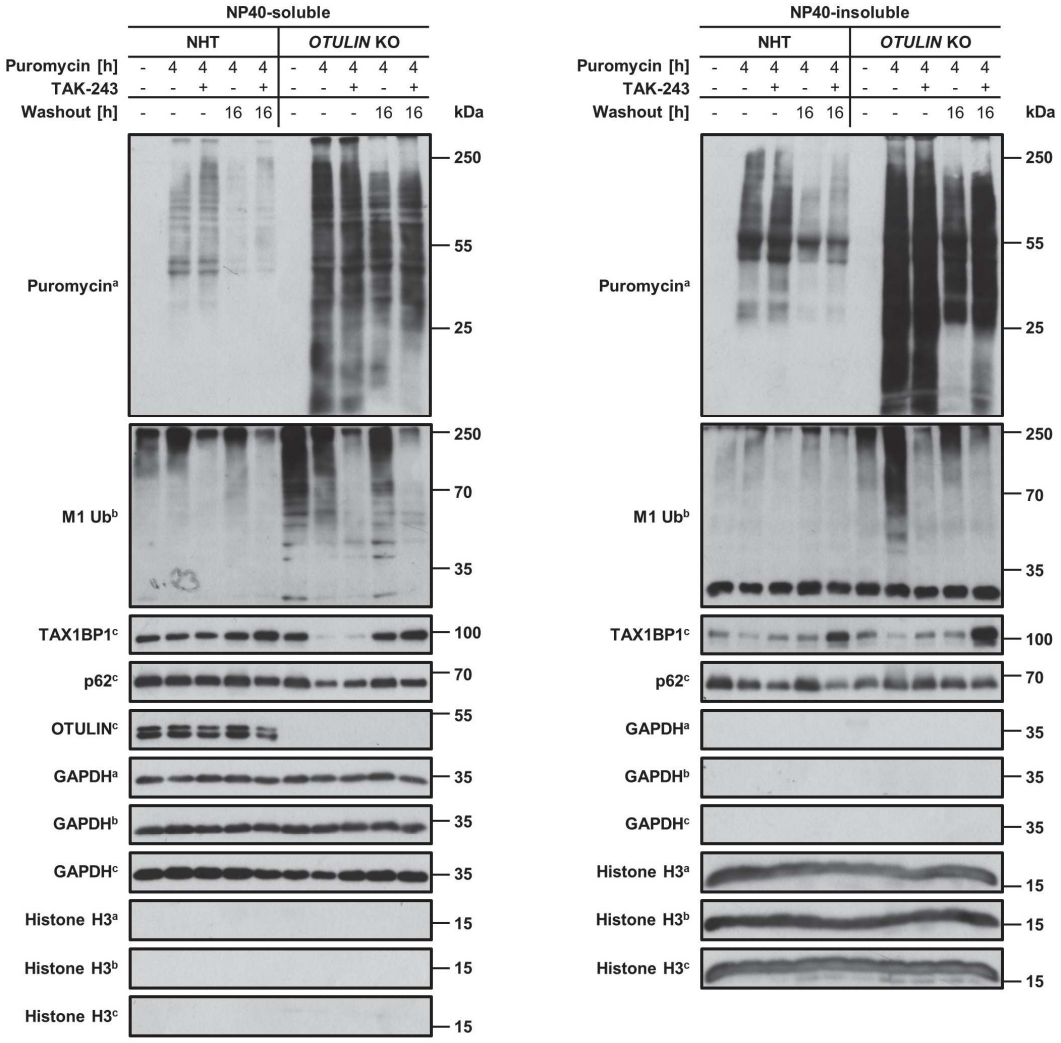

Figure 15. Clearance of puromycin-labeled peptides is ubiquitin-dependent.

Western blot analysis of puromycin, M1 poly-Ub, TAX1BP1, p62 and OTULIN expression in the NP40-soluble and NP40-insoluble fractions of MZ-54 NHT and *OTULIN* KO GBM cells, pre-treated with TAK-243 (200 nM) for 1 h, followed by treatment with puromycin (10 µg/ml) for 4 h and puromycin washout for 16 h. GAPDH and histone H3 were used as loading controls for the NP40-soluble and -insoluble fractions, respectively. Representative blots of two independent experiments are shown.

5.3 Role of OTULIN and M1 poly-Ub in lysophagy

5.3.1 M1 poly-Ub accumulates at damaged lysosomes

In addition to enrichment of TAX1BP1 in the autophagosomes of *OTULIN* KO cells, galectin-3, which serves important functions in lysophagy, was also upregulated, indicating a potential role of OTULIN and M1 poly-Ub in the response to lysosomal damage and the regulation of lysophagy. To address this, LMP and lysophagy was induced with the lysosomotropic drug LLOMe. LLOMe treatment increased M1 poly-Ub levels and this was particularly prominent upon loss of OTULIN. In addition, LLOMe-induced galectin-3 degradation and LC3 lipidation was enhanced in OTULIN-deficient

cells (**Figure 16A**). Immunofluorescence staining revealed that LLOMe-induced lysosomal damage triggers accumulation of M1 poly-Ub in punctate structures which colocalize with the lysosomal membrane protein LAMP1 (**Figure 16B**).

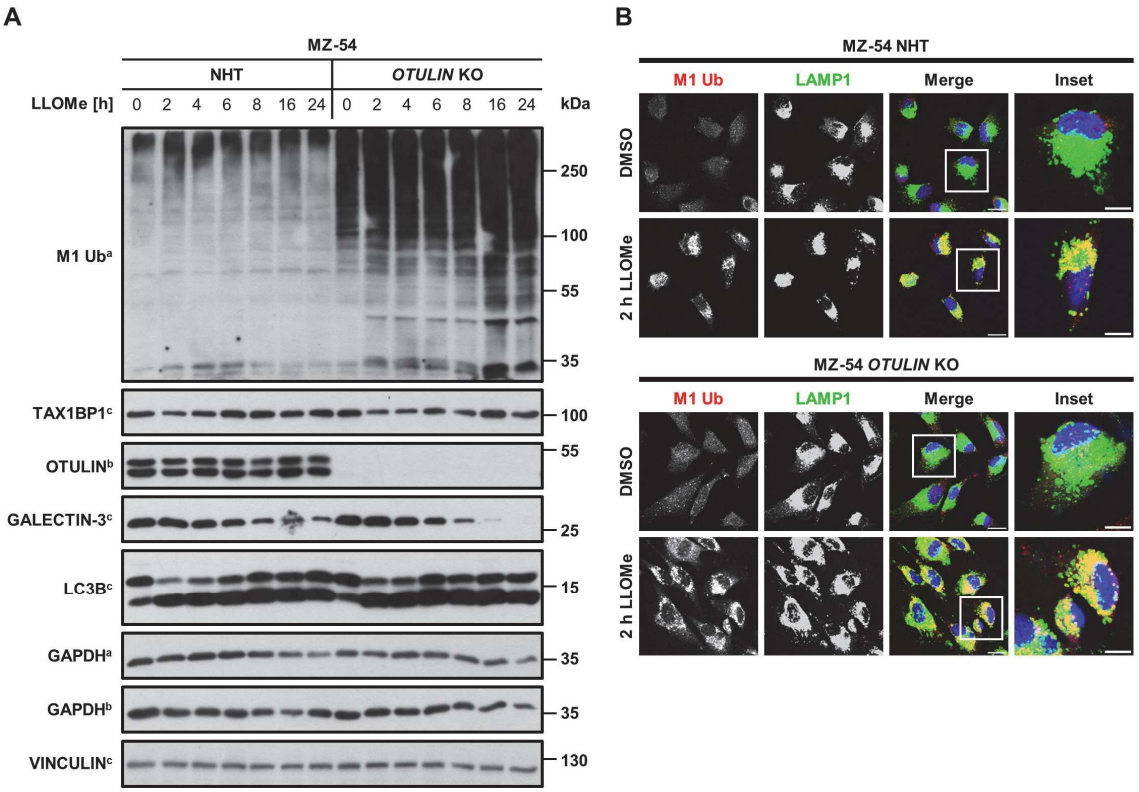

Figure 16. M1 poly-Ub accumulates at damaged lysosomes.

A. Western blot analysis of M1 poly-Ub, TAX1BP1, OTULIN, galectin-3 and LC3B expression in MZ-54 NHT and *OTULIN* KO GBM cells, treated with LLOMe (500 µM) for the indicated time points. GAPDH and vinculin were used as loading controls. Representative blots of two independent experiments are shown. **B.** Representative immunofluorescence staining of M1 poly-Ub and LAMP1 in MZ-54 NHT and *OTULIN* KO GBM cells, treated with LLOMe (500 µM) for 2 h. Scale bar: 20 µm (10 µm for insets).

5.3.2 TAX1BP1 localizes to M1 poly-Ub modified lysosomes in response to lysosomal damage

Ubiquitination of damaged lysosomes recruits the autophagy machinery including ATG8 proteins and selective autophagy receptors such as p62 or TAX1BP1 [100,108]. In agreement with this, LLOMe treatment induced formation of TAX1BP1 puncta at M1 poly-Ub-positive structures (**Figure 17A**), and TAX1BP1 puncta also partially colocalized with LAMP1 (**Figure 17B**).

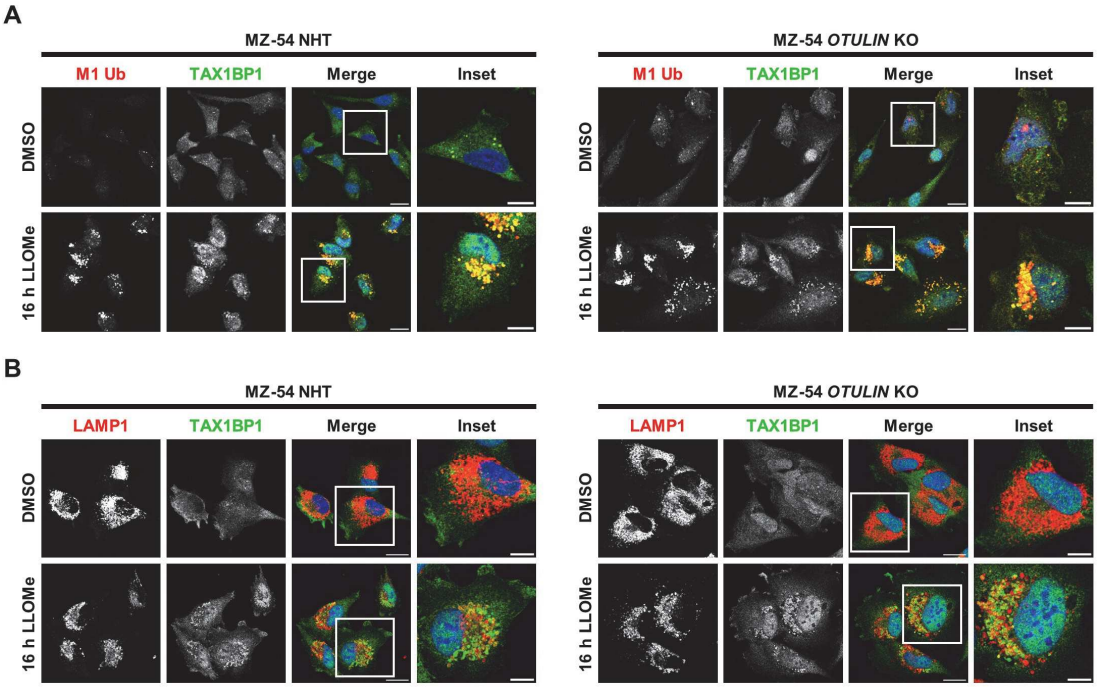

Figure 17. TAX1BP1 is recruited to damaged lysosomes and colocalizes with LLOMe-induced M1 poly-Ub puncta.

A. Representative immunofluorescence staining of M1 poly-Ub and TAX1BP1 in MZ-54 NHT and *OTULIN* KO GBM cells treated with LLOMe (500 µM) for 16 h. Scale bar: 20 µm (10 µm for insets). **B.** Idem as A, but MZ-54 NHT and *OTULIN* KO GBM cells treated with LLOMe (500 µM) for 16 h were stained for LAMP1 and TAX1BP1. Scale bar: 20 µm (10 µm for insets).

5.3.3 Effect of OTULIN depletion on the lysophagic flux

LMP induces the recruitment of galectins to damaged lysosomes where they bind to exposed intraluminal glycans and initiate lysophagy [95]. Immunofluorescence staining confirmed LLOMe-induced formation of galectin-3 puncta which partially colocalized with M1 poly-Ub (**Figure 18A**). To address if the clearance of galectin-3 puncta (as readout for the lysophagic flux) is affected by loss of OTULIN, co-staining of galectin-3 and LAMP1 was performed after LLOMe treatment and washout (**Figure 18B**). However, the degradation of galectin-3 puncta was only slightly enhanced in OTULIN-depleted cells (**Figure 18B and 18C**).

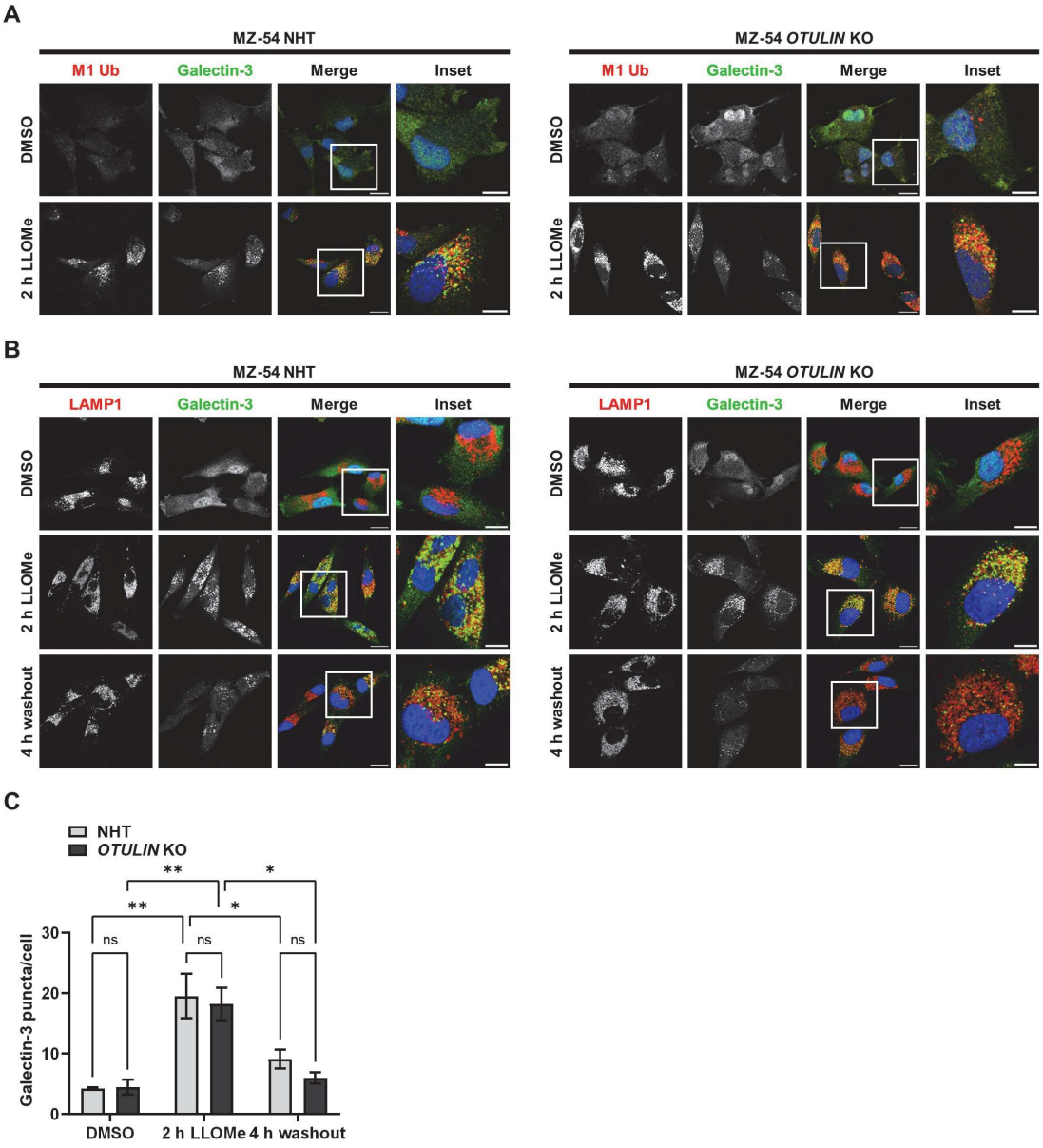

Figure 18. Clearance of galectin-3 puncta after lysosomal damage might be affected by loss of OTULIN.

A. Representative immunofluorescence staining of M1 poly-Ub and galectin-3 in MZ-54 NHT and *OTULIN* KO GBM cells, treated with LLOMe (500 µM) for 2 h. Scale bar: 20 µm (10 µm for insets). **B.** Idem as A, but after treatment of MZ-54 NHT and *OTULIN* KO GBM cells with LLOMe (500 µM) for 2 h, LLOMe was washed out and cells were incubated in fresh medium for additional 4 h and stained for LAMP1 and galectin-3. Scale bar: 20 µm (10 µm for insets). **C.** Quantification of galectin-3 puncta. Mean and SEM of 38 cells from three independent experiments are shown. * $p < 0.05$, ** $p < 0.01$, ns: not significant. Statistical significance was determined with two-way ANOVA followed by Tukey's multiple comparisons tests.

5.3.4 OTULIN and M1 poly-Ub control TBK1 activation after lysosomal damage

TBK1 is known to be activated in response to lysosomal damage through phosphorylation on serine 172. Phosphorylated TBK1 localizes to galectin-3-positive

puncta and inhibition of TBK1 phosphorylation decreases the lysophagic flux [108]. Therefore, TBK1 phosphorylation was analyzed after LLOMe-induced lysophagy. LLOMe treatment enhanced TBK1 phosphorylation and this effect was more pronounced in OTULIN-deficient cells (**Figure 19A**). Furthermore, inhibition of LUBAC activity with the small molecule inhibitor HOIPIN-8 partially prevented LLOMe-triggered TBK1 phosphorylation (**Figure 19B**). Together, these results suggest that TBK1 activation at damaged lysosomes is dependent on M1 poly-Ub and OTULIN.

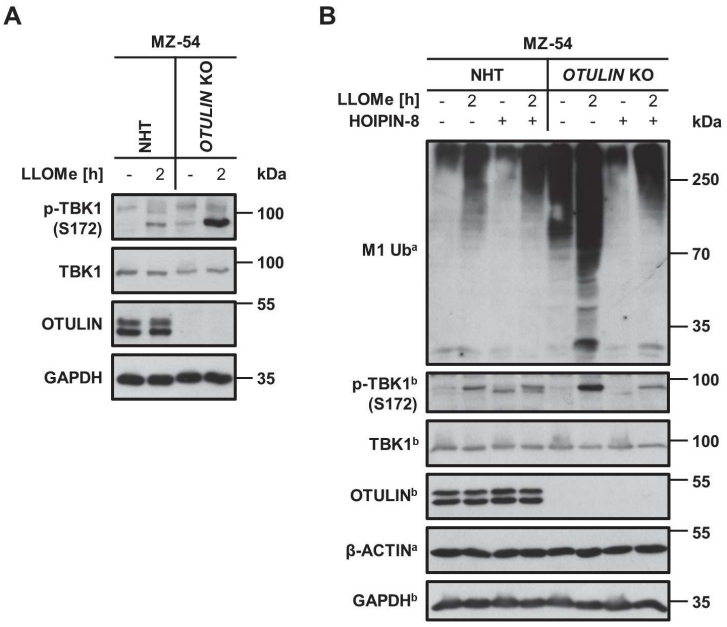

Figure 19. Loss of OTULIN increases TBK1 phosphorylation in response to lysosomal damage.

A. Western blot analysis of p-TBK1 (S172), TBK1 and OTULIN expression in MZ-54 NHT and *OTULIN* KO GBM cells treated with LLOMe (500 µM) for 2 h. GAPDH was used as loading control. Representative blots of two independent experiments are shown. **B.** Idem as A, but MZ-54 NHT and *OTULIN* KO GBM cells were pre-treated with HOIPIN-8 (30 µM) for 24 h before addition of LLOMe (500 µM) for 2 h. β-Actin and GAPDH were used as loading controls. Representative blots of two independent experiments are shown.

5.3.5 OTULIN depletion does not affect nuclear translocation of TFEB in response to lysosomal damage

Under basal conditions, the transcription factor TFEB is held inactive through mTORC1-mediated phosphorylation and sequestration in the cytosol by 14-3-3 proteins [63,64]. Lysosomal damage inhibits mTORC1, thereby inducing dephosphorylation of TFEB, release from 14-3-3 proteins and translocation in the nucleus where it activates the expression of genes implicated in autophagy and lysosomal biogenesis [65]. Therefore, a potential role of OTULIN in the regulation of TFEB activation after lysosomal damage was investigated. Western blot analysis revealed that LLOMe treatment induced a shift of the TFEB band in whole cell lysates (WCL) (**Figure 20A**), indicating dephosphorylation

of TFEB. In addition, nuclear fractionation confirmed translocation of TFEB in the nucleus after LLOMe treatment, but there were no differences between OTULIN-depleted cells and control cells (**Figure 20B**). Thus, OTULIN does not seem to affect nuclear translocation of TFEB in response to lysosomal damage.

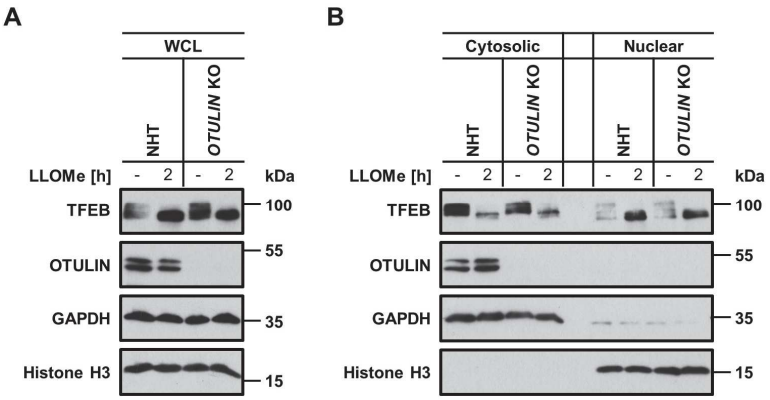

Figure 20. LLOMe-induced nuclear translocation of TFEB is not affected by loss of OTULIN expression.

A. Western blot analysis of TFEB and OTULIN expression in whole cell lysates (WCL) of MZ-54 NHT and *OTULIN* KO GBM cells treated with LLOMe (500 µM) for 2 h. GAPDH and Histone H3 were used as loading controls. Representative blots of two independent experiments are shown. **B.** Idem as A, but protein expression was analyzed in the cytosolic and nuclear fraction of MZ-54 NHT and *OTULIN* KO GBM cells treated with LLOMe (500 µM) for 2 h. GAPDH and Histone H3 were used as loading controls for the cytosolic and nuclear fraction, respectively. Representative blots of two independent experiments are shown.

5.3.6 Accumulation of M1 poly-Ub at damaged lysosomes induces local NF-κB activation

In xenophagy, M1 poly-Ub at the surface of bacteria creates a signaling platform for NEMO recruitment and local NF-κB activation in an OTULIN-dependent manner [111]. To investigate if M1 poly-Ub at damaged lysosomes serves similar functions, immunofluorescence staining of NEMO and M1 poly-Ub was performed after LLOMe-induced lysosomal damage. In OTULIN-deficient cells, LLOMe induced formation of NEMO-positive punctate structures which partially colocalized with M1 poly-Ub puncta (**Figure 21A and 21C**) and LAMP1 (**Figure 21B and 21D**).

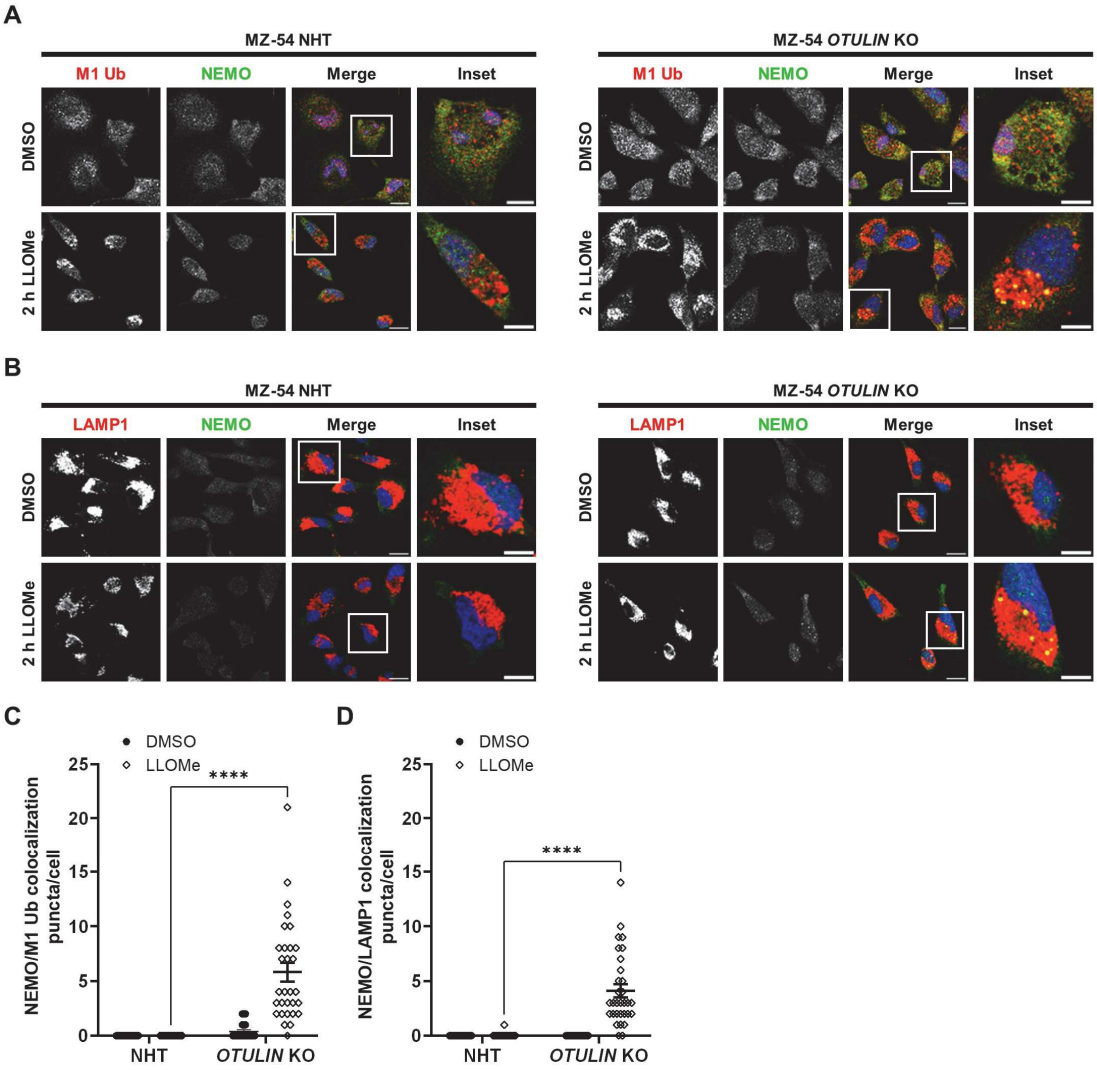

Figure 21. M1 poly-Ub accumulation at damaged lysosomes induces local recruitment of NEMO.

A. Representative immunofluorescence staining of M1 poly-Ub and NEMO in MZ-54 NHT and *OTULIN* KO GBM cells, treated with LLOMe (500 µM) for 2 h. Scale bar: 20 µm (10 µm for insets). **B.** Idem as A, but MZ-54 NHT and *OTULIN* KO GBM cells treated with LLOMe (500 µM) for 2 h were stained for LAMP1 and NEMO. Scale bar: 20 µm (10 µm for insets). **C.** Quantification of NEMO- and M1 poly-Ub-positive puncta from A. Mean and SEM of 30 cells from four independent microscopic views are shown. **** $p < 0.0001$. **D.** Quantification of NEMO- and LAMP1-positive puncta from B. Mean and SEM of 31 cells from four independent microscopic views are shown. **** $p < 0.0001$. Statistical significance in (**C**) and (**D**) was determined with two-way ANOVA followed by Tukey's multiple comparisons tests. This experiment was performed by M. Dietrich.

Furthermore, LLOMe treatment induced IKKα/β phosphorylation at M1 poly-Ub- (**Figure 22A and 22C**) and LAMP1-positive structures (**Figure 22B and 22D**) upon loss of OTULIN expression.

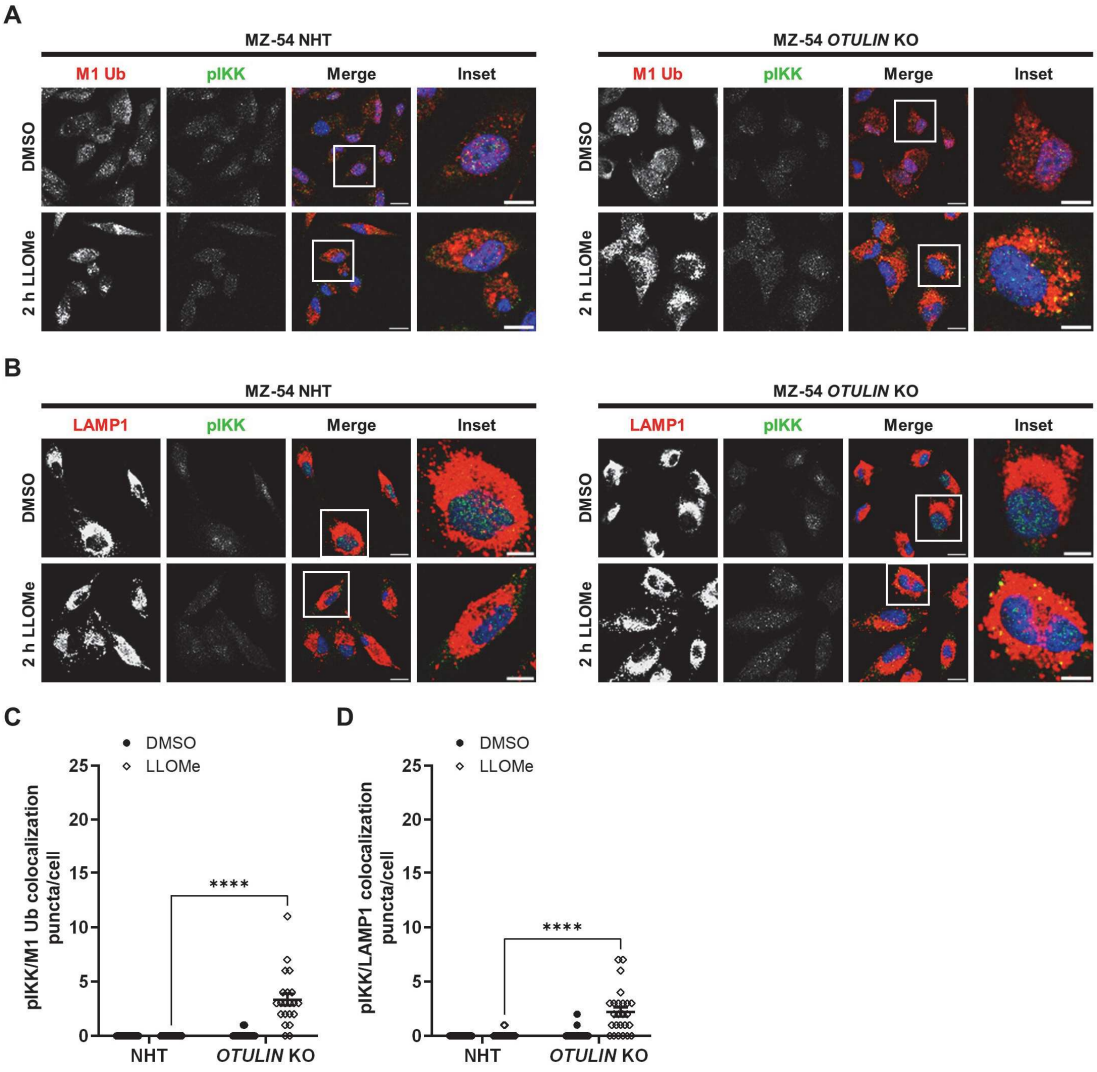

Figure 22. Lysosomal damage induces IKK phosphorylation on M1 poly-Ub-modified lysosomes in an OTULIN-dependent manner.

A. Representative immunofluorescence staining of M1 poly-Ub and pIKKα/β (Ser176/180) in MZ-54 NHT and *OTULIN* KO GBM cells, treated with LLOMe (500 µM) for 2 h. Scale bar: 20 µm (10 µm for insets). **B.** Idem as A, but MZ-54 NHT and *OTULIN* KO GBM cells treated with LLOMe (500 µM) for 2 h were stained for LAMP1 and pIKKα/β (Ser176/180). Scale bar: 20 µm (10 µm for insets). **C.** Quantification of M1 poly-Ub- and pIKKα/β (Ser176/180)-positive puncta from A. Mean and SEM of 21 cells from four independent microscopic views are shown. **** $p < 0.0001$. **D.** Quantification of NEMO- and pIKKα/β (Ser176/180)-positive puncta from B. Mean and SEM of 25 cells from four independent microscopic views are shown. **** $p < 0.0001$. Statistical significance in (**C**) and (**D**) was determined with two-way ANOVA followed by Tukey's multiple comparisons tests. This experiment was performed by M. Dietrich.

Inhibition of LUBAC activity with HOIPIN-8 greatly reduced the formation of NEMO puncta at M1 poly-Ub-modified lysosomes (**Figure 23A and 23B**), indicating a requirement of M1 poly-Ub for local recruitment of NEMO to damaged lysosomes.

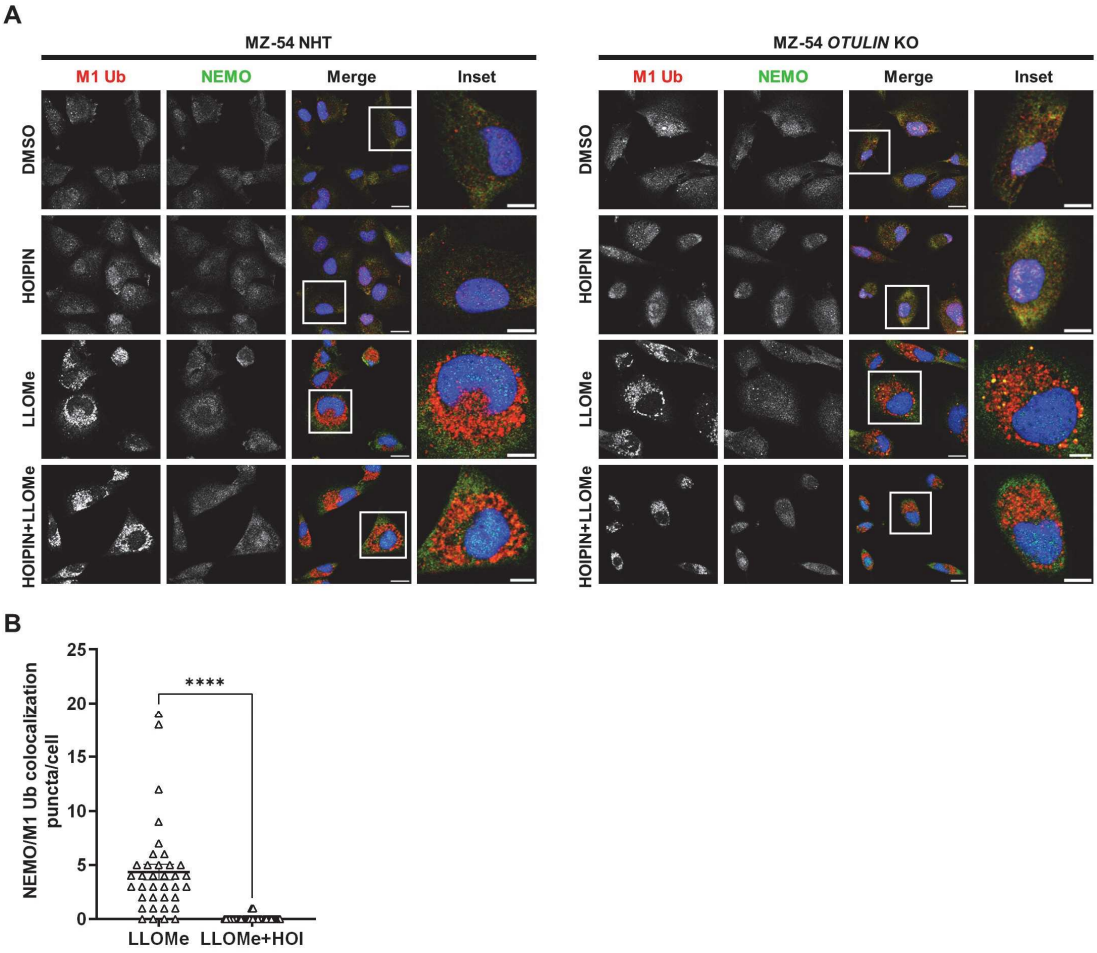

Figure 23. HOIPIN-8-mediated HOIP inhibition decreases LLOMe-induced formation of NEMO puncta.

A. Representative immunofluorescence staining of M1 poly-Ub and NEMO in MZ-54 NHT and *OTULIN* KO GBM cells, pre-treated with HOIPIN-8 (HOI, 30 µM) for 1 h before addition of LLOMe (500 µM) for 2 h. Scale bar: 20 µm (10 µm for insets). **B.** Quantification of NEMO- and M1 poly-Ub-positive puncta in *OTULIN* KO cells from A. Mean and SEM of 36 cells from at least five independent microscopic views are shown. **** $p < 0.0001$. Statistical significance was determined with unpaired t-test. This experiment was performed by M. Dietrich.

Similarly, inhibition of IKKβ with TPCA-1 almost completely prevented IKK phosphorylation at M1 poly-Ub-modified lysosomes in *OTULIN* KO cells (**Figure 24A and 24B**).

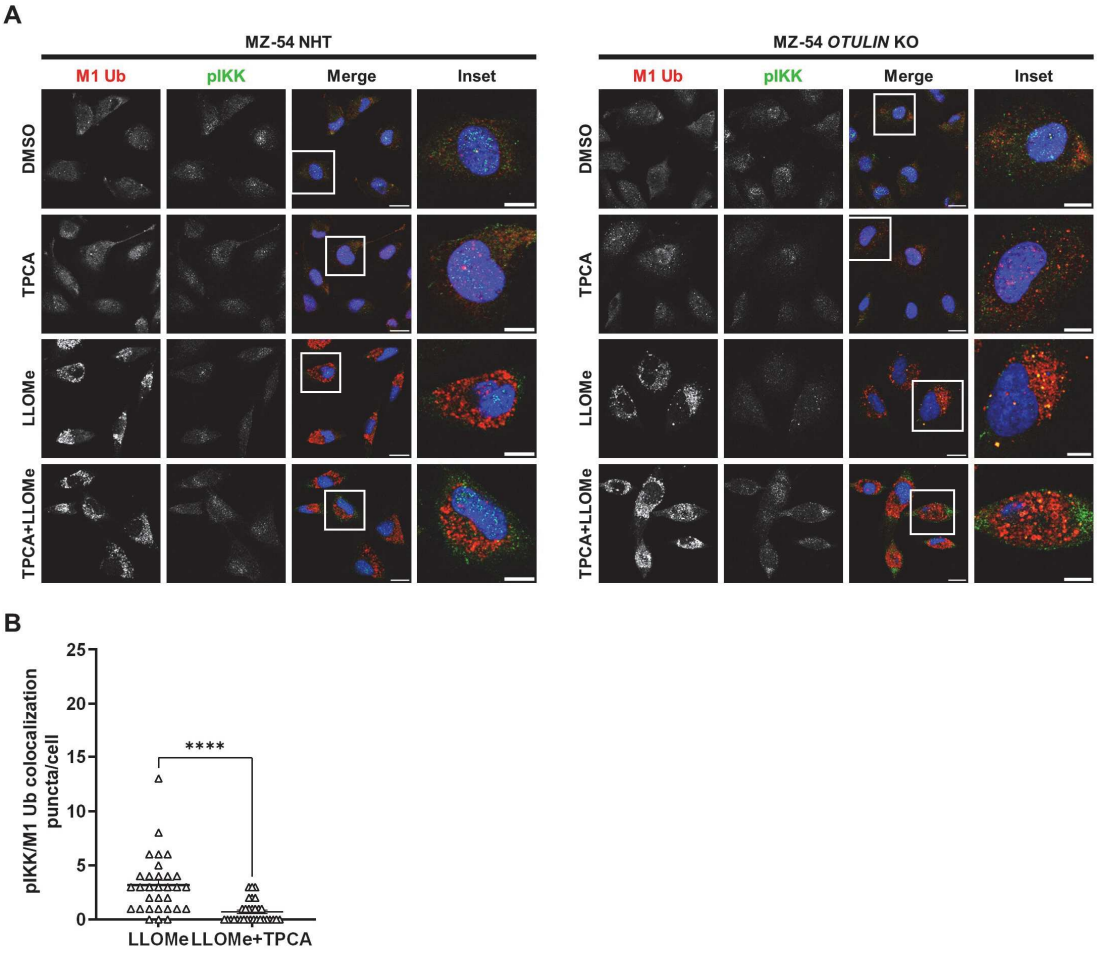

Figure 24. Inhibition of IKKβ with TPCA-1 prevents IKK phosphorylation at LLOMe-induced M1 poly-Ub puncta.

A. Representative immunofluorescence staining of M1 poly-Ub and pIKKα/β (Ser176/180) in MZ-54 NHT and *OTULIN* KO GBM cells, pre-treated with TPCA-1 (TPCA, 5 µM) for 1 h before addition of LLOMe (500 µM) for 2 h. Scale bar: 20 µm (10 µm for insets). **B.** Quantification of M1 poly-Ub- and pIKKα/β (Ser176/180)-positive puncta in *OTULIN* KO cells from A. Mean and SEM of 31 cells from at least six independent microscopic views are shown. **** $p < 0.0001$. Statistical significance was determined with unpaired t-test. This experiment was performed by M. Dietrich.

Local recruitment of NEMO and activation of IKK also prominently increased the expression of the NF-κB target genes *IL6* (**Figure 25A**), *IL8* (**Figure 25B**) and *TNFA* (**Figure 25C**) in OTULIN-deficient but not in control cells.

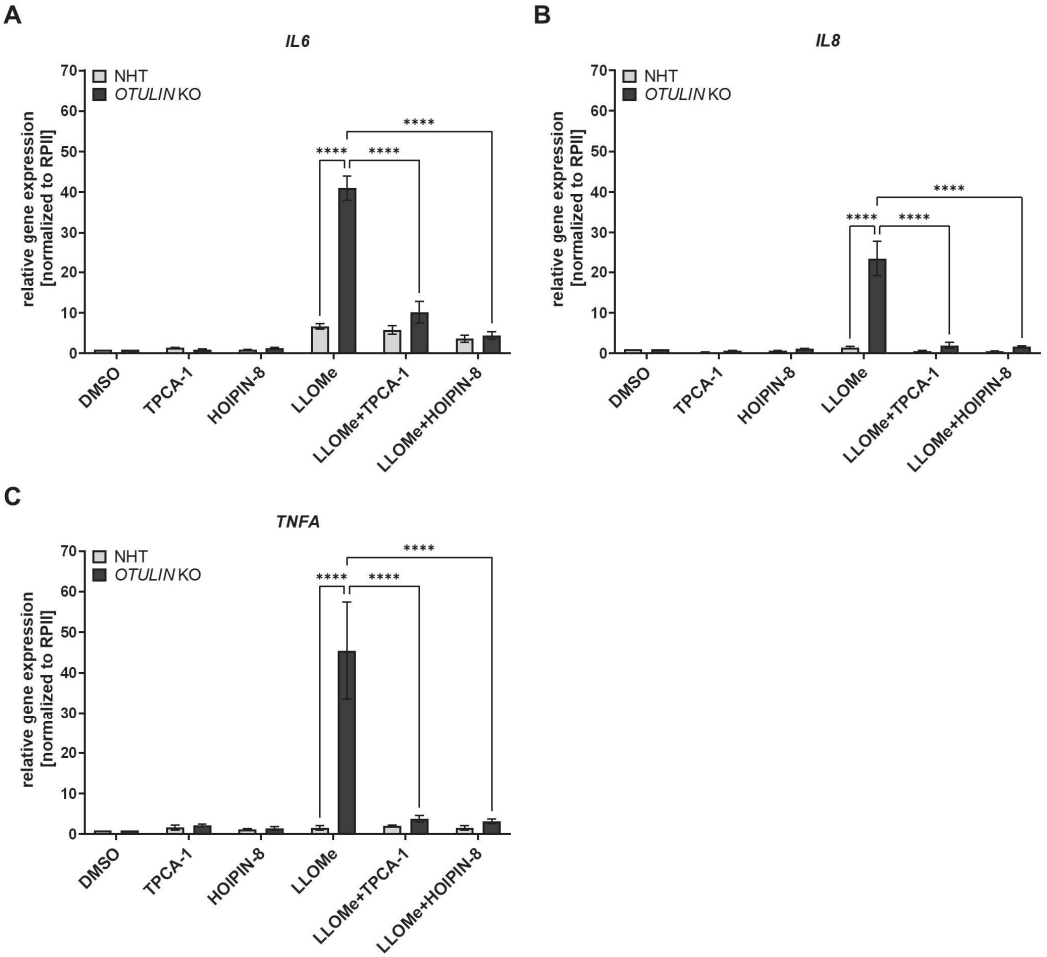

Figure 25. M1 poly-Ub accumulation at damaged lysosomes induces NF-κB target gene activation in an OTULIN-dependent manner.

mRNA expression levels of *IL6* (**A**), *IL8* (**B**) and *TNFA* (**C**) were analyzed by qRT-PCR of MZ-54 NHT and *OTULIN* KO GBM cells, pre-treated with HOIPIN-8 (30 μM) and TPCA-1 (5 μM) for 1 h and treated with LLOMe (500 μM) for 4 h. Fold increase of mRNA levels is shown relative to DMSO control with mean and SEM of at least three independent experiments performed in triplicates. **** $p < 0.0001$. Statistical significance was determined with two-way ANOVA followed by Tukey's multiple comparisons tests. This experiment was performed by M. Dietrich.

5.3.7 M1 poly-Ub accumulation and NF-κB activation requires K63 poly-Ub deposited on damaged lysosomes

In TNFR1 signaling, LUBAC is recruited to K63-ubiquitinated RIPK1 and conjugates M1 poly-Ub chains to RIPK1, thereby leading to the recruitment of the IKK complex and subsequent NF-κB activation [203,263,295]. To investigate if K63 poly-Ub is also required for the formation of M1 poly-Ub chains at damaged lysosomes and local NF-κB activation, the dimeric K63 poly-Ub specific E2 enzyme UbcH13-UEV1a was inhibited with NSC697923. As expected, NSC697923 strongly decreased the accumulation of K63 poly-Ub puncta at lysosomes in response to LLOMe-induced lysosomal damage (**Figure 26A**). Interestingly, NSC697923 also prominently diminished LLOMe-induced M1 poly-

Ub modification of damaged lysosomes (**Figure 26B**), indicating that the formation of M1 poly-Ub chains at damaged lysosomes is dependent on pre-formed K63 poly-Ub.

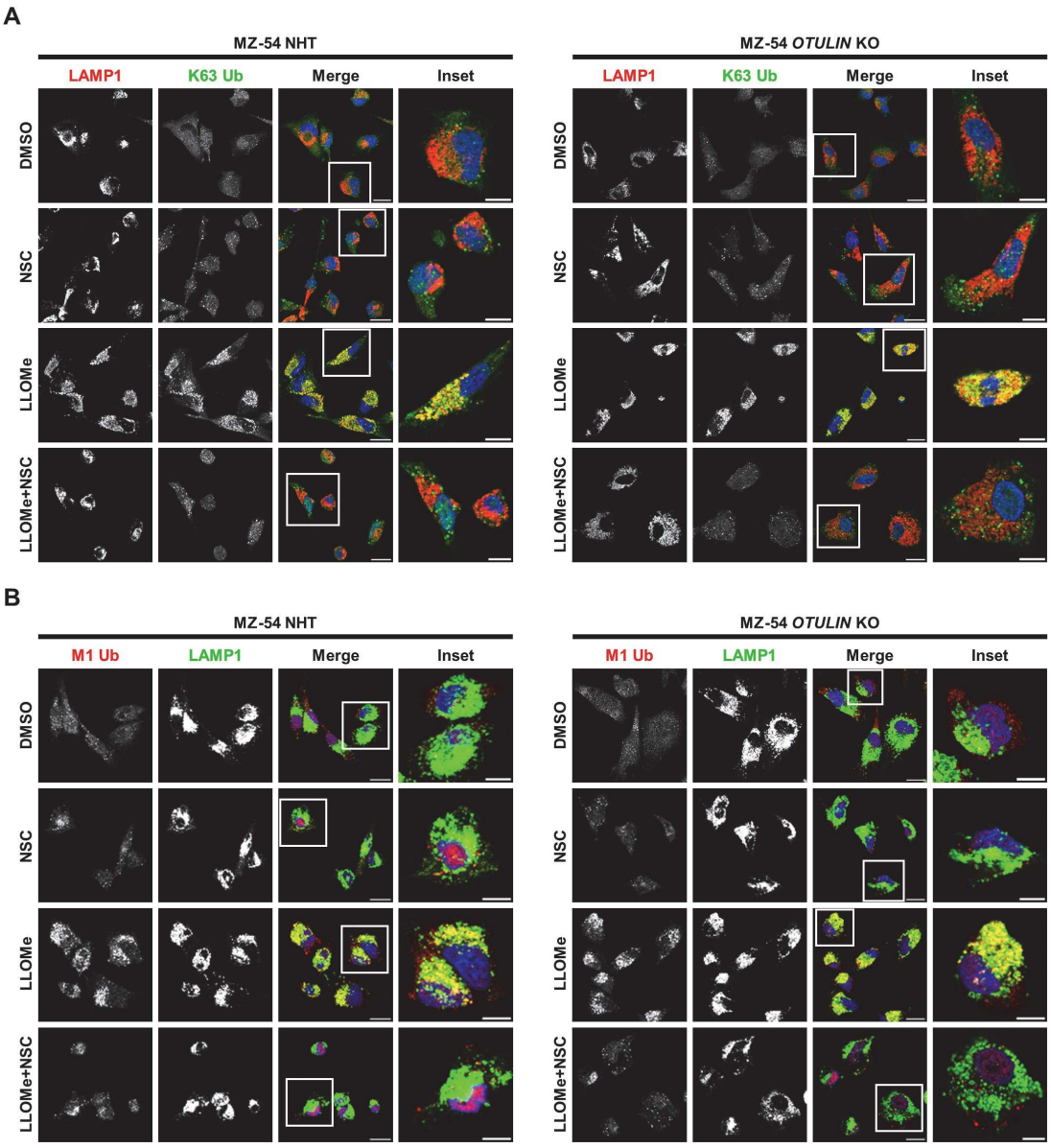

Figure 26. Formation of M1 poly-Ub chains at damaged lysosomes relies on K63 poly-Ub.

A. Representative immunofluorescence staining of LAMP1 and K63 poly-Ub in MZ-54 NHT and *OTULIN* KO GBM cells pre-treated with NSC697923 (NSC, 2.5 µM) for 1 h and treated with LLOMe (500 µM) for 2 h. Scale bar: 20 µm (10 µm for insets). **B.** Idem as A, but MZ-54 NHT and *OTULIN* KO GBM cells were stained for M1 poly-Ub and LAMP1. Scale bar: 20 µm (10 µm for insets). This experiment was performed by M. Dietrich.

Furthermore, NSC697923 prevented the accumulation of NEMO puncta at M1 poly-Ub-positive structures in response to LLOMe treatment (**Figure 27A and 27B**) and significantly blocked LLOMe-induced upregulation of the NF-κB target genes *IL6* and *IL8* (**Figure 27C and 27D**). Thus, recruitment of NEMO to damaged lysosomes and local NF-κB activation relies on K63 poly-Ub.

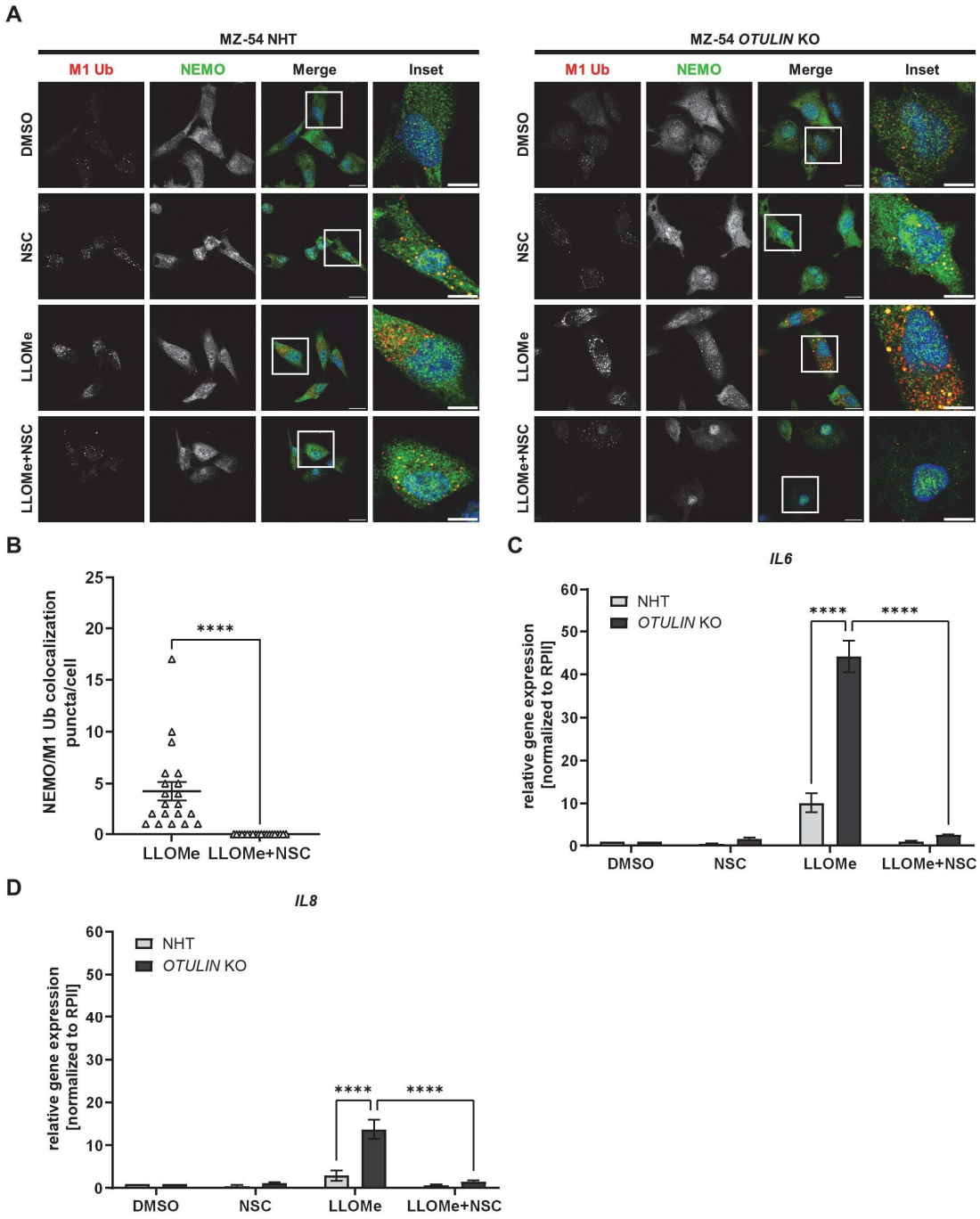

Figure 27. Local recruitment of NEMO to damaged lysosomes and NF-κB activation depends on K63 poly-Ub.

A. Representative immunofluorescence staining of M1 poly-Ub and NEMO in MZ-54 NHT and *OTULIN* KO GBM cells pre-treated with NSC697923 (NSC, 2.5 μM) for 1 h and treated with LLOMe (500 μM) for 2 h. Scale bar: 20 μm (10 μm for insets). **B.** Quantification of M1 poly-Ub- and NEMO-positive puncta in *OTULIN* KO cells from A. Mean and SEM of 20 cells from four independent microscopic views are shown. **** $p < 0.0001$. **C. & D.** mRNA expression levels of *IL6* and *IL8* were analyzed by qRT-PCR of MZ-54 NHT and *OTULIN* KO GBM cells pre-treated with NSC697923 (NSC, 2.5 μM) for 1 h and treated with LLOMe (500 μM) for 4 h. Fold increase of mRNA levels is shown relative to DMSO control with mean and SEM of at least three independent experiments performed in triplicates. **** $p < 0.0001$. Statistical significance was determined with unpaired t-test (**B**) and two-way ANOVA followed by Tukey's multiple comparisons tests (**C&D**). This experiment was performed by M. Dietrich.

5.3.8 Lysophagy serves pro-survival roles during LMP-induced cell death

LLOMe-induced LMP causes release of cathepsins in the cytosol, thereby activating apoptosis [342]. Furthermore, M1 poly-Ub has an important role in the regulation of TNFR1-mediated cell death [304-306]. Thus, the role of OTULIN and M1 poly-Ub in the regulation of lysosome-dependent cell death pathways was investigated. LLOMe treatment induced cell death in MZ-54 *OTULIN* KO and NHT control cells, which was inhibited by the pan-caspase inhibitor zVAD.fmk, verifying that LLOMe induces caspase-dependent apoptosis (**Figure 28A**) [342]. To address if autophagy and M1 poly-Ub control LMP-induced cell death, OTULIN expression was silenced in wild-type and Penta KO HeLa cells (**Figure 28B**), deficient of the five major autophagy receptors OPTN, NDP52, TAX1BP1, p62 and NBR1 [114], followed by LLOMe treatment in combination with pepstatin A- and CA-074-mediated inhibition of lysosomal proteases. Already pepstatin A and CA-074 treatment alone enhanced cell death in Penta KO cells with knockdown of OTULIN. In addition, cathepsin inhibition sensitized both WT and Penta KO cells to LLOMe-induced cell death and this effect was even more pronounced after silencing of OTULIN (**Figure 28C**). Together, this suggests pro-survival functions of autophagy in the response to lysosomal damage.

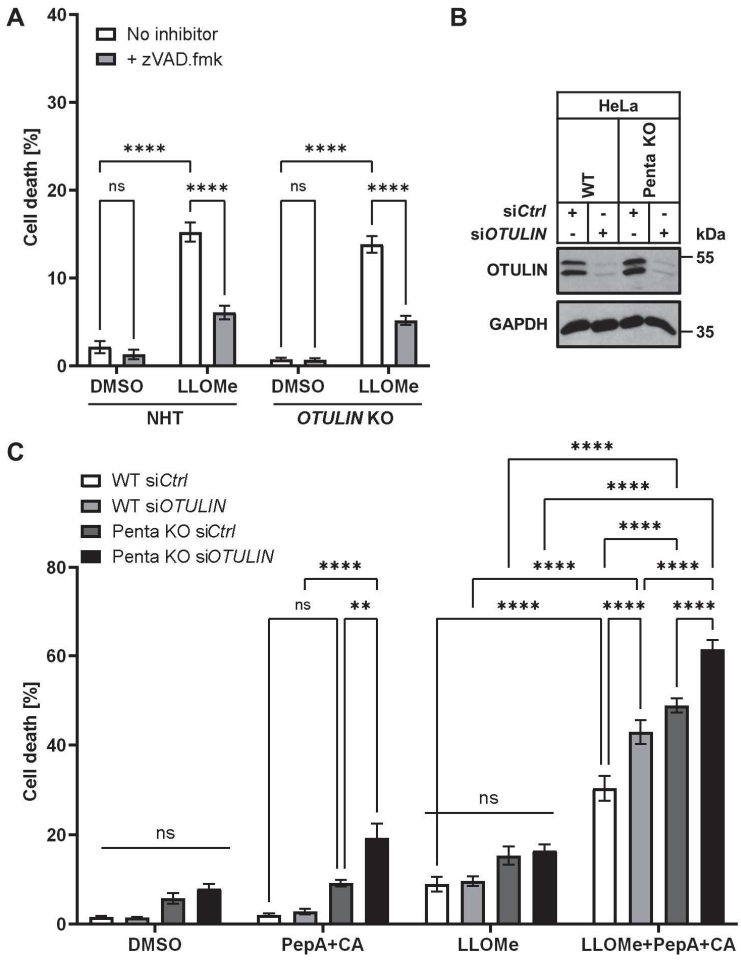

Figure 28. Lysophagy serves pro-survival roles during LMP-induced cell death.

Figure 28. Continued.

A. Cell death analysis of MZ-54 NHT and *OTULIN* KO GBM cells treated with LLOMe (2 mM) and zVAD.fmk (20 µM) for 24 h. Cell death was assessed by measuring the propidium iodide (PI) uptake as fraction of total nuclei determined by Hoechst counterstaining using high-content fluorescence microscopy. Mean and SEM of three independent experiments are shown. **** $p < 0.0001$, ns: not significant. **B.** Western blot analysis of OTULIN expression in HeLa WT and Penta KO cells after knockdown of OTULIN to confirm silencing of protein expression. GAPDH was used as loading control. Representative blots of three independent experiments are shown. **C.** Cell death analysis after knockdown of OTULIN in HeLa WT and Penta KO cells and treatment with LLOMe (2 mM) and Pepstatin A (10 µM) and CA-074 (10 µM) for 24 h. Cell death was assessed by measuring the propidium iodide (PI) uptake as fraction of total nuclei determined by Hoechst counterstaining using high-content fluorescence microscopy. Mean and SEM of three independent experiments are shown. ** $p < 0.01$, **** $p < 0.0001$, ns: not significant. Statistical significance was determined with ANOVA followed by Tukey's multiple comparisons tests. This experiment was performed by M. Dietrich.

5.3.9 Role of M1 poly-Ub in the response to lysosomal damage in human dopaminergic neurons and primary mouse cortical neurons

Lysosomal dysfunction is a characteristic hallmark of many NDs, including PD, AD and ALS [343-345]. Therefore, the role of M1 poly-Ub after lysosomal damage was examined in human induced pluripotent stem cells (iPSC)-derived dopaminergic neurons (DA-iPSn) and in primary mouse embryonic cortical neurons. LLOMe treatment induced the formation of M1 poly-Ub- and galectin-3 puncta at damaged lysosomes (**Figure 29A**) and significantly increased colocalization of M1 poly-Ub and galectin-3 in LLOMe-treated DA-iPSn (**Figure 29B**). Similarly, super-resolution structured illumination microscopy (SR-SIM) after incubation of primary mouse embryonic cortical neurons with LLOMe revealed an accumulation and partial colocalization of M1 poly-Ub, galectin-3 and LAMP1 (**Figure 29C**). 3D-reconstruction of a confocal section showed that M1 poly-Ub enveloped a subset of LAMP1- and galectin-3-positive lysosomes (**Figure 29D**), verifying that damaged lysosomes in primary mouse neurons are also modified with M1 poly-Ub.

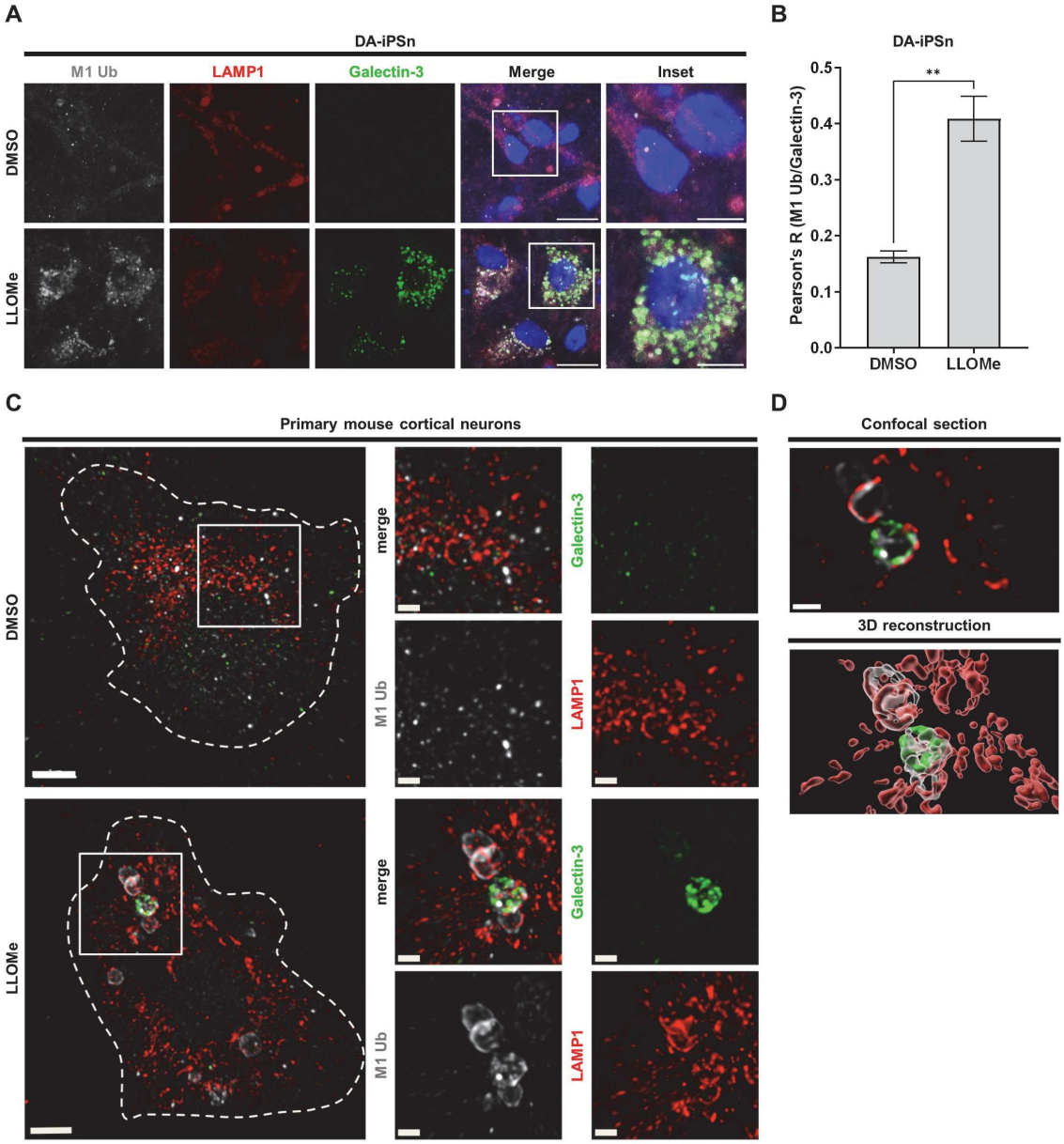

Figure 29. M1 poly-Ub increases at damaged lysosomes in human dopaminergic neurons and primary mouse cortical neurons.

A. Representative immunofluorescence staining of M1 poly-Ub, LAMP1 and galectin-3 in iPSC-derived DA neurons treated with LLOMe (500 µM) for 30 min. Scale bar: 20 µm (10 µm for insets). This experiment was performed by Denise Balta. **B.** Pearson correlation coefficients of M1 poly-Ub/galectin-3 staining from A. Data are shown as mean and SEM from three replicates and at least ten images per replicate. ** $p < 0.01$. Statistical significance was determined with unpaired t-test. **C.** Representative super-resolution structured illumination microscopy (SR-SIM) immunofluorescence staining of LAMP1, M1 poly-Ub and galectin-3 in DMSO and LLOMe treated (2 mM for 2 h) primary mouse cortical neurons (cell soma is outlined) after seven days in vitro (DIV). Scale bar: 3 µm (1 µm for insets). This experiment was performed by Verian Bader. **D.** Precise localization of the antibody signals from (**C**) in a single confocal section of a galectin-3-positive lysosome (upper panel) and an Imaris-assisted 3D-reconstruction of the respective area (lower panel). Scale bar: 1 µm.

6 Discussion

Protein ubiquitination serves key functions in the control of bulk and selective autophagy. Multiple E3 ligases and DUBs mediate ubiquitination or deubiquitination of core autophagy proteins to regulate different steps of the autophagy pathway. Examples include TNF receptor-associated factor 6 (TRAF6)-catalyzed K63 ubiquitination of ULK1 to enhance autophagy initiation [54], RING finger protein 2 (RNF2)-promoted K48 ubiquitination of AMBRA1 to target it for proteasomal degradation [346] or USP19-mediated deubiquitination of Beclin-1 to enhance its stability [347]. Furthermore, in selective autophagy, ubiquitination of cargo proteins enables recruitment of Ub-binding autophagy receptors which link the autophagic cargo to ATG8 proteins on growing autophagosomal membranes (e.g. SCF^{FBXO27}-mediated ubiquitination of lysosomal glycoproteins to trigger recruitment of the autophagy machinery during lysophagy [100]). Of note, LUBAC- and OTULIN-controlled M1 ubiquitination is also implicated in the control of autophagy initiation and maturation [309] and in selective autophagy of bacteria after pathogen infection [111]. This study identified OTULIN as a negative regulator of the autophagic flux and revealed OTULIN-dependent autophagy cargo candidates which are implicated in selective forms of autophagy such as aggrephagy and lysophagy. Follow-up experiments confirmed a role of M1 poly-Ub and OTULIN in aggrephagy and showed that damaged lysosomes are modified with M1 poly-Ub chains, thereby creating a signaling platform for NEMO and IKK complex recruitment and local NF-κB activation.

6.1 Function of OTULIN in the control of autophagy

The findings of this study suggest an inhibitory effect of OTULIN on autophagy induction and the autophagic flux. Loss of OTULIN enhanced LC3 lipidation and LC3 puncta formation in response to autophagy induction and electron microscopy revealed a higher number of DGCs in OTULIN-deficient cells. Furthermore, BafA1-mediated blockade of autophagy increased LC3-II accumulation in *OTULIN* KO cells, indicating that the autophagic flux is enhanced upon loss of OTULIN. These data partially correspond with a previous study which identified the ULK1 complex subunit ATG13 as a putative substrate of LUBAC- and OTULIN-controlled M1 ubiquitination. The authors show that modification of ATG13 with M1 poly-Ub chains enhanced ATG13 protein stability. Silencing of OTULIN expression promoted autophagy initiation but had a repressive effect on autophagy maturation [309]. In this work, the stimulating effect on autophagy induction upon loss of OTULIN could be confirmed. However, the western blot analysis after BafA1 treatment suggested that OTULIN deficiency rather increases than represses the autophagic flux. Furthermore, no increased stability of ATG13 in *OTULIN*

KO MZ-54 GBM cells could be observed (data not shown). This raises the possibility that in addition to regulating autophagy via M1 ubiquitination of ATG13, LUBAC and OTULIN may control autophagy via different cell type- and context-specific mechanisms. Thus, other proteins of the autophagy pathway might also be substrates for OTULIN- and LUBAC-regulated M1 ubiquitination. It can also be hypothesized that OTULIN and M1 poly-Ub regulate autophagy via additional, yet unknown mechanisms. Interestingly, a previous study suggested a role for OTULIN and M1 poly-Ub in the regulation of mTOR signaling. In humans, OTULIN deficiency causes ORAS, an inflammatory disease which is characterized by symptoms such as fever, diarrhea and arthritis. Furthermore, ORAS patients can suffer from a progressive steatotic liver disease [281,283]. Similarly, mice with hepatocyte-specific deletion of OTULIN develop steatohepatitis which is caused by hyperactivation of mTOR and can be reduced with the mTOR inhibitor rapamycin [282]. The kinase mTOR has key functions in the control of cell growth and metabolism and is present in two complexes, mTORC1 and mTORC2 [50]. Since mTORC1 is a master negative regulator of autophagy [348], it can be speculated that OTULIN and M1 poly-Ub also control autophagy activity via mTOR.

6.2 OTULIN-dependent effects on autophagy cargo proteins

The autophagosome content profiling revealed changes in the autophagosome content upon loss of OTULIN expression. The significantly up- and downregulated proteins in the autophagosomes of OTULIN-depleted cells included organelle-specific, endosomal and lysosomal proteins but also different proteins which are known to regulate autophagy. One of the significantly upregulated proteins in the autophagosomes of *OTULIN* KO cells was the autophagy receptor TAX1BP1 and further experiments indicated that TAX1BP1 degradation is regulated in an OTULIN-dependent manner. TAX1BP1 is implicated in different types of selective autophagy, including lysophagy [108], aggrephagy [113], mitophagy [114] and xenophagy [339]. Like many SARs, TAX1BP1 contains two UBDs, UBZ1 and UBZ2, and was shown to bind to K48 poly-Ub, K63 poly-Ub and M1 tetra-Ub *in vitro* [339]. In addition, a previous study revealed that TAX1BP1 binds to M1-ubiquitinated RIPK1 in an UBZ1/2-dependent manner, thereby recruiting FIP200 and the autophagy machinery to promote RIPK1 degradation via LC3-independent autophagy [340]. Since loss of OTULIN strongly increases cellular M1 poly-Ub levels, it can be hypothesized that in OTULIN-deficient cells, the recruitment of TAX1BP1 to M1 ubiquitinated proteins is enhanced and consequently, also the engulfment of TAX1BP1 together with M1 ubiquitinated autophagic cargo in autophagosomes is increased and leads to the observed changes in the autophagosome content of *OTULIN* KO cells. In addition to enrichment of TAX1BP1 in the

autophagosomes of OTULIN-deficient cells some lysosomal (e.g. RAB11A) and mitochondrial proteins (e.g. TOMM40, VDAC3) were upregulated as well, indicating that OTULIN might affect lysosomal homeostasis, lysophagy and mitophagy.

6.3 OTULIN- and M1 poly-Ub-mediated regulation of aggrephagy

A previous study identified TAX1BP1 as an aggrephagy receptor promoting the clearance of ubiquitinated toxic protein aggregates [113]. Since the enrichment of TAX1BP1 in the autophagosomes of OTULIN-deficient cells suggested a role of M1 poly-Ub and OTULIN in aggrephagy, protein aggregation was induced with puromycin. Puromycin causes premature termination of translation, thereby triggering accumulation of DRiPs which are subsequently removed via aggrephagy [113,126]. OTULIN deficiency increased the formation of M1 poly-Ub and K63 poly-Ub-labeled puncta in response to puromycin-induced proteotoxic stress. Furthermore, TAX1BP1 and p62 were recruited to puromycin-induced M1 poly-Ub-positive foci and loss of OTULIN strikingly increased M1 ubiquitinated insoluble proteins and reduced the levels of soluble TAX1BP1 and p62 in response to puromycin treatment. Of note, the formation of puromycin-labeled proteins was greatly enhanced in OTULIN-deficient cells and the clearance of these peptides after puromycin washout seemed to be delayed compared to control cells. These data indicate a link between OTULIN, M1 poly-Ub and aggrephagy. Aggrephagy is tightly controlled by different SARs, such as p62 and TAX1BP1 [75,113]. Previous studies revealed that p62 oligomers bind to ubiquitinated protein aggregates to assemble them in larger condensates by LLPS which is supported by NBR1 [136,138,139]. TAX1BP1 localizes to these condensates by binding to NBR1 and subsequently promotes autophagosome formation by recruitment of FIP200 via its SKICH domain [136,138,349]. Of note, M1 poly-Ub is also implicated in the clearance of protein aggregates. It was shown previously that the LUBAC subunit HOIP modifies polyQ-Htt aggregates with M1 poly-Ub, thereby mediating recruitment of NEMO to these aggregates [260]. In addition, a recent study revealed that binding of NEMO to M1-ubiquitinated protein aggregates promotes p62-mediated autophagic degradation of misfolded proteins by the following two mechanisms: first, NEMO enhances M1 ubiquitination at protein aggregates. Second, the interaction of NEMO with M1 poly-Ub forms a mobile phase-separated aggregate surface, thereby facilitating local concentration of p62 by co-condensation which leads to more efficient autophagosomal clearance of protein aggregates [350]. Based on this, the data of this work which reveal an increased number of M1 poly-Ub-positive puncta colocalizing with p62 and TAX1BP1 and more insoluble M1 ubiquitinated proteins in OTULIN-deficient cells suggest that

OTULIN might negatively regulate labeling of protein aggregates with M1 poly-Ub, recruitment of autophagy receptors to these aggregates and their subsequent autophagic degradation. In contrast to this, the finding that the retention of puromycin-labeled peptides seems to be prolonged upon loss of OTULIN rather suggests a positive effect of OTULIN on the clearance of protein aggregates. Thus, it remains to be addressed how exactly OTULIN regulates aggrephagy. Therefore, it could be helpful to study the role of OTULIN in another model of proteotoxic stress, for example by overexpression of aggregation-prone proteins such as polyQ-Htt [351]. The use of the translation inhibitor puromycin for induction of protein aggregation has the disadvantage that the observed effects in OTULIN-deficient cells can not only be related to aggrephagy but also to differences in translation. To address if OTULIN controls the rate of protein translation, the methionine analog L-azidohomoalanine (AHA) which labels newly synthesized proteins could be used [352].

6.4 Role of OTULIN and M1 poly-Ub in the response to lysosomal damage

Since the autophagy receptor TAX1BP1 is also implicated in lysophagy [108], LMP was induced in OTULIN-deficient cells to investigate a potential function of OTULIN and M1 poly-Ub in the response to lysosomal damage. Interestingly, M1 poly-Ub strongly accumulated at damaged lysosomes in a K63 poly-Ub-dependent manner and colocalized with TAX1BP1 and galectin-3 puncta. So far, the ubiquitination machinery in lysophagy and the substrate proteins are only incompletely understood. It is known that ubiquitination of damaged lysosomes occurs in a hierarchical manner and involves different types of Ub chains. While K63-linked Ub chains appear on damaged lysosomes very early after lysosomal damage (~ 30 min) and mediate recruitment of Ub-binding autophagy receptors and the core autophagy machinery, K48 ubiquitination of damaged lysosomes is delayed (~ 2 h after LMP) [82,104]. Different E2 Ub-conjugating enzymes, E3 Ub ligases and DUBs were identified to regulate ubiquitination of damaged lysosomes. Thus, the E3 ligase TRIM16 is recruited by galectin-3 to mediate ubiquitination of damaged lysosomes, thereby triggering recruitment of components of the ULK1 and PI3KC3 complex and promoting phagophore formation [96]. In addition, the E3 ligases SCF^{FBXO27} and CUL4A-DDB1-WDFY1 drive ubiquitination (mainly with K48 Ub chains) of lysosomal membrane proteins [100,101] and the DUB YOD1 acts together with the AAA-ATPase p97, UBXD1 and PLAA to remove K48-linked Ub chains from damaged lysosomes and drive their clearance via lysophagy [103]. Of note, the E2 Ub-conjugating enzyme UBE2QL1 controls K48 ubiquitination and p97 recruitment to

damaged lysosomes, but the associating E3 Ub ligase of UBE2QL1 has not been identified so far [104].

The finding that permeabilized lysosomes are modified with M1 poly-Ub extents the current knowledge about the ubiquitination machinery implicated in lysophagy. Furthermore, it raises the question about the functional role of M1 poly-Ub and OTULIN in lysophagy. To address the effect of OTULIN on the lysophagic flux, clearance of galectin-3 puncta was monitored after LLOMe washout. The loss of galectin-3 puncta was slightly enhanced in OTULIN-deficient cells indicating that OTULIN and M1 poly-Ub might regulate the lysophagic flux. However, measuring the clearance of galectin-3 puncta as readout for the lysophagic flux has the disadvantage that not only lysophagy but also other pathways of the ELDR (e.g. ESCRT-mediated repair of damaged lysosomes, TFEB-mediated transcriptional regulation) contribute to the elimination of galectin-3-positive damaged lysosomes [353]. Thus, clearance of galectin-3 puncta does not specifically reflect the lysophagic activity. Recently, the lysophagy flux reporter TMEM192-mKeima has been described in which the lysosomal transmembrane protein 192 (TMEM192) is fused to the fluorescent protein mKeima [353]. mKeima is resistant to cleavage by lysosomal proteases and its excitation is pH-dependent: at a neutral pH, mKeima is excited at a wavelength of 440 nm, but at acidic pH its excitation wavelength increases to 590 nm [354]. An increase in the 590/440 nm ratio reflects the transport of mKeima from a neutral into an acidic environment (e.g. lysosomal lumen) and can therefore be used as a measure for the lysophagic flux. It was shown that LLOMe-induced TMEM192-mKeima puncta are cleared independently of the ESCRT machinery and TFEB, making TMEM192-mKeima to a more specific lysophagy reporter than galectin-3-based probes [353]. Thus, to investigate a potential role of OTULIN in the regulation of the lysophagic flux, TMEM192-mKeima might be a better readout. It is also possible that M1 poly-Ub accumulation at damaged lysosomes serves other functions than regulation of the lysophagic flux. It was shown that in response to TNFα treatment, LUBAC localizes to mitochondria and mediates accumulation of M1 poly-Ub chains at mitochondria. This subsequently leads to recruitment of NEMO and formation of a signaling platform for local NF-κB activation at mitochondria. However, TNFα-induced mitochondrial M1 ubiquitination has no effect on mitophagy [355]. Thus, it can be speculated that damage-induced M1 ubiquitination of lysosomes has no functional role in lysophagy, but regulates other cellular processes.

6.5 TBK1 activation after lysosomal damage is regulated by OTULIN and M1 poly-Ub

The results of this study revealed that LLOMe-induced phosphorylation of TBK1 at S172, which activates its kinase activity, is enhanced in OTULIN-deficient cells. In addition, HOIPIN-8-mediated LUBAC inhibition decreased TBK1 phosphorylation in response to LLOMe treatment, indicating that M1 poly-Ub and OTULIN control TBK1 activation at damaged lysosomes. Consistently, it has been described previously that TBK1 phosphorylation is enhanced in catalytically inactive Otulin$^{C129A/C129A}$Ripk3$^{-/-}$ Casp8$^{-/-}$ bone marrow-derived macrophages (BMDMs) [248]. TBK1 is known to have key functions in both selective and bulk autophagy. For example, in mitophagy and xenophagy, TBK1 is recruited to the ubiquitinated autophagic cargo and mediates phosphorylation of autophagy receptors such as OPTN, NDP52, TAX1BP1 and p62, thereby increasing their binding affinity to Ub and LC3 and promoting autophagy [116,117,119,356,357]. Of note, activation of TBK1 at damaged lysosomes was also described previously and shown to be required for the lysophagic flux [108], which corresponds with the LLOMe-induced TBK1 phosphorylation observed in this study. Furthermore, TBK1 controls different steps during starvation-induced bulk autophagy, for example by direct and indirect regulation of mTORC1 activity [358-360] or by phosphorylating STX17 to promote assembly of the ULK1 complex [361].

6.6 Nuclear translocation of TFEB is not controlled by OTULIN

TFEB has a key role in the regulation of autophagic and lysosomal gene expression. Under basal conditions, mTORC1-mediated phosphorylation leads to sequestration of TFEB in the cytosol by 14-3-3 proteins [63,64]. Lysosomal damage induces release of TFEB from 14-3-3 proteins and its nuclear translocation to activate the expression of genes implicated in autophagy and lysosomal biogenesis [65]. Thus, one question in this study was if OTULIN regulates the response to lysosomal damage via TFEB. However, no differences in the nuclear translocation of TFEB could be observed upon loss of OTULIN, indicating that TFEB activity is not controlled by OTULIN and M1 poly-Ub.

6.7 M1 poly-Ub at damaged lysosomes serves as platform for local NF-κB activation

In TNFR1 signaling, LUBAC is recruited to K63-ubiquitinated RIPK1 and subsequently conjugates M1 poly-Ub chains to RIPK1, thereby leading to the recruitment of the IKK complex and subsequent NF-κB activation [263,295,296]. Similarly, the M1 poly-Ub coat which is formed around bacteria during pathogen infection (e.g. *Salmonella typhimurium*)

builds a signaling platform for local NEMO recruitment and NF-κB activation in an OTULIN-dependent manner [111,289]. To address if M1 poly-Ub at damaged lysosomes has comparable functions, NF-κB activation was investigated after LLOMe-induced lysosomal damage. LLOMe treatment triggered formation of NEMO-positive puncta which colocalized with M1 poly-Ub and the lysosomal marker LAMP1. Furthermore, IKK was phosphorylated and activated at M1 poly-Ub-modified lysosomes to promote induction of the NF-κB target genes *IL6*, *IL8* and *TNFA*. Importantly, NEMO recruitment, IKK complex activation and induction of NF-κB target gene expression was only observed in OTULIN-deficient cells, corresponding to the essential function of OTULIN as regulator of NF-κB activation during xenophagy [111]. As described above (see 6.5), TBK1 activation in response to lysosomal damage was enhanced upon loss of OTULIN. Interestingly, it was shown that during TNFα signaling, LUBAC-mediated M1 ubiquitination of TNFR1 enables recruitment of TBK1 and IKKε to phosphorylate RIPK1 and prevent RIPK1-dependent cell death. More precisely, NEMO binds to M1 poly-Ub chains and recruits TRAF family member associated NF-κB activator (TANK) and NAK-associated protein 1 (NAP1) which both associate with TBK1 and thereby mediate recruitment of TBK1 to TNFR1 [362]. In addition, TBK1 is activated on a mitochondrial NF-κB signaling platform in response to TNFR1 activation [355]. These data suggest that TBK1 activation upon induction of lysosomal damage occurs via similar mechanisms as in the case of TNFR1 signaling.

6.8 K63 poly-Ub is required for M1 ubiquitination of damaged lysosomes and local NF-κB activation

In immune receptor signaling, M1 poly-Ub chains are often attached to K63 poly-Ub chains on adapter proteins of RSCs, thereby forming K63-M1 poly-Ub hybrid chains [363]. Furthermore, it was shown that in many cases, M1 poly-Ub depends on pre-deposited K63 poly-Ub chains [302]. Activation of TNFR1 signaling induces recruitment of LUBAC to K63-ubiquitinated RIPK1 and LUBAC subsequently conjugates M1 poly-Ub chains to RIPK1 and additional proteins such as NEMO, thereby leading to activation of the IKK complex and NF-κB target gene expression [203,294]. The results of this study revealed that the accumulation of M1 poly-Ub at damaged lysosomes could be blocked by inhibition of the K63 poly-Ub specific E2 enzyme UbcH13-UEV1a. In addition, local recruitment of NEMO and NF-κB activation was abolished by inhibition of K63 ubiquitination. This suggests that LUBAC-mediated M1 poly-Ub modification of damaged lysosomes and local NF-κB activation depends on pre-formed K63 poly-Ub chains in a similar manner as in the case of immune receptor signaling pathways such as TNFR1 or NOD1 and NOD2 signaling [297,298].

6.9 Lysophagy serves pro-survival functions in the response to lysosomal damage

LLOMe-induced LMP triggers the release of cathepsins in the cytosol where they activate caspase-mediated apoptosis by cleavage of the pro-apoptotic protein Bid [364], degradation of anti-apoptotic B-cell lymphoma 2 (Bcl-2) family members such as Bcl-2, Bcl-x_L or Mcl-1 [365] and the release of cytochrome c [366]. In addition, lysosomal damage also induces other cell death pathways such as necroptosis [367,368] or ferroptosis [369,370]. In this study, LMP activated caspase-dependent cell death in both control and OTULIN-depleted cells. Interestingly, LLOMe-induced cell death was higher after cathepsin inhibition and increased further upon loss of the five major autophagy receptors or OTULIN, indicating that lysophagy serves pro-survival functions during lysosomal damage by removing damaged lysosomes to prevent leakage of harmful substances such as cathepsins in the cytosol. Of note, a cell-protective function of lysophagy was also described recently in another study. Li *et al.* showed that Ras GTPase-activating protein-binding protein 1 (G3BP1) promotes lysophagy by inhibition of mTOR signaling, thereby preventing ferroptotic cell death caused by ROS production and release of free iron from damaged lysosomes [370,371]. M1 poly-Ub critically regulates TNFR1-mediated cell death by activating the pro-survival NF-κB pathway [304-306]. Since knockdown of OTULIN increased cell death in response to LMP induction and cathepsin inhibition, it can be speculated that M1 poly-Ub also serves cell death-regulating functions during lysosomal damage.

6.10 Modeling the response to lysosomal damage in primary human and mouse neurons

Neurons display enhanced sensitivity to lysosomal damage and dysregulation of lysosomal function is often associated with the development of NDs such as PD, AD and ALS [343-345]. Importantly, M1 poly-Ub is linked to different types of NDs. For example, in ALS, M1 poly-Ub chains were detected on TDP-43-positive aggregates which colocalized with the LUBAC components HOIP and sharpin and the autophagy receptor OPTN [320]. Similarly, a subset of tau aggregates in AD is modified with M1 poly-Ub chains [319]. Therefore, the role of M1 poly-Ub in the response to lysosomal damage was investigated in human dopaminergic neurons and primary mouse neurons as a physiologically more relevant model. LLOMe-mediated lysosomal damage induced accumulation of M1 poly-Ub which colocalized with galectin-3 puncta at damaged lysosomes. This indicates that the response to lysosomal damage is conserved in primary human and mouse neurons, underlining the importance of M1 poly-Ub in cellular

responses to lysosomal damage. Further research and a better understanding about the functional consequences of M1 ubiquitination of damaged lysosomes in primary neurons might help to develop new treatment strategies for NDs with lysosomal dysfunction.

6.11 Limitations and Outlook

In this work, the role of LUBAC- and OTULIN-controlled M1 ubiquitination in the regulation of bulk and selective autophagy was addressed. Previously, Chu *et al.* reported that OTULIN deficiency increases LUBAC-mediated M1 ubiquitination and protein stability of ATG13, thereby promoting autophagy initiation but blocking autophagy maturation due to extended phagophore expansion [309]. Characterization of CRISPR/Cas9-mediated *OTULIN* KO MZ-54 GBM cells confirmed OTULIN as a negative regulator of autophagy induction, but also suggested an inhibitory effect of OTULIN on the autophagic flux which is in contrast to the study of Chu *et al.* [309]. One explanation for this could be that LUBAC- and OTULIN-mediated control of autophagy occurs in a cell type- and context-dependent manner and further experiments would be required to confirm this assumption. Of note, the autophagic flux was only investigated with BafA1 in this study and use of the tandem fluorescent autophagy reporter mRFP-EGFP-LC3 [372] could be helpful to verify these results. Furthermore, other mechanisms how OTULIN and M1 poly-Ub might regulate autophagy were not investigated in this work. Since OTULIN deficiency in mice was linked to hyperactivation of mTOR signaling [282] and mTORC1 has a key role in the negative regulation of autophagy [348], it would be interesting to analyze mTOR activity and signaling in OTULIN-deficient MZ-54 GBM cells. Of note, the conclusions of this study are mainly based on observations made in OTULIN-deficient cells. To confirm and strengthen these results the effect of HOIP genetic knockout on autophagy could be investigated and rescue experiments with WT or catalytically inactive OTULIN could be performed.

The autophagosome content profiling revealed OTULIN-specific differences in autophagy cargo proteins. Of note, the autophagy receptor TAX1BP1 and the glycan-binding protein galectin-3 were upregulated in the autophagosomes of OTULIN-depleted cells and further experiments suggested OTULIN-dependent autophagic degradation of TAX1BP1. Since TAX1BP1 regulates different forms of selective autophagy including aggrephagy [113] and lysophagy [108] and galectin-3 is implicated in lysophagy [95,96], follow-up experiments focussed on studying the function of OTULIN and M1 poly-Ub in the context of aggrephagy and lysophagy. However, since other OTULIN-dependent autophagy cargo candidates included mitochondrial (e.g. TOMM40, VDAC3) proteins, it would also be interesting to address a potential role of OTULIN in the regulation of mitophagy in future research.

Analysis of the function of OTULIN and M1 poly-Ub in the regulation of aggrephagy indicated that OTULIN has an inhibitory effect on the labeling of puromycin-induced protein aggregates with M1 poly-Ub and the recruitment of p62 and TAX1BP1 to these aggregates. However, if OTULIN promotes or rather delays the clearance of protein aggregates was not deciphered in this study and remains to be investigated. Since TAX1BP1 was described to control the clearance of protein aggregates [113] and OTULIN deficiency strongly decreased the levels of soluble TAX1BP1 in response to puromycin treatment, it can be speculated that OTULIN regulates aggregate clearance via TAX1BP1, but further experiments would be needed to verify this assumption. Of note, this study solely used puromycin to model protein aggregation. Given that puromycin inhibits protein translation, differences observed in puromycin-treated OTULIN-depleted cells can also be due to changes in the translation rate. To circumvent this issue, proteotoxic stress could be induced with an alternative model, for example the overexpression of aggregation-prone proteins such as polyQ-Htt [351], or newly synthesized proteins could be labeled with the methionine analog AHA [352] to address if OTULIN affects the translation rate of TAX1BP1 and p62. Since accumulation of protein aggregates is characteristic for many NDs such as AD, PD or ALS [122,123,183], the use of primary neurons would be an interesting model to investigate the role of OTULIN and M1 poly-Ub in aggrephagy in a physiologically more relevant system.

While K48 and K63 ubiquitination is known to regulate lysophagy [82,104], M1 poly-Ub chains have not been detected on damaged lysosomes so far. This work revealed that induction of lysosomal damage resulted in strong accumulation of M1 poly-Ub at damaged lysosomes, suggesting a novel function of M1 poly-Ub in the control of lysophagy. However, further experiments are needed to prove that LUBAC localizes to damaged lysosomes and to identify lysosomal substrates for M1 ubiquitination. To address the functional role of M1 poly-Ub in lysophagy, clearance of galectin-3 puncta was assessed after induction of lysosomal damage. The clearance of galectin-3 puncta was slightly enhanced upon loss of OTULIN, indicating that OTULIN-controlled M1 poly-Ub regulates the lysophagic flux. However, monitoring the clearance of galectin-3 puncta has the disadvantage that it does not only reflect the lysophagic flux but also other processes of the ELDR such as ESCRT-mediated repair of damaged lysosomes [353]. Use of the lysophagy flux reporter TMEM192-mKeima as a more specific readout for the lysophagic flux might help to confirm M1 poly-Ub-mediated regulation of lysophagy activity. In addition, further experiments could investigate the contribution of galectin-8 in the regulation of lysophagy. Galectin-8 was shown to localize to pathogen-damaged lysosomal membranes and recruit NDP52 in an Ub-independent manner to activate lysophagy [97]. Of note, this work showed that accumulation of M1 poly-Ub at damaged

lysosomes requires pre-deposited K63 poly-Ub. This is consistent with previous studies describing the recruitment of LUBAC to K63-ubiquitinated proteins of immune receptor signaling complexes [203,294]. However, the identity of the E3 ligase responsible for K63 ubiquitination of damaged lysosomes was not investigated in this study. To date, the E2 and E3 enzymes mediating K63 ubiquitination in lysophagy are unknown. Large scale methods such as genome-wide CRISPR/Cas9 or siRNA screening could be used in future studies to address this.

This study demonstrated that loss of OTULIN enhances TBK1 activation in response to LLOMe-induced lysosomal damage. Phosphorylation and activation of TBK1 has been linked previously with an increase in the lysophagic flux [108]. Furthermore, in other types of selective autophagy such as mitophagy or xenophagy, activated TBK1 phosphorylates autophagy receptors including p62, OPTN or NDP52, thereby enhancing binding to Ub and LC3 [116-119]. However, the substrates of TBK1 in lysophagy remain unknown and future studies should aim to identify them.

LUBAC-mediated assembly of M1 poly-Ub has a key role in NF-κB activation downstream of immune receptors such as TNFR1 [263,295,296]. Similarly, invading bacteria are coated with M1 poly-Ub during xenophagy, thereby forming a platform for local NEMO recruitment and NF-κB activation to restrict bacterial growth [111,289]. In this study, induction of lysosomal damage triggered the formation of NEMO- and pIKK-positive foci at M1 poly-Ub-modified lysosomes and upregulated the expression of NF-κB target genes in an OTULIN- and K63 poly-Ub-dependent manner. However, the functional role of NF-κB activation in response to lysosomal damage remains to be addressed.

Since it is well known that lysosomal damage can activate cell death pathways such as caspase-dependent apoptosis [342], necroptosis [367,368] or ferroptosis [369,370], the function of OTULIN and M1 poly-Ub in lysosome-dependent cell death was investigated in this work. Cathepsin inhibition and loss of the five major autophagy receptors increased LLOMe-induced cell death, suggesting pro-survival functions of lysophagy during lysosomal damage. This corresponds with a previous study describing that G3BP1-mediated lysophagy induction reduces ferroptotic cell death [370]. Silencing of OTULIN enhanced cell death after LMP induction and cathepsin inhibition. This indicates that OTULIN participates in the regulation of cell death during lysosomal damage, possibly by controlling the autophagy flux via M1 poly-Ub. To further characterize the role of M1 poly-Ub in lysosome-dependent cell death, LUBAC function could be blocked by genetic knockout of HOIP or use of the HOIPIN inhibitor HOIPIN-8. In addition, OTULIN-dependent NF-κB activation in response to lysosomal damage might also have regulatory functions in lysosome-dependent cell death. Previously, it was demonstrated

that binding of TNFα to TNFR1 results in the production of the lysosomotropic agent sphingosine which in turn triggers LMP and release of cathepsin B in the cytosol followed by induction of apoptosis [373-375]. Of note, NF-κB activation protects cells from TNFα-induced lysosome-dependent apoptosis by upregulation of the NF-κB target serine protease inhibitor 2A (Spi2A), an inhibitor of different cytosolic cysteine cathepsins including cathepsin B [376]. Future research could address the contribution of NF-κB in the control of LMP-induced cell death, for example by inhibition of IKKβ with TPCA-1.

Lysosomal damage also induced accumulation of M1 poly-Ub at galectin-3-positive lysosomes in human dopaminergic neurons and in primary mouse embryonic cortical neurons, confirming the data obtained in MZ-54 and HeLa cells and strengthening the functional relevance of M1 poly-Ub in the response to lysosomal damage. Genetic depletion of OTULIN expression could help to further characterize the role of M1 poly-Ub in the regulation of lysosomal integrity in neurons. This might also have important implications for the understanding of NDs such as PD, AD or ALS which are often associated with defects in lysosomal function [343-345].

7 Deutsche Zusammenfassung

Bei Autophagie handelt es sich um einen katabolischen Prozess, bei dem zytoplasmatische Bestandteile (engl. c*argo*) in neu gebildeten, vesikelförmigen Autophagosomen mit einer Doppelmembran eingeschlossen und nach Fusion des Autophagosom mit einem Lysosom zum Autolysosom durch lysosomale saure Hydrolasen abgebaut werden. Die Abbauprodukte stehen wieder für den Stoffwechsel zur Verfügung, weshalb Autophagie eine wichtige Rolle bei der Aufrechterhaltung der zellulären Homöostase spielt. Man unterscheidet drei Hauptformen von Autophagie: Makroautophagie, Mikroautophagie und Chaperon-vermittelte Autophagie. Dabei stellt Makroautophagie die gängigste Art von Autophagie dar und wird im Folgenden nur noch als „Autophagie“ bezeichnet. Der Ablauf des Autophagie-Signalweges wird maßgeblich durch das Zusammenspiel von verschiedenen Proteinkomplexen reguliert, welche zu einem großen Teil von Mitgliedern der ATG (engl. *autophagy-related protein*) Proteinfamilie gebildet werden. Induktion von Autophagie, welche durch Stressfaktoren wie Nährstoffmangel, DNA-Schäden oder reaktive Sauerstoffspezies erfolgen kann, führt zunächst zur Nukleation des Phagophor an spezifischen Phosphatidylinositol-3-Phosphat (PI3P)-reichen Stellen des endoplasmatischen Retikulums (ER), den sogenannten Omegasomen. Anschließend kommt es zur Erweiterung des Phagophor (Expansion), wobei zwei Ubiquitin-ähnliche Konjugationssysteme eine wichtige Rolle spielen, der ATG12~ATG5-ATG16L Komplex und die ATG8 Proteine MAP1LC3/LC3 (engl. *microtubule-associated proteins 1A*/*1B light chain 3*) und GABARAP (engl. *γ-aminobutyric acid receptor-associated protein*). LC3 und GABARAP werden während der Expansion des Phagophor prozessiert und durch Konjugation mit dem Lipid Phosphatidylethanolamin (PE) in der Membran des wachsenden Phagophor verankert. Das Phagophor verschließt sich zu einem vesikelförmigen Autophagosom, welches nach seiner Reifung mit einem Lysosom zu einem Autolysosom fusioniert. Im Autolysosom werden die zytoplasmatischen Bestandteile durch lysosomale Hydrolasen abgebaut, deren katalytische Aktivität abhängig vom sauren pH im Lysosom ist.

Bei der sogenannten *bulk* Autophagie werden zytoplasmatische Bestandteile zufällig in Autophagosomen eingeschlossen und abgebaut. Im Gegensatz dazu kommt es bei der selektiven Autophagie zum spezifischen Abbau von zum Beispiel geschädigten Zellorganellen, Proteinaggregaten oder Pathogenen. Das *Cargo* für selektive Autophagie wird üblicherweise mit Ubiquitin-Ketten als Abbausignal markiert, welche der Erkennung der Substrate durch Autophagie-Rezeptoren dienen. Die meisten Autophagie-Rezeptoren besitzen sowohl eine Ubiquitin-Bindedomäne (UBD), über die sie an das ubiquitinierte *Cargo* binden, sowie eine LIR (engl. *LC3-interacting region*) Domäne, die die Interaktion mit LC3 auf der autophagosomalen Membran ermöglicht.

Auf diese Weise bringen Autophagie-Rezeptoren das für den Abbau bestimmte *Cargo* in räumliche Nähe mit dem entstehenden Autophagosom. Dieses bildet sich um das Rezeptor-gebundene *Cargo*, welches nach Fusion mit einem Lysosom abgebaut wird. Manche Autophagie-Rezeptoren sind spezifisch für eine Art von selektiver Autophagie, während andere an verschiedenen Formen von selektiver Autophagie beteiligt sind.

Verschiedene Stimuli wie oxidativer Stress, neurotoxische Aggregate, Pathogene oder lysosomotrophe Substanzen können lysosomale Membran-Permeabilisierung (LMP) hervorrufen. Die damit verbundene Freisetzung von Protonen, reaktiven Sauerstoffspezies und lysosomalen Enzymen ins Zytosol ist sehr schädlich für die Zelle und kann lysosomalen Zelltod induzieren. Für die Aufrechterhaltung der zellulären Funktion ist es deshalb von Bedeutung, geschädigte Lysosomen schnellstmöglich zu reparieren oder abzubauen. Den Abbau von Lysosomen durch Autophagie bezeichnet man als Lysophagie. Lysophagie wird dadurch initiiert, dass infolge von lysosomalen Schaden Glykane auf der lysosomalen Membran exponiert werden und zur Lokalisation von Galektinen und der Ubiquitin-Maschinerie an den Lysosomen führen. Im Folgenden werden Autophagie-Rezeptoren (u.a. p62, TAX1BP1 (engl. *Tax1-binding protein 1*, OPTN (Optineurin)) und andere Schlüsselproteine des Autophagie-Signalweges (ULK1 (engl. *Unc-51-like kinase 1*), ATG16L) zu den ubiquitinierten Lysosomen rekrutiert und es kommt zum Abbau der geschädigten Lysosomen durch noch intakte Lysosomen. Auch wenn bereits K63 und K48 Poly-Ubiquitinierung auf geschädigten Lysosomen nachgewiesen werden konnte, sind die Enzyme, die die Ubiquitinierung von geschädigten Lysosomen regulieren, weitgehend unbekannt und es ist nicht klar, ob noch andere Typen von Ubiquitin-Ketten an Lysophagie beteiligt sind.

Ähnlich wie die Schädigung von Lysosomen stellt auch die Akkumulation von Proteinaggregaten eine potenzielle Bedrohung für die zelluläre Integrität dar und ist charakteristisch für verschiedene neurodegenerative Krankheiten wie Alzheimer, Parkinson oder Chorea Huntington. Der Abbau von Proteinaggregaten durch selektive Autophagie wird Aggrephagie genannt und ist wichtig für die Aufrechterhaltung der Protein Homöostase (Proteostase). Aggrephagie hat viele Gemeinsamkeiten zu Lysophagie. So kommt es ebenfalls zur Markierung der Proteinaggregate mit Ubiquitin, was der Erkennung durch Autophagie-Rezeptoren dient, die wiederum die Verbindung zu LC3 auf der autophagosomalen Membran bilden. Autophagie-Rezeptoren, die bei Aggrephagie eine Rolle spielen, sind zum Beispiel p62, TAX1BP1, NBR1 (engl. *Next to BRCA1 gene 1*), OPTN und TOLLIP (engl. *Toll-interacting protein*). Außerdem sind noch weitere Proteine wie ALFY (engl. *Autophagy-linked FYVE protein*), WDR81 (engl. *WD repeat-containing protein 81*) oder TECPR1 (engl. *Tectonin beta-propeller repeat-containing protein 1*) an der Regulation von Aggrephagie beteiligt.

Die Ubiquitinierung ist eine der häufigsten posttranslationalen Proteinmodifikationen. Dabei kommt es durch das Zusammenspiel von E1 Ubiquitin-aktivierenden Enzymen, E2 Ubiquitin-konjugierenden Enzymen und E3 Ubiquitin Ligasen zur kovalenten Bindung des Proteins Ubiquitin an Substratproteine. Es gibt verschiedene Formen von Ubiquitinierung. Bei der Mono-Ubiquitinierung wird das Substratprotein mit nur einem Ubiquitin-Molekül modifiziert, wohingegen bei der Poly-Ubiquitinierung eine Ubiquitin-Kette an das Substratprotein gebunden wird. Dabei können weitere Ubiquitin Monomere entweder an einen von sieben Lysin-Resten (K6, K11, K27, K29, K33, K48 und K63) ligiert werden oder an das Methionin am N-Terminus von Ubiquitin (M1). Lineare (M1) Ubiquitinierung wird durch den E3 Ligase Komplex LUBAC (eng. *linear ubiquitin chain assembly complex*) katalysiert, der aus der E3 Ubiquitin Ligase HOIP (engl. *HOIL-1-interacting protein*) sowie den Proteinen HOIL-1 (engl. *heme-oxidized IRP2 Ubiquitin ligase 1*) und Sharpin (engl. *shank-associated RH domain-interacting protein*) zusammengesetzt ist. Der Abbau von M1 Ubiquitin-Ketten erfolgt durch die Deubiquitinasen OTULIN (engl. *OTU domain-containing DUB with linear linkage specificity*) und CYLD (Cylindromatosis). Während OTULIN spezifisch für M1 Ubiquitin ist, schneidet CYLD sowohl K63 als auch M1 Ubiquitin. CYLD interagiert mit HOIP über das Adaptor-Protein SPATA2, wohingegen OTULIN direkt mit seiner PIM (engl. *PUB interaction motif*) Domäne an die PUB (engl. *peptide N-glycosidase/UBA*) Domäne von HOIP bindet. Eine zentrale Funktion von M1 Ubiquitin ist die Kontrolle von Immunrezeptor-assoziierten Signalwegen, wie dem TNFR1 (engl. *tumor necrosis factor receptor 1*) Signalweg, und damit verbunden die Aktivierung des NF-κB (engl. *nuclear factor-κB*) Signalweges, der das Zellüberleben kontrolliert. Als Gegenspieler von LUBAC hat CYLD eine inhibierende Wirkung auf die NF-κB Aktivität, die Rolle von OTULIN im NF-κB Signalweg ist jedoch Zelltyp- und Kontext-abhängig. So hat OTULIN teils einen negativen Effekt auf die NF-κB Aktivität, in anderen Studien konnte aber gezeigt werden, dass OTULIN die Auto-Ubiquitinierung von HOIP verhindert und somit die Aktivität von HOIP aufrechterhält. Dementsprechend steigen die zellulären M1 Ubiquitin Level bei einem Verlust der katalytischen Aktivität von OTULIN stark an und es kommt zu einer reduzierten NF-κB Aktivität. M1 Ubiquitin spielt auch eine Rolle bei der Regulation von Autophagie. So konnte gezeigt werden, dass LUBAC durch M1 Ubiquitinierung von ATG13 die Induktion von Autophagie und die Autophagosom-Reifung kontrolliert. M1 Ubiquitin reguliert außerdem die selektive Autophagie von Pathogenen (Xenophagie). Nach Infektion mit *Salmonella typhimurium* wird die Hülle der eingedrungenen Bakterien mit M1 Ubiquitin modifiziert, was zur Rekrutierung der Autophagie-Rezeptoren p62 und OPTN führt und den lysosomalen Abbau der Bakterien vorantreibt. Zudem bilden die M1 Ubiquitin-Ketten auf der Oberfläche der Bakterien eine Plattform zur Rekrutierung von

NEMO (engl. *NF-κB essential modulator*). Dadurch kommt es zur lokalen NF-κB Aktivierung und zu einer erhöhten Ausschüttung von pro-inflammatorischen Zytokinen, die die bakterielle Proliferation vermindern.

Das Ziel dieser Studie war es, die Rolle von OTULIN und LUBAC in der Regulation von (selektiver) Autophagie weiter zu charakterisieren. Dafür wurde zunächst mittels der CRISPR/Cas9-Technologie das für OTULIN codierende Gen in der Glioblastom-Zelllinie MZ-54 ausgeschaltet. Die Zellen wurden dann mit den Autophagie-auslösenden Substanzen Torin1 und Loperamid (LOP) behandelt und interessanterweise war die durch Torin1- und LOP-induzierte LC3 Lipidierung in *OTULIN* KO Zellen im Vergleich zu Kontrollzellen (NHT, engl. *non-human target*) erhöht. Ebenso kam es in OTULIN-defizienten Zellen infolge von LOP-induzierter Autophagie zu einer verstärkten Bildung von LC3 Punkten, die nach Induktion von Autophagie auf charakteristische Weise im Fluoreszenzmikroskop zu erkennen sind. Die Wirkung von OTULIN auf den autophagischen Flux wurde außerdem mithilfe von Bafilomycin A1 (BafA1) untersucht. Durch Hemmung der lysosomalen H^+-ATPase verhindert BafA1 die Azidifizierung der Lysosomen und damit den Abbau des *Cargo*-Materials in den Autophagosomen. Nach Behandlung mit BafA1 war die Lipidierung von LC3 ebenfalls in *OTULIN* KO Zellen erhöht. Um potenzielle Unterschiede in der Morphologie der Zellen nach Ausschalten der OTULIN Expression zu charakterisieren, wurde eine elektronenmikroskopische Analyse nach Behandlung mit LOP durchgeführt. Diese zeigte eine Zunahme von degradativen Kompartimenten und Autophagosomen nach Depletion von OTULIN. Zusammengefasst deuten diese Daten daraufhin, dass OTULIN die Induktion von Autophagie und den autophagischen Flux negativ reguliert. Da OTULIN und LUBAC bereits in der Regulation von Xenophagie beschrieben sind, sollte im Folgenden untersucht werden, ob OTULIN auch andere Arten von selektiver Autophagie kontrolliert, beziehungsweise ob bestimmte *Cargo*-Proteine in Abhängigkeit von OTULIN verändert abgebaut werden. Dafür wurde der Inhalt der Autophagosomen von *OTULIN* KO und Kontrollzellen mittels Massenspektrometrie untersucht. Tatsächlich waren verschiedene Proteine in den Autophagosomen von OTULIN-defizienten Zellen signifikant hoch- beziehungsweise runterreguliert, darunter sowohl solche, die an der Regulation von Autophagie beteiligt sind (TAX1BP1, Galektin-3) sowie Organell-spezifische (TOMM40) und endosomale und lysosomale Proteine (RAB11A). Folgende Experimente wiesen darauf hin, dass der lysosomale Abbau von TAX1BP1 durch OTULIN kontrolliert wird. Da TAX1BP1 als Autophagie-Rezeptor sowohl an der Regulation von Lysophagie und Aggrephagie beteiligt ist und Galektin-3 auch eine wichtige Funktion in Lysophagie hat, wurde im Weiteren eine potenzielle Rolle von OTULIN und M1 Ubiquitin in Aggrephagie und Lysophagie untersucht.

Zur Induktion von Proteinaggregation und Aggrephagie wurde der Translationsinhibitor Puromycin verwendet. Nach Behandlung mit Puromycin war in *OTULIN* KO Zellen die Bildung von M1 ubiquitinierten unlöslichen Proteinen deutlich erhöht und es kam zu einer Abnahme von TAX1BP1 und p62 in der löslichen Proteinfraktion. Außerdem konnte in OTULIN-defizienten Zellen ein Anstieg der mit Puromycin-markierten Proteine beobachtet werden und der Abbau von diesen nach Auswaschen von Puromycin schien verlangsamt zu sein. Zusammengefasst deutet dies auf eine regulatorische Funktion von OTULIN in Aggrephagie hin.

Um die Rolle von OTULIN und M1 Ubiquitin in Lysophagie zu untersuchen, wurde LMP mit der lysosomotrophen Substanz LLOMe induziert. Dies führte sowohl in Kontrollzellen als auch in *OTULIN* KO Zellen zu einer starken Akkumulation von M1 Ubiquitin-positiven Punkten auf den geschädigten Lysosomen. Eine Western Blot Analyse zeigte außerdem, dass bei Verlust von OTULIN die durch LLOMe-induzierte LC3 Lipidierung und der Abbau von Galektin-3 verstärkt ist. Auch konnte mittels Fluoreszenzmikroskopie beobachtet werden, dass die Anzahl von Galektin-3-positiven Punkten nach Auswaschen von LLOMe in OTULIN-defizienten Zellen geringer war, was einen erhöhten lysophagischen Flux bei Verlust der OTULIN Expression suggeriert.

Weil es bei Xenophagie auf den mit M1 Ubiquitin-modifizierten Bakterien zur lokalen NF-κB Aktivierung kommt und Xenophagie viele Parallelen zu Lysophagie aufweist, wurde untersucht, ob ein ähnlicher Mechanismus auch bei Lysophagie auftritt. Tatsächlich führte die Induktion von LMP in OTULIN-defizienten Zellen zur Rekrutierung von NEMO zu den geschädigten Lysosomen, sowie zur Aktivierung des IKK (engl. *inhibitor of κB (IκB) kinase*) Komplexes und zur Induktion von NF-κB Zielgenen. Dies war abhängig von der vorherigen Modifikation der geschädigten Lysosomen mit K63 Ubiquitin. Auch kam es bei Verlust der OTULIN Expression zu einer verstärkten Aktivierung der Kinase TBK1 (engl. *TANK-binding kinase 1*) infolge von lysosomalen Schaden. Da bekannt ist, dass lysosomaler Schaden Zelltod hervorrufen kann, wurde die Rolle von OTULIN und M1 poly-Ub in Lysosom-abhängigen Zelltod untersucht. Der durch LMP induzierte Zelltod war durch Inhibition von lysosomalen Abbau und Verlust von OTULIN erhöht. Dies deutet darauf hin, dass Lysosom-abhängiger Zelltod durch OTULIN reguliert wird und Lysophagie eine protektive Rolle während lysosomalen Schaden besitzt. Abschließend konnte gezeigt werden, dass es nach Induktion von LMP auch in humanen dopaminergen Neuronen und primären Maus-Neuronen zur Akkumulation von M1 Ubiquitin auf Galektin-3-positiven Lysosomen kommt.

In der vorliegenden Arbeit wurde eine negative Rolle von OTULIN in der Aktivierung von Autophagie und des autophagischen Flux nachgewiesen. Außerdem konnte gezeigt werden, dass OTULIN und M1 Ubiquitin an der Regulation von Aggrephagie und

Lysophagie beteiligt sind. Die Induktion von LMP führte zu einer Akkumulation von M1 Ubiquitin auf den geschädigten Lysosomen. Zudem dienten die mit M1 Ubiquitin-markierten Lysosomen als Plattformen zur lokalen NF-κB Aktivierung in Abhängigkeit von OTULIN und K63 Ubiquitin. Auch in humanen dopaminergen Neuronen und primären Maus-Neuronen kam es infolge von LMP zur Markierung von Galektin-3-positiven Lysosomen mit M1 Ubiquitin, was die Wichtigkeit von M1 Ubiquitin in der zellulären Antwort auf lysosomalen Schaden unterstreicht und möglicherweise auch von Bedeutung bei der Untersuchung von neurodegenerativen Krankheiten ist, die häufig mit lysosomaler Dysfunktion assoziiert sind.

8 References

1. Dikic, I. and Z. Elazar, *Mechanism and medical implications of mammalian autophagy.* Nature reviews Molecular cell biology, 2018. **19**(6): p. 349-364.
2. De Duve, C. *The lysosome concept*. in *Ciba Foundation Symposium-Anterior pituitary secretion (Book I of Colloquia on Endocrinology)*. 1963. Wiley Online Library.
3. Tsukada, M. and Y. Ohsumi, *Isolation and characterization of autophagy-defective mutants of Saccharomyces cerevisiae.* FEBS letters, 1993. **333**(1-2): p. 169-174.
4. Lu, G., Y. Wang, Y. Shi, et al., *Autophagy in health and disease: From molecular mechanisms to therapeutic target.* MedComm, 2022. **3**(3): p. e150.
5. Wang, L., D.J. Klionsky, and H.-M. Shen, *The emerging mechanisms and functions of microautophagy.* Nature Reviews Molecular Cell Biology, 2023. **24**(3): p. 186-203.
6. Cuervo, A.M. and E. Wong, *Chaperone-mediated autophagy: roles in disease and aging.* Cell research, 2014. **24**(1): p. 92-104.
7. Kaushik, S., U. Bandyopadhyay, S. Sridhar, et al., *Chaperone-mediated autophagy at a glance.* Journal of cell science, 2011. **124**(4): p. 495-499.
8. Mizushima, N. and M. Komatsu, *Autophagy: renovation of cells and tissues.* Cell, 2011. **147**(4): p. 728-741.
9. Yu, L., Y. Chen, and S.A. Tooze, *Autophagy pathway: Cellular and molecular mechanisms.* Autophagy, 2018. **14**(2): p. 207-215.
10. Biazik, J., P. Ylä-Anttila, H. Vihinen, et al., *Ultrastructural relationship of the phagophore with surrounding organelles.* Autophagy, 2015. **11**(3): p. 439-451.
11. Hollenstein, D.M. and C. Kraft, *Autophagosomes are formed at a distinct cellular structure.* Current opinion in cell biology, 2020. **65**: p. 50-57.
12. Zachari, M. and I.G. Ganley, *The mammalian ULK1 complex and autophagy initiation.* Essays in biochemistry, 2017. **61**(6): p. 585-596.
13. Matsunaga, K., T. Saitoh, K. Tabata, et al., *Two Beclin 1-binding proteins, Atg14L and Rubicon, reciprocally regulate autophagy at different stages.* Nature cell biology, 2009. **11**(4): p. 385-396.
14. Nishimura, T. and S.A. Tooze, *Emerging roles of ATG proteins and membrane lipids in autophagosome formation.* Cell discovery, 2020. **6**(1): p. 32.
15. Itakura, E., C. Kishi, K. Inoue, et al., *Beclin 1 forms two distinct phosphatidylinositol 3-kinase complexes with mammalian Atg14 and UVRAG.* Molecular biology of the cell, 2008. **19**(12): p. 5360-5372.
16. Polson, H.E., J. de Lartigue, D.J. Rigden, et al., *Mammalian Atg18 (WIPI2) localizes to omegasome-anchored phagophores and positively regulates LC3 lipidation.* Autophagy, 2010. **6**(4): p. 506-522.
17. Axe, E.L., S.A. Walker, M. Manifava, et al., *Autophagosome formation from membrane compartments enriched in phosphatidylinositol 3-phosphate and dynamically connected to the endoplasmic reticulum.* The Journal of cell biology, 2008. **182**(4): p. 685-701.

18. Ravikumar, B., K. Moreau, L. Jahreiss, et al., *Plasma membrane contributes to the formation of pre-autophagosomal structures.* Nature cell biology, 2010. **12**(8): p. 747-757.

19. Hailey, D.W., A.S. Rambold, P. Satpute-Krishnan, et al., *Mitochondria supply membranes for autophagosome biogenesis during starvation.* Cell, 2010. **141**(4): p. 656-667.

20. De Tito, S., J.H. Hervás, A.R. Van Vliet, et al., *The Golgi as an assembly line to the autophagosome.* Trends in biochemical sciences, 2020. **45**(6): p. 484-496.

21. Puri, C., M. Renna, C.F. Bento, et al., *Diverse autophagosome membrane sources coalesce in recycling endosomes.* Cell, 2013. **154**(6): p. 1285-1299.

22. Dupont, N., S. Chauhan, J. Arko-Mensah, et al., *Neutral lipid stores and lipase PNPLA5 contribute to autophagosome biogenesis.* Current Biology, 2014. **24**(6): p. 609-620.

23. Nakatogawa, H., *Two ubiquitin-like conjugation systems that mediate membrane formation during autophagy.* Essays in biochemistry, 2013. **55**: p. 39-50.

24. Shpilka, T., H. Weidberg, S. Pietrokovski, et al., *Atg8: an autophagy-related ubiquitin-like protein family.* Genome biology, 2011. **12**(7): p. 1-11.

25. Kirisako, T., Y. Ichimura, H. Okada, et al., *The reversible modification regulates the membrane-binding state of Apg8/Aut7 essential for autophagy and the cytoplasm to vacuole targeting pathway.* The Journal of cell biology, 2000. **151**(2): p. 263-276.

26. Mizushima, N., *The ATG conjugation systems in autophagy.* Current opinion in cell biology, 2020. **63**: p. 1-10.

27. Hamasaki, M., N. Furuta, A. Matsuda, et al., *Autophagosomes form at ER–mitochondria contact sites.* Nature, 2013. **495**(7441): p. 389-393.

28. Stolz, A., A. Ernst, and I. Dikic, *Cargo recognition and trafficking in selective autophagy.* Nature cell biology, 2014. **16**(6): p. 495-501.

29. Wesch, N., V. Kirkin, and V.V. Rogov, *Atg8-family proteins—structural features and molecular interactions in autophagy and beyond.* Cells, 2020. **9**(9): p. 2008.

30. Hanada, T., N.N. Noda, Y. Satomi, et al., *The Atg12-Atg5 conjugate has a novel E3-like activity for protein lipidation in autophagy.* Journal of Biological Chemistry, 2007. **282**(52): p. 37298-37302.

31. Lystad, A.H., S.R. Carlsson, L.R. de la Ballina, et al., *Distinct functions of ATG16L1 isoforms in membrane binding and LC3B lipidation in autophagy-related processes.* Nature cell biology, 2019. **21**(3): p. 372-383.

32. Martens, S. and D. Fracchiolla, *Activation and targeting of ATG8 protein lipidation.* Cell discovery, 2020. **6**(1): p. 23.

33. Dooley, H.C., M. Razi, H.E. Polson, et al., *WIPI2 links LC3 conjugation with PI3P, autophagosome formation, and pathogen clearance by recruiting Atg12–5-16L1.* Molecular cell, 2014. **55**(2): p. 238-252.

34. Fracchiolla, D., C. Chang, J.H. Hurley, et al., *A PI3K-WIPI2 positive feedback loop allosterically activates LC3 lipidation in autophagy.* Journal of Cell Biology, 2020. **219**(7): p. e201912098.

35. Takahashi, Y., H. He, Z. Tang, et al., *An autophagy assay reveals the ESCRT-III component CHMP2A as a regulator of phagophore closure.* Nature communications, 2018. **9**(1): p. 2855.

36. Takahashi, Y., X. Liang, T. Hattori, et al., *VPS37A directs ESCRT recruitment for phagophore closure.* Journal of Cell Biology, 2019. **218**(10): p. 3336-3354.

37. Kauffman, K.J., S. Yu, J. Jin, et al., *Delipidation of mammalian Atg8-family proteins by each of the four ATG4 proteases.* Autophagy, 2018. **14**(6): p. 992-1010.

38. Yu, Z.-Q., T. Ni, B. Hong, et al., *Dual roles of Atg8− PE deconjugation by Atg4 in autophagy.* Autophagy, 2012. **8**(6): p. 883-892.

39. Jahreiss, L., F.M. Menzies, and D.C. Rubinsztein, *The itinerary of autophagosomes: from peripheral formation to kiss-and-run fusion with lysosomes.* Traffic, 2008. **9**(4): p. 574-587.

40. Itakura, E., C. Kishi-Itakura, and N. Mizushima, *The hairpin-type tail-anchored SNARE syntaxin 17 targets to autophagosomes for fusion with endosomes/lysosomes.* Cell, 2012. **151**(6): p. 1256-1269.

41. Morelli, E., P. Ginefra, V. Mastrodonato, et al., *Multiple functions of the SNARE protein Snap29 in autophagy, endocytic, and exocytic trafficking during epithelial formation in Drosophila.* Autophagy, 2014. **10**(12): p. 2251-2268.

42. Diao, J., R. Liu, Y. Rong, et al., *ATG14 promotes membrane tethering and fusion of autophagosomes to endolysosomes.* Nature, 2015. **520**(7548): p. 563-566.

43. McEwan, D.G., D. Popovic, A. Gubas, et al., *PLEKHM1 regulates autophagosome-lysosome fusion through HOPS complex and LC3/GABARAP proteins.* Molecular cell, 2015. **57**(1): p. 39-54.

44. Jiang, P., T. Nishimura, Y. Sakamaki, et al., *The HOPS complex mediates autophagosome–lysosome fusion through interaction with syntaxin 17.* Molecular biology of the cell, 2014. **25**(8): p. 1327-1337.

45. Mijaljica, D., M. Prescott, and R.J. Devenish, *V-ATPase engagement in autophagic processes.* Autophagy, 2011. **7**(6): p. 666-668.

46. Kuma, A. and N. Mizushima. *Physiological role of autophagy as an intracellular recycling system: with an emphasis on nutrient metabolism*. in *Seminars in cell & developmental biology*. 2010. Elsevier.

47. Shang, L., S. Chen, F. Du, et al., *Nutrient starvation elicits an acute autophagic response mediated by Ulk1 dephosphorylation and its subsequent dissociation from AMPK.* Proceedings of the National Academy of Sciences, 2011. **108**(12): p. 4788-4793.

48. Wileman, T., *Autophagy as a defence against intracellular pathogens.* Essays in biochemistry, 2013. **55**: p. 153-163.

49. Moreau, K., S. Luo, and D.C. Rubinsztein, *Cytoprotective roles for autophagy.* Current opinion in cell biology, 2010. **22**(2): p. 206-211.

50. Jhanwar-Uniyal, M., A.G. Amin, J.B. Cooper, et al., *Discrete signaling mechanisms of mTORC1 and mTORC2: Connected yet apart in cellular and molecular aspects.* Advances in biological regulation, 2017. **64**: p. 39-48.

51. Kim, J., M. Kundu, B. Viollet, et al., *AMPK and mTOR regulate autophagy through direct phosphorylation of Ulk1.* Nature cell biology, 2011. **13**(2): p. 132-141.

52. Puente, C., R.C. Hendrickson, and X. Jiang, *Nutrient-regulated phosphorylation of ATG13 inhibits starvation-induced autophagy.* Journal of Biological Chemistry, 2016. **291**(11): p. 6026-6035.

53. Yuan, H.-X., R.C. Russell, and K.-L. Guan, *Regulation of PIK3C3/VPS34 complexes by MTOR in nutrient stress-induced autophagy.* Autophagy, 2013. **9**(12): p. 1983-1995.

54. Nazio, F., F. Strappazzon, M. Antonioli, et al., *mTOR inhibits autophagy by controlling ULK1 ubiquitylation, self-association and function through AMBRA1 and TRAF6.* Nature cell biology, 2013. **15**(4): p. 406-416.

55. Wan, W., Z. You, Y. Xu, et al., *mTORC1 phosphorylates acetyltransferase p300 to regulate autophagy and lipogenesis.* Molecular cell, 2017. **68**(2): p. 323-335. e6.

56. Wan, W., Z. You, L. Zhou, et al., *mTORC1-regulated and HUWE1-mediated WIPI2 degradation controls autophagy flux.* Molecular cell, 2018. **72**(2): p. 303-315. e6.

57. Hardie, D.G., *AMPK and autophagy get connected.* The EMBO journal, 2011. **30**(4): p. 634-635.

58. Gwinn, D.M., D.B. Shackelford, D.F. Egan, et al., *AMPK phosphorylation of raptor mediates a metabolic checkpoint.* Molecular cell, 2008. **30**(2): p. 214-226.

59. Inoki, K., T. Zhu, and K.-L. Guan, *TSC2 mediates cellular energy response to control cell growth and survival.* Cell, 2003. **115**(5): p. 577-590.

60. Alers, S., A.S. Löffler, S. Wesselborg, et al., *Role of AMPK-mTOR-Ulk1/2 in the regulation of autophagy: cross talk, shortcuts, and feedbacks.* Molecular and cellular biology, 2012. **32**(1): p. 2-11.

61. Kim, J., Y.C. Kim, C. Fang, et al., *Differential regulation of distinct Vps34 complexes by AMPK in nutrient stress and autophagy.* Cell, 2013. **152**(1): p. 290-303.

62. Sridharan, S., K. Jain, and A. Basu, *Regulation of autophagy by kinases.* Cancers, 2011. **3**(2): p. 2630-2654.

63. Martina, J.A., Y. Chen, M. Gucek, et al., *MTORC1 functions as a transcriptional regulator of autophagy by preventing nuclear transport of TFEB.* Autophagy, 2012. **8**(6): p. 903-914.

64. Xu, Y., J. Ren, X. He, et al., *YWHA/14-3-3 proteins recognize phosphorylated TFEB by a noncanonical mode for controlling TFEB cytoplasmic localization.* Autophagy, 2019. **15**(6): p. 1017-1030.

65. Settembre, C., C. Di Malta, V.A. Polito, et al., *TFEB links autophagy to lysosomal biogenesis.* science, 2011. **332**(6036): p. 1429-1433.

66. Mammucari, C., G. Milan, V. Romanello, et al., *FoxO3 controls autophagy in skeletal muscle in vivo.* Cell metabolism, 2007. **6**(6): p. 458-471.

67. Sanchez, A.M., A. Csibi, A. Raibon, et al., *AMPK promotes skeletal muscle autophagy through activation of forkhead FoxO3a and interaction with Ulk1.* Journal of cellular biochemistry, 2012. **113**(2): p. 695-710.

68. Sakamaki, J.-i., S. Wilkinson, M. Hahn, et al., *Bromodomain protein BRD4 is a transcriptional repressor of autophagy and lysosomal function.* Molecular cell, 2017. **66**(4): p. 517-532. e9.

69. Maejima, I., A. Takahashi, H. Omori, et al., *Autophagy sequesters damaged lysosomes to control lysosomal biogenesis and kidney injury.* The EMBO journal, 2013. **32**(17): p. 2336-2347.

70. Ashrafi, G. and T. Schwarz, *The pathways of mitophagy for quality control and clearance of mitochondria.* Cell Death & Differentiation, 2013. **20**(1): p. 31-42.

71. Bernales, S., K.L. McDonald, and P. Walter, *Autophagy counterbalances endoplasmic reticulum expansion during the unfolded protein response.* PLoS biology, 2006. **4**(12): p. e423.

72. Kraft, C., A. Deplazes, M. Sohrmann, et al., *Mature ribosomes are selectively degraded upon starvation by an autophagy pathway requiring the Ubp3p/Bre5p ubiquitin protease.* Nature cell biology, 2008. **10**(5): p. 602-610.

73. Manjithaya, R., T.Y. Nazarko, J.-C. Farré, et al., *Molecular mechanism and physiological role of pexophagy.* FEBS letters, 2010. **584**(7): p. 1367-1373.

74. Schulze, R.J., A. Sathyanarayan, and D.G. Mashek, *Breaking fat: The regulation and mechanisms of lipophagy.* Biochimica et Biophysica Acta (BBA)-Molecular and Cell Biology of Lipids, 2017. **1862**(10): p. 1178-1187.

75. Bauer, B., S. Martens, and L. Ferrari, *Aggrephagy at a glance.* Journal of Cell Science, 2023. **136**(10): p. jcs260888.

76. Bauckman, K.A., N. Owusu-Boaitey, and I.U. Mysorekar, *Selective autophagy: xenophagy.* Methods, 2015. **75**: p. 120-127.

77. Faruk, M.O., Y. Ichimura, and M. Komatsu, *Selective autophagy.* Cancer science, 2021. **112**(10): p. 3972-3978.

78. Kirkin, V., D.G. McEwan, I. Novak, et al., *A role for ubiquitin in selective autophagy.* Molecular cell, 2009. **34**(3): p. 259-269.

79. Kraft, C., M. Peter, and K. Hofmann, *Selective autophagy: ubiquitin-mediated recognition and beyond.* Nature cell biology, 2010. **12**(9): p. 836-841.

80. Wild, P., D.G. McEwan, and I. Dikic, *The LC3 interactome at a glance.* Journal of cell science, 2014. **127**(1): p. 3-9.

81. Johansen, T. and T. Lamark, *Selective autophagy: ATG8 family proteins, LIR motifs and cargo receptors.* Journal of molecular biology, 2020. **432**(1): p. 80-103.

82. Papadopoulos, C., B. Kravic, and H. Meyer, *Repair or lysophagy: dealing with damaged lysosomes.* Journal of molecular biology, 2020. **432**(1): p. 231-239.

83. Zhang, K.R., C.S. Jankowski, R. Marshall, et al., *Oxidative stress induces lysosomal membrane permeabilization and ceramide accumulation in retinal pigment epithelial cells.* Disease Models & Mechanisms, 2023. **16**(7).

84. Gómez-Sintes, R., M.D. Ledesma, and P. Boya, *Lysosomal cell death mechanisms in aging.* Ageing research reviews, 2016. **32**: p. 150-168.

85. Boya, P. and G. Kroemer, *Lysosomal membrane permeabilization in cell death.* Oncogene, 2008. **27**(50): p. 6434-6451.

86. Hornung, V., F. Bauernfeind, A. Halle, et al., *Silica crystals and aluminum salts activate the NALP3 inflammasome through phagosomal destabilization.* Nature immunology, 2008. **9**(8): p. 847-856.

87. Terman, A., T. Kurz, B. Gustafsson, et al., *Lysosomal labilization.* IUBMB life, 2006. **58**(9): p. 531-539.

88. Papadopoulos, C. and H. Meyer, *Detection and clearance of damaged lysosomes by the endo-lysosomal damage response and lysophagy.* Current Biology, 2017. **27**(24): p. R1330-R1341.

89. Balogi, Z., G. Multhoff, T.K. Jensen, et al., *Hsp70 interactions with membrane lipids regulate cellular functions in health and disease.* Progress in Lipid Research, 2019. **74**: p. 18-30.

90. Kirkegaard, T., A.G. Roth, N.H. Petersen, et al., *Hsp70 stabilizes lysosomes and reverts Niemann–Pick disease-associated lysosomal pathology.* Nature, 2010. **463**(7280): p. 549-553.

91. Sardiello, M., M. Palmieri, A. Di Ronza, et al., *A gene network regulating lysosomal biogenesis and function.* Science, 2009. **325**(5939): p. 473-477.

92. Zoncu, R. and R.M. Perera, *Built to last: lysosome remodeling and repair in health and disease.* Trends in Cell Biology, 2022. **32**(7): p. 597-610.

93. Radulovic, M., K.O. Schink, E.M. Wenzel, et al., *ESCRT-mediated lysosome repair precedes lysophagy and promotes cell survival.* The EMBO journal, 2018. **37**(21): p. e99753.

94. Hung, Y.-H., L.M.-W. Chen, J.-Y. Yang, et al., *Spatiotemporally controlled induction of autophagy-mediated lysosome turnover.* Nature communications, 2013. **4**(1): p. 2111.

95. Hoyer, M.J., S. Swarup, and J.W. Harper, *Mechanisms Controlling Selective Elimination of Damaged Lysosomes.* Current opinion in physiology, 2022: p. 100590.

96. Chauhan, S., S. Kumar, A. Jain, et al., *TRIMs and galectins globally cooperate and TRIM16 and galectin-3 co-direct autophagy in endomembrane damage homeostasis.* Developmental cell, 2016. **39**(1): p. 13-27.

97. Thurston, T.L., M.P. Wandel, N. von Muhlinen, et al., *Galectin 8 targets damaged vesicles for autophagy to defend cells against bacterial invasion.* Nature, 2012. **482**(7385): p. 414-418.

98. Jia, J., Y.P. Abudu, A. Claude-Taupin, et al., *Galectins control mTOR in response to endomembrane damage.* Molecular cell, 2018. **70**(1): p. 120-135. e8.

99. Glenn, K.A., R.F. Nelson, H.M. Wen, et al., *Diversity in tissue expression, substrate binding, and SCF complex formation for a lectin family of ubiquitin ligases.* Journal of Biological Chemistry, 2008. **283**(19): p. 12717-12729.

100. Yoshida, Y., S. Yasuda, T. Fujita, et al., *Ubiquitination of exposed glycoproteins by SCFFBXO27 directs damaged lysosomes for autophagy.* Proceedings of the National Academy of Sciences, 2017. **114**(32): p. 8574-8579.

101. Teranishi, H., K. Tabata, M. Saeki, et al., *Identification of CUL4A-DDB1-WDFY1 as an E3 ubiquitin ligase complex involved in initiation of lysophagy.* Cell Reports, 2022. **40**(11): p. 111349.

102. Huett, A., R.J. Heath, J. Begun, et al., *The LRR and RING domain protein LRSAM1 is an E3 ligase crucial for ubiquitin-dependent autophagy of intracellular Salmonella Typhimurium.* Cell host & microbe, 2012. **12**(6): p. 778-790.

103. Papadopoulos, C., P. Kirchner, M. Bug, et al., *VCP/p97 cooperates with YOD 1, UBXD 1 and PLAA to drive clearance of ruptured lysosomes by autophagy.* The EMBO journal, 2017. **36**(2): p. 135-150.

104. Koerver, L., C. Papadopoulos, B. Liu, et al., *The ubiquitin-conjugating enzyme UBE 2 QL 1 coordinates lysophagy in response to endolysosomal damage.* EMBO reports, 2019. **20**(10): p. e48014.

105. Bai, Y., G. Yu, H.-M. Zhou, et al., *PTP4A2 promotes lysophagy by dephosphorylation of VCP/p97 at Tyr805.* Autophagy, 2023. **19**(5): p. 1562-1581.

106. Gallagher, E.R. and E.L. Holzbaur, *The selective autophagy adaptor p62/SQSTM1 forms phase condensates regulated by HSP27 that facilitate the clearance of damaged lysosomes via lysophagy.* Cell Reports, 2023. **42**(2).

107. Bussi, C., J.M. Peralta Ramos, D.S. Arroyo, et al., *Alpha-synuclein fibrils recruit TBK1 and OPTN to lysosomal damage sites and induce autophagy in microglial cells.* Journal of cell science, 2018. **131**(23): p. jcs226241.

108. Eapen, V.V., S. Swarup, M.J. Hoyer, et al., *Quantitative proteomics reveals the selectivity of ubiquitin-binding autophagy receptors in the turnover of damaged lysosomes by lysophagy.* Elife, 2021. **10**: p. e72328.

109. Bhattacharya, A., R. Mukherjee, S.K. Kuncha, et al., *A lysosome membrane regeneration pathway depends on TBC1D15 and autophagic lysosomal reformation proteins.* Nature Cell Biology, 2023. **25**(5): p. 685-698.

110. Wong, Y.C. and E.L. Holzbaur, *Optineurin is an autophagy receptor for damaged mitochondria in parkin-mediated mitophagy that is disrupted by an ALS-linked mutation.* Proceedings of the National Academy of Sciences, 2014. **111**(42): p. E4439-E4448.

111. Van Wijk, S.J., F. Fricke, L. Herhaus, et al., *Linear ubiquitination of cytosolic Salmonella Typhimurium activates NF-κB and restricts bacterial proliferation.* Nature microbiology, 2017. **2**(7): p. 1-10.

112. Verlhac, P., C. Viret, and M. Faure, *Dual function of CALCOCO2/NDP52 during xenophagy.* Autophagy, 2015. **11**(6): p. 965-966.

113. Sarraf, S.A., H.V. Shah, G. Kanfer, et al., *Loss of TAX1BP1-Directed Autophagy Results in Protein Aggregate Accumulation in the Brain.* Molecular cell, 2022. **82**(7): p. 1383.

114. Lazarou, M., D.A. Sliter, L.A. Kane, et al., *The ubiquitin kinase PINK1 recruits autophagy receptors to induce mitophagy.* Nature, 2015. **524**(7565): p. 309-314.

115. Kageyama, S., S.R. Gudmundsson, Y.-S. Sou, et al., *p62/SQSTM1-droplet serves as a platform for autophagosome formation and anti-oxidative stress response.* Nature communications, 2021. **12**(1): p. 16.

116. Richter, B., D.A. Sliter, L. Herhaus, et al., *Phosphorylation of OPTN by TBK1 enhances its binding to Ub chains and promotes selective autophagy of damaged mitochondria.* Proceedings of the National Academy of Sciences, 2016. **113**(15): p. 4039-4044.

117. Wild, P., H. Farhan, D.G. McEwan, et al., *Phosphorylation of the autophagy receptor optineurin restricts Salmonella growth.* Science, 2011. **333**(6039): p. 228-233.

118. Thurston, T.L., G. Ryzhakov, S. Bloor, et al., *The TBK1 adaptor and autophagy receptor NDP52 restricts the proliferation of ubiquitin-coated bacteria.* Nature immunology, 2009. **10**(11): p. 1215-1221.

119. Heo, J.-M., A. Ordureau, J.A. Paulo, et al., *The PINK1-PARKIN mitochondrial ubiquitylation pathway drives a program of OPTN/NDP52 recruitment and TBK1 activation to promote mitophagy.* Molecular cell, 2015. **60**(1): p. 7-20.

120. Corkery, D.P., S. Castro-Gonzalez, A. Knyazeva, et al., *An ATG12-ATG5-TECPR1 E3-like complex regulates unconventional LC3 lipidation at damaged lysosomes.* EMBO reports, 2023. **24**(9): p. e56841.

121. Menzies, F.M., A. Fleming, A. Caricasole, et al., *Autophagy and neurodegeneration: pathogenic mechanisms and therapeutic opportunities.* Neuron, 2017. **93**(5): p. 1015-1034.

122. Emin, D., Y.P. Zhang, E. Lobanova, et al., *Small soluble α-synuclein aggregates are the toxic species in Parkinson's disease.* Nature communications, 2022. **13**(1): p. 5512.

123. Li, S. and A.M. Stern, *Bioactive human Alzheimer brain soluble Aβ: pathophysiology and therapeutic opportunities.* Molecular Psychiatry, 2022. **27**(8): p. 3182-3191.

124. Kim, Y.E., M.S. Hipp, A. Bracher, et al., *Molecular chaperone functions in protein folding and proteostasis.* Annual review of biochemistry, 2013. **82**: p. 323-355.

125. Pohl, C. and I. Dikic, *Cellular quality control by the ubiquitin-proteasome system and autophagy.* Science, 2019. **366**(6467): p. 818-822.

126. Lamark, T. and T. Johansen, *Aggrephagy: selective disposal of protein aggregates by macroautophagy.* International journal of cell biology, 2012. **2012**.

127. Gatica, D., V. Lahiri, and D.J. Klionsky, *Cargo recognition and degradation by selective autophagy.* Nature cell biology, 2018. **20**(3): p. 233-242.

128. Khaminets, A., C. Behl, and I. Dikic, *Ubiquitin-dependent and independent signals in selective autophagy.* Trends in cell biology, 2016. **26**(1): p. 6-16.

129. Kirkin, V., T. Lamark, Y.-S. Sou, et al., *A role for NBR1 in autophagosomal degradation of ubiquitinated substrates.* Molecular cell, 2009. **33**(4): p. 505-516.

130. Korac, J., V. Schaeffer, I. Kovacevic, et al., *Ubiquitin-independent function of optineurin in autophagic clearance of protein aggregates.* Journal of cell science, 2013. **126**(2): p. 580-592.

131. Lu, K., I. Psakhye, and S. Jentsch, *Autophagic clearance of polyQ proteins mediated by ubiquitin-Atg8 adaptors of the conserved CUET protein family.* Cell, 2014. **158**(3): p. 549-563.

132. Pankiv, S., T.H. Clausen, T. Lamark, et al., *p62/SQSTM1 binds directly to Atg8/LC3 to facilitate degradation of ubiquitinated protein aggregates by autophagy.* Journal of biological chemistry, 2007. **282**(33): p. 24131-24145.

133. Babinchak, W.M. and W.K. Surewicz, *Liquid–liquid phase separation and its mechanistic role in pathological protein aggregation.* Journal of molecular biology, 2020. **432**(7): p. 1910-1925.

134. Mathieu, C., R.V. Pappu, and J.P. Taylor, *Beyond aggregation: Pathological phase transitions in neurodegenerative disease.* Science, 2020. **370**(6512): p. 56-60.

135. Wegmann, S., B. Eftekharzadeh, K. Tepper, et al., *Tau protein liquid–liquid phase separation can initiate tau aggregation.* The EMBO journal, 2018. **37**(7): p. e98049.

136. Turco, E., A. Savova, F. Gere, et al., *Reconstitution defines the roles of p62, NBR1 and TAX1BP1 in ubiquitin condensate formation and autophagy initiation.* Nature communications, 2021. **12**(1): p. 5212.

137. Lamark, T., M. Perander, H. Outzen, et al., *Interaction codes within the family of mammalian Phox and Bem1p domain-containing proteins.* Journal of Biological Chemistry, 2003. **278**(36): p. 34568-34581.

138. Agudo-Canalejo, J., S.W. Schultz, H. Chino, et al., *Wetting regulates autophagy of phase-separated compartments and the cytosol.* Nature, 2021. **591**(7848): p. 142-146.

139. Sun, D., R. Wu, J. Zheng, et al., *Polyubiquitin chain-induced p62 phase separation drives autophagic cargo segregation.* Cell research, 2018. **28**(4): p. 405-415.

140. Ma, X., C. Lu, Y. Chen, et al., *CCT2 is an aggrephagy receptor for clearance of solid protein aggregates.* Cell, 2022. **185**(8): p. 1325-1345. e22.

141. Gestaut, D., A. Limatola, L. Joachimiak, et al., *The ATP-powered gymnastics of TRiC/CCT: an asymmetric protein folding machine with a symmetric origin story.* Current opinion in structural biology, 2019. **55**: p. 50-58.

142. Behrends, C., C.A. Langer, R. Boteva, et al., *Chaperonin TRiC promotes the assembly of polyQ expansion proteins into nontoxic oligomers.* Molecular cell, 2006. **23**(6): p. 887-897.

143. Kitamura, A., H. Kubota, C.-G. Pack, et al., *Cytosolic chaperonin prevents polyglutamine toxicity with altering the aggregation state.* Nature cell biology, 2006. **8**(10): p. 1163-1169.

144. Long, J., T.P. Garner, M.J. Pandya, et al., *Dimerisation of the UBA domain of p62 inhibits ubiquitin binding and regulates NF-κB signalling.* Journal of molecular biology, 2010. **396**(1): p. 178-194.

145. Walinda, E., D. Morimoto, K. Sugase, et al., *Solution structure of the ubiquitin-associated (UBA) domain of human autophagy receptor NBR1 and its interaction with ubiquitin and polyubiquitin.* Journal of Biological Chemistry, 2014. **289**(20): p. 13890-13902.

146. Grice, G.L. and J.A. Nathan, *The recognition of ubiquitinated proteins by the proteasome.* Cellular and molecular life sciences, 2016. **73**: p. 3497-3506.

147. Tan, J.M., E.S. Wong, V.L. Dawson, et al., *Lysine 63-linked polyubiquitin potentially partners with p62 to promote the clearance of protein inclusions by autophagy.* Autophagy, 2008. **4**(2): p. 251-253.

148. Tan, J.M., E.S. Wong, D.S. Kirkpatrick, et al., *Lysine 63-linked ubiquitination promotes the formation and autophagic clearance of protein inclusions associated with neurodegenerative diseases.* Human molecular genetics, 2008. **17**(3): p. 431-439.

149. Cabe, M., D.J. Rademacher, A.B. Karlsson, et al., *PB1 and UBA domains of p62 are essential for aggresome-like induced structure formation.* Biochemical and biophysical research communications, 2018. **503**(4): p. 2306-2311.

150. Lim, J., M.L. Lachenmayer, S. Wu, et al., *Proteotoxic stress induces phosphorylation of p62/SQSTM1 by ULK1 to regulate selective autophagic clearance of protein aggregates.* PLoS genetics, 2015. **11**(2): p. e1004987.

151. Schlütermann, D., N. Berleth, J. Deitersen, et al., *FIP200 controls the TBK1 activation threshold at SQSTM1/p62-positive condensates.* Scientific Reports, 2021. **11**(1): p. 1-18.

152. Filimonenko, M., P. Isakson, K.D. Finley, et al., *The selective macroautophagic degradation of aggregated proteins requires the PI3P-binding protein Alfy.* Molecular cell, 2010. **38**(2): p. 265-279.

153. Simonsen, A., H.C. Birkeland, D.J. Gillooly, et al., *Alfy, a novel FYVE-domain-containing protein associated with protein granules and autophagic membranes.* Journal of cell science, 2004. **117**(18): p. 4239-4251.

154. Fox, L.M., K. Kim, C.W. Johnson, et al., *Huntington's disease pathogenesis is modified in vivo by Alfy/Wdfy3 and selective macroautophagy.* Neuron, 2020. **105**(5): p. 813-821. e6.

155. Clausen, T.H., T. Lamark, P. Isakson, et al., *p62/SQSTM1 and ALFY interact to facilitate the formation of p62 bodies/ALIS and their degradation by autophagy.* Autophagy, 2010. **6**(3): p. 330-344.

156. Yoon, M.J., B. Choi, E.J. Kim, et al., *UXT chaperone prevents proteotoxicity by acting as an autophagy adaptor for p62-dependent aggrephagy.* Nature communications, 2021. **12**(1): p. 1955.

157. Wetzel, L., S. Blanchard, S. Rama, et al., *TECPR1 promotes aggrephagy by direct recruitment of LC3C autophagosomes to lysosomes.* Nature communications, 2020. **11**(1): p. 2993.

158. Tedesco, B., L. Vendredy, V. Timmerman, et al., *The chaperone-assisted selective autophagy complex dynamics and dysfunctions.* Autophagy, 2023: p. 1-23.

159. Johnston, J.A., C.L. Ward, and R.R. Kopito, *Aggresomes: a cellular response to misfolded proteins.* The Journal of cell biology, 1998. **143**(7): p. 1883-1898.

160. Kawaguchi, Y., J.J. Kovacs, A. McLaurin, et al., *The deacetylase HDAC6 regulates aggresome formation and cell viability in response to misfolded protein stress.* Cell, 2003. **115**(6): p. 727-738.

161. Arndt, V., N. Dick, R. Tawo, et al., *Chaperone-assisted selective autophagy is essential for muscle maintenance.* Current Biology, 2010. **20**(2): p. 143-148.

162. Gamerdinger, M., A.M. Kaya, U. Wolfrum, et al., *BAG3 mediates chaperone-based aggresome-targeting and selective autophagy of misfolded proteins.* EMBO reports, 2011. **12**(2): p. 149-156.

163. Iwata, A., B.E. Riley, J.A. Johnston, et al., *HDAC6 and microtubules are required for autophagic degradation of aggregated huntingtin.* Journal of Biological Chemistry, 2005. **280**(48): p. 40282-40292.

164. Weller, M., W. Wick, K. Aldape, et al., *Glioma.* Nature reviews Disease primers, 2015. **1**(1): p. 1-18.

165. Chen, R., M. Smith-Cohn, A.L. Cohen, et al., *Glioma subclassifications and their clinical significance.* Neurotherapeutics, 2017. **14**: p. 284-297.

166. Batash, R., N. Asna, P. Schaffer, et al., *Glioblastoma multiforme, diagnosis and treatment; recent literature review.* Current medicinal chemistry, 2017. **24**(27): p. 3002-3009.

167. Razavi, S.-M., K.E. Lee, B.E. Jin, et al., *Immune evasion strategies of glioblastoma.* Frontiers in surgery, 2016. **3**: p. 11.

168. Fabbro-Peray, P., S. Zouaoui, A. Darlix, et al., *Association of patterns of care, prognostic factors, and use of radiotherapy–temozolomide therapy with survival in patients with newly diagnosed glioblastoma: a French national population-based study.* Journal of Neuro-oncology, 2019. **142**: p. 91-101.

169. Grochans, S., A.M. Cybulska, D. Simińska, et al., *Epidemiology of glioblastoma multiforme–literature review.* Cancers, 2022. **14**(10): p. 2412.

170. Louis, D.N., A. Perry, P. Wesseling, et al., *The 2021 WHO classification of tumors of the central nervous system: a summary.* Neuro-oncology, 2021. **23**(8): p. 1231-1251.

171. Marinković, M., M. Šprung, M. Buljubašić, et al., *Autophagy modulation in cancer: current knowledge on action and therapy.* Oxidative Medicine and Cellular Longevity, 2018. **2018**.

172. Zielke, S., N. Meyer, M. Mari, et al., *Loperamide, pimozide, and STF-62247 trigger autophagy-dependent cell death in glioblastoma cells.* Cell death & disease, 2018. **9**(10): p. 994.

173. Kinzler, M.N., S. Zielke, S. Kardo, et al., *STF-62247 and pimozide induce autophagy and autophagic cell death in mouse embryonic fibroblasts.* Scientific Reports, 2020. **10**(1): p. 687.

174. Zein, L., S. Fulda, D. Kögel, et al., *Organelle-specific mechanisms of drug-induced autophagy-dependent cell death.* Matrix Biology, 2021. **100**: p. 54-64.

175. Jawhari, S., B. Bessette, S. Hombourger, et al., *Autophagy and TrkC/NT-3 signaling joined forces boost the hypoxic glioblastoma cell survival.* Carcinogenesis, 2017. **38**(6): p. 592-603.

176. Zhang, X., W. Li, C. Wang, et al., *Inhibition of autophagy enhances apoptosis induced by proteasome inhibitor bortezomib in human glioblastoma U87 and U251 cells.* Molecular and cellular biochemistry, 2014. **385**: p. 265-275.

177. Chakrabarti, M., D.J. Klionsky, and S.K. Ray, *miR-30e blocks autophagy and acts synergistically with proanthocyanidin for inhibition of AVEN and BIRC6 to increase apoptosis in glioblastoma stem cells and glioblastoma SNB19 cells.* PLoS One, 2016. **11**(7): p. e0158537.

178. Fulda, S., *Cell death-based treatment of glioblastoma.* Cell death & disease, 2018. **9**(2): p. 121.

179. Zielke, S., S. Kardo, L. Zein, et al., *ATF4 links ER stress with reticulophagy in glioblastoma cells.* Autophagy, 2021. **17**(9): p. 2432-2448.

180. Josset, E., H. Burckel, G. Noel, et al., *The mTOR inhibitor RAD001 potentiates autophagic cell death induced by temozolomide in a glioblastoma cell line.* Anticancer research, 2013. **33**(5): p. 1845-1851.

181. Rosenfeld, M.R., X. Ye, J.G. Supko, et al., *A phase I/II trial of hydroxychloroquine in conjunction with radiation therapy and concurrent and adjuvant temozolomide in patients with newly diagnosed glioblastoma multiforme.* Autophagy, 2014. **10**(8): p. 1359-1368.

182. Taylor, M.A., B.C. Das, and S.K. Ray, *Targeting autophagy for combating chemoresistance and radioresistance in glioblastoma.* Apoptosis, 2018. **23**(11-12): p. 563-575.

183. Nixon, R.A., *The role of autophagy in neurodegenerative disease.* Nature medicine, 2013. **19**(8): p. 983-997.

184. Fecto, F., J. Yan, S.P. Vemula, et al., *SQSTM1 mutations in familial and sporadic amyotrophic lateral sclerosis.* Archives of neurology, 2011. **68**(11): p. 1440-1446.

185. Walden, H. and M.M. Muqit, *Ubiquitin and Parkinson's disease through the looking glass of genetics.* Biochemical Journal, 2017. **474**(9): p. 1439-1451.

186. Spilman, P., N. Podlutskaya, M.J. Hart, et al., *Inhibition of mTOR by rapamycin abolishes cognitive deficits and reduces amyloid-β levels in a mouse model of Alzheimer's disease.* PloS one, 2010. **5**(4): p. e9979.

187. Spencer, B., R. Potkar, M. Trejo, et al., *Beclin 1 gene transfer activates autophagy and ameliorates the neurodegenerative pathology in α-synuclein models of Parkinson's and Lewy body diseases.* Journal of Neuroscience, 2009. **29**(43): p. 13578-13588.

188. Kieburtz, K., M.P. McDermott, T.S. Voss, et al., *A randomized, placebo-controlled trial of latrepirdine in Huntington disease.* Archives of neurology, 2010. **67**(2): p. 154-160.

189. Miller, R., S. Smith, J. Murphy, et al., *A clinical trial of verapamil in amyotrophic lateral sclerosis.* Muscle & Nerve: Official Journal of the American Association of Electrodiagnostic Medicine, 1996. **19**(4): p. 511-515.

190. Regnard, C., R. Twycross, M. Mihalyo, et al., *Loperamide.* Journal of pain and symptom management, 2011. **42**(2): p. 319-323.

191. Merritt, J., B. Brown, and S. Tomlinson, *Loperamide and calmodulin.* The Lancet, 1982. **319**(8266): p. 283.

192. Church, J., E.J. Fletcher, K. Abdel-Hamid, et al., *Loperamide blocks high-voltage-activated calcium channels and N-methyl-D-aspartate-evoked responses in rat and mouse cultured hippocampal pyramidal neurons.* Molecular pharmacology, 1994. **45**(4): p. 747-757.

193. Sadeque, A.J., C. Wandel, H. He, et al., *Increased drug delivery to the brain by P-glycoprotein inhibition.* Clinical Pharmacology & Therapeutics, 2000. **68**(3): p. 231-237.

194. Zhang, L., J. Yu, H. Pan, et al., *Small molecule regulators of autophagy identified by an image-based high-throughput screen.* Proceedings of the National Academy of Sciences, 2007. **104**(48): p. 19023-19028.

195. Thiele, D.L. and P.E. Lipsky, *The action of leucyl-leucine methyl ester on cytotoxic lymphocytes requires uptake by a novel dipeptide-specific facilitated transport system and dipeptidyl peptidase I-mediated conversion to membranolytic products.* The Journal of experimental medicine, 1990. **172**(1): p. 183-194.

196. Thiele, D.L. and P.E. Lipsky, *Mechanism of L-leucyl-L-leucine methyl ester-mediated killing of cytotoxic lymphocytes: dependence on a lysosomal thiol protease, dipeptidyl peptidase I, that is enriched in these cells.* Proceedings of the National Academy of Sciences, 1990. **87**(1): p. 83-87.

197. Skowyra, M.L., P.H. Schlesinger, T.V. Naismith, et al., *Triggered recruitment of ESCRT machinery promotes endolysosomal repair.* Science, 2018. **360**(6384): p. eaar5078.

198. Uchimoto, T., H. Nohara, R. Kamehara, et al., *Mechanism of apoptosis induced by a lysosomotropic agent, L-Leucyl-L-Leucine methyl ester.* Apoptosis, 1999. **4**: p. 357-362.

199. Finley, D., *Recognition and processing of ubiquitin-protein conjugates by the proteasome.* Annual review of biochemistry, 2009. **78**: p. 477-513.

200. Jin, L., A. Williamson, S. Banerjee, et al., *Mechanism of ubiquitin-chain formation by the human anaphase-promoting complex.* Cell, 2008. **133**(4): p. 653-665.

201. Matsumoto, M.L., K.E. Wickliffe, K.C. Dong, et al., *K11-linked polyubiquitination in cell cycle control revealed by a K11 linkage-specific antibody.* Molecular cell, 2010. **39**(3): p. 477-484.

202. Yuan, W.-C., Y.-R. Lee, S.-Y. Lin, et al., *K33-linked polyubiquitination of coronin 7 by Cul3-KLHL20 ubiquitin E3 ligase regulates protein trafficking.* Molecular cell, 2014. **54**(4): p. 586-600.

203. Gerlach, B., S.M. Cordier, A.C. Schmukle, et al., *Linear ubiquitination prevents inflammation and regulates immune signalling.* Nature, 2011. **471**(7340): p. 591-596.

204. Ikeda, F., Y.L. Deribe, S.S. Skånland, et al., *SHARPIN forms a linear ubiquitin ligase complex regulating NF-κB activity and apoptosis.* Nature, 2011. **471**(7340): p. 637-641.

205. Vijay-Kumar, S., C.E. Bugg, and W.J. Cook, *Structure of ubiquitin refined at 1.8 Åresolution.* Journal of molecular biology, 1987. **194**(3): p. 531-544.

206. Dikic, I., S. Wakatsuki, and K.J. Walters, *Ubiquitin-binding domains—from structures to functions.* Nature reviews Molecular cell biology, 2009. **10**(10): p. 659-671.

207. Kamadurai, H.B., J. Souphron, D.C. Scott, et al., *Insights into ubiquitin transfer cascades from a structure of a UbcH5B∼ ubiquitin-HECTNEDD4L complex.* Molecular cell, 2009. **36**(6): p. 1095-1102.

208. Reyes-Turcu, F.E., J.R. Horton, J.E. Mullally, et al., *The ubiquitin binding domain ZnF UBP recognizes the C-terminal diglycine motif of unanchored ubiquitin.* Cell, 2006. **124**(6): p. 1197-1208.

209. Rahighi, S., F. Ikeda, M. Kawasaki, et al., *Specific recognition of linear ubiquitin chains by NEMO is important for NF-κB activation.* Cell, 2009. **136**(6): p. 1098-1109.

210. Sloper-Mould, K.E., J.C. Jemc, C.M. Pickart, et al., *Distinct functional surface regions on ubiquitin.* Journal of Biological Chemistry, 2001. **276**(32): p. 30483-30489.

211. Schulman, B.A. and J. Wade Harper, *Ubiquitin-like protein activation by E1 enzymes: the apex for downstream signalling pathways.* Nature reviews Molecular cell biology, 2009. **10**(5): p. 319-331.

212. Ye, Y. and M. Rape, *Building ubiquitin chains: E2 enzymes at work.* Nature reviews Molecular cell biology, 2009. **10**(11): p. 755-764.

213. Buetow, L. and D.T. Huang, *Structural insights into the catalysis and regulation of E3 ubiquitin ligases.* Nature reviews Molecular cell biology, 2016. **17**(10): p. 626-642.

214. Clague, M.J., C. Heride, and S. Urbé, *The demographics of the ubiquitin system.* Trends in cell biology, 2015. **25**(7): p. 417-426.

215. Smit, J.J. and T.K. Sixma, *RBR E3-ligases at work.* EMBO reports, 2014. **15**(2): p. 142-154.

216. Foot, N., T. Henshall, and S. Kumar, *Ubiquitination and the regulation of membrane proteins.* Physiological reviews, 2017. **97**(1): p. 253-281.

217. Akutsu, M., I. Dikic, and A. Bremm, *Ubiquitin chain diversity at a glance.* Journal of cell science, 2016. **129**(5): p. 875-880.

218. Meyer, H.-J. and M. Rape, *Enhanced protein degradation by branched ubiquitin chains.* Cell, 2014. **157**(4): p. 910-921.

219. Kane, L.A., M. Lazarou, A.I. Fogel, et al., *PINK1 phosphorylates ubiquitin to activate Parkin E3 ubiquitin ligase activity.* Journal of Cell Biology, 2014. **205**(2): p. 143-153.

220. Ohtake, F., Y. Saeki, K. Sakamoto, et al., *Ubiquitin acetylation inhibits polyubiquitin chain elongation.* EMBO reports, 2015. **16**(2): p. 192-201.

221. Flotho, A. and F. Melchior, *Sumoylation: a regulatory protein modification in health and disease.* Annual review of biochemistry, 2013. **82**: p. 357-385.

222. Enchev, R.I., B.A. Schulman, and M. Peter, *Protein neddylation: beyond cullin–RING ligases.* Nature reviews Molecular cell biology, 2015. **16**(1): p. 30-44.

223. Haas, A.L., P. Ahrens, P. Bright, et al., *Interferon induces a 15-kilodalton protein exhibiting marked homology to ubiquitin.* Journal of Biological Chemistry, 1987. **262**(23): p. 11315-11323.

224. Husnjak, K. and I. Dikic, *Ubiquitin-binding proteins: decoders of ubiquitin-mediated cellular functions.* Annual review of biochemistry, 2012. **81**: p. 291-322.

225. Komander, D. and M. Rape, *The ubiquitin code.* Annual review of biochemistry, 2012. **81**: p. 203-229.

226. Swatek, K.N. and D. Komander, *Ubiquitin modifications.* Cell research, 2016. **26**(4): p. 399-422.

227. Clague, M.J., I. Barsukov, J.M. Coulson, et al., *Deubiquitylases from genes to organism.* Physiological reviews, 2013. **93**(3): p. 1289-1315.

228. Kwasna, D., S.A.A. Rehman, J. Natarajan, et al., *Discovery and characterization of ZUFSP/ZUP1, a distinct deubiquitinase class important for genome stability.* Molecular cell, 2018. **70**(1): p. 150-164. e6.

229. Rehman, S.A.A., Y.A. Kristariyanto, S.-Y. Choi, et al., *MINDY-1 is a member of an evolutionarily conserved and structurally distinct new family of deubiquitinating enzymes.* Molecular cell, 2016. **63**(1): p. 146-155.

230. Clague, M.J., S. Urbé, and D. Komander, *Breaking the chains: deubiquitylating enzyme specificity begets function.* Nature reviews Molecular cell biology, 2019. **20**(6): p. 338-352.

231. Mevissen, T.E. and D. Komander, *Mechanisms of deubiquitinase specificity and regulation.* Annual review of biochemistry, 2017. **86**: p. 159-192.

232. Faesen, A.C., M.P. Luna-Vargas, P.P. Geurink, et al., *The differential modulation of USP activity by internal regulatory domains, interactors and eight ubiquitin chain types.* Chemistry & biology, 2011. **18**(12): p. 1550-1561.

233. Keusekotten, K., P.R. Elliott, L. Glockner, et al., *OTULIN antagonizes LUBAC signaling by specifically hydrolyzing Met1-linked polyubiquitin.* Cell, 2013. **153**(6): p. 1312-1326.

234. Mevissen, T.E., Y. Kulathu, M.P. Mulder, et al., *Molecular basis of Lys11-polyubiquitin specificity in the deubiquitinase Cezanne.* Nature, 2016. **538**(7625): p. 402-405.

235. Bremm, A., S.M. Freund, and D. Komander, *Lys11-linked ubiquitin chains adopt compact conformations and are preferentially hydrolyzed by the deubiquitinase Cezanne.* Nature structural & molecular biology, 2010. **17**(8): p. 939-947.

236. Cunningham, C.N., J.M. Baughman, L. Phu, et al., *USP30 and parkin homeostatically regulate atypical ubiquitin chains on mitochondria.* Nature cell biology, 2015. **17**(2): p. 160-169.

237. Sato, Y., K. Okatsu, Y. Saeki, et al., *Structural basis for specific cleavage of Lys6-linked polyubiquitin chains by USP30.* Nature structural & molecular biology, 2017. **24**(11): p. 911-919.

238. Gersch, M., C. Gladkova, A.F. Schubert, et al., *Mechanism and regulation of the Lys6-selective deubiquitinase USP30.* Nature structural & molecular biology, 2017. **24**(11): p. 920-930.

239. Hospenthal, M.K., S.M. Freund, and D. Komander, *Assembly, analysis and architecture of atypical ubiquitin chains.* Nature structural & molecular biology, 2013. **20**(5): p. 555-565.

240. Mevissen, T.E., M.K. Hospenthal, P.P. Geurink, et al., *OTU deubiquitinases reveal mechanisms of linkage specificity and enable ubiquitin chain restriction analysis.* Cell, 2013. **154**(1): p. 169-184.

241. Lee, B.-H., Y. Lu, M.A. Prado, et al., *USP14 deubiquitinates proteasome-bound substrates that are ubiquitinated at multiple sites.* Nature, 2016. **532**(7599): p. 398-401.

242. Zhang, X.-y., H. Pfeiffer, A. Thorne, et al., *USP22, an hSAGA subunit and potential cancer stem cell marker, reverses the polycomb-catalyzed ubiquitylation of histone H2A.* Cell cycle, 2008. **7**(11): p. 1522-1524.

243. Sobhian, B., G. Shao, D.R. Lilli, et al., *RAP80 targets BRCA1 to specific ubiquitin structures at DNA damage sites.* Science, 2007. **316**(5828): p. 1198-1202.

244. Bonacci, T., A. Suzuki, G.D. Grant, et al., *Cezanne/OTUD 7B is a cell cycle-regulated deubiquitinase that antagonizes the degradation of APC/C substrates.* The EMBO journal, 2018. **37**(16): p. e98701.

245. Fiil, B.K., R.B. Damgaard, S.A. Wagner, et al., *OTULIN restricts Met1-linked ubiquitination to control innate immune signaling.* Molecular cell, 2013. **50**(6): p. 818-830.

246. Hrdinka, M., B.K. Fiil, M. Zucca, et al., *CYLD limits Lys63-and Met1-linked ubiquitin at receptor complexes to regulate innate immune signaling.* Cell reports, 2016. **14**(12): p. 2846-2858.

247. Draber, P., S. Kupka, M. Reichert, et al., *LUBAC-recruited CYLD and A20 regulate gene activation and cell death by exerting opposing effects on linear ubiquitin in signaling complexes.* Cell reports, 2015. **13**(10): p. 2258-2272.

248. Heger, K., K.E. Wickliffe, A. Ndoja, et al., *OTULIN limits cell death and inflammation by deubiquitinating LUBAC.* Nature, 2018. **559**(7712): p. 120-124.

249. Herhaus, L., A.B. Perez-Oliva, G. Cozza, et al., *Casein kinase 2 (CK2) phosphorylates the deubiquitylase OTUB1 at Ser16 to trigger its nuclear localization.* Science signaling, 2015. **8**(372): p. ra35-ra35.

250. Coornaert, B., M. Baens, K. Heyninck, et al., *T cell antigen receptor stimulation induces MALT1 paracaspase–mediated cleavage of the NF-κB inhibitor A20.* Nature immunology, 2008. **9**(3): p. 263-271.

251. Dixit, V.M., S. Green, V. Sarma, et al., *Tumor necrosis factor-alpha induction of novel gene products in human endothelial cells including a macrophage-specific chemotaxin.* Journal of Biological Chemistry, 1990. **265**(5): p. 2973-2978.

252. Kirisako, T., K. Kamei, S. Murata, et al., *A ubiquitin ligase complex assembles linear polyubiquitin chains.* The EMBO journal, 2006. **25**(20): p. 4877-4887.

253. Yamanaka, K., H. Ishikawa, Y. Megumi, et al., *Identification of the ubiquitin–protein ligase that recognizes oxidized IRP2.* Nature cell biology, 2003. **5**(4): p. 336-340.

254. Tokunaga, F., T. Nakagawa, M. Nakahara, et al., *SHARPIN is a component of the NF-κB-activating linear ubiquitin chain assembly complex.* Nature, 2011. **471**(7340): p. 633-636.

255. Sasaki, K. and K. Iwai, *LUBAC-mediated linear ubiquitination in tissue homeostasis and disease.* The Journal of Biochemistry, 2023: p. mvad045.

256. Schaeffer, V., M. Akutsu, M.H. Olma, et al., *Binding of OTULIN to the PUB domain of HOIP controls NF-κB signaling.* Molecular cell, 2014. **54**(3): p. 349-361.

257. Elliott, P.R., S.V. Nielsen, P. Marco-Casanova, et al., *Molecular basis and regulation of OTULIN-LUBAC interaction.* Molecular cell, 2014. **54**(3): p. 335-348.

258. Elliott, P.R., D. Leske, M. Hrdinka, et al., *SPATA2 links CYLD to LUBAC, activates CYLD, and controls LUBAC signaling.* Molecular cell, 2016. **63**(6): p. 990-1005.

259. Kupka, S., D. De Miguel, P. Draber, et al., *SPATA2-mediated binding of CYLD to HOIP enables CYLD recruitment to signaling complexes.* Cell reports, 2016. **16**(9): p. 2271-2280.

260. van Well, E.M., V. Bader, M. Patra, et al., *A protein quality control pathway regulated by linear ubiquitination.* The EMBO journal, 2019. **38**(9): p. e100730.

261. Fujita, H., A. Tokunaga, S. Shimizu, et al., *Cooperative domain formation by homologous motifs in HOIL-1L and SHARPIN plays a crucial role in LUBAC stabilization.* Cell reports, 2018. **23**(4): p. 1192-1204.

262. Sato, Y., H. Fujita, A. Yoshikawa, et al., *Specific recognition of linear ubiquitin chains by the Npl4 zinc finger (NZF) domain of the HOIL-1L subunit of the linear*

ubiquitin chain assembly complex. Proceedings of the National Academy of Sciences, 2011. **108**(51): p. 20520-20525.

263. Fujita, H., S. Rahighi, M. Akita, et al., *Mechanism underlying IκB kinase activation mediated by the linear ubiquitin chain assembly complex.* Molecular and cellular biology, 2014. **34**(7): p. 1322-1335.

264. Smit, J.J., D. Monteferrario, S.M. Noordermeer, et al., *The E3 ligase HOIP specifies linear ubiquitin chain assembly through its RING-IBR-RING domain and the unique LDD extension.* The EMBO journal, 2012. **31**(19): p. 3833-3844.

265. Stieglitz, B., R.R. Rana, M.G. Koliopoulos, et al., *Structural basis for ligase-specific conjugation of linear ubiquitin chains by HOIP.* Nature, 2013. **503**(7476): p. 422-426.

266. Fuseya, Y., H. Fujita, M. Kim, et al., *The HOIL-1L ligase modulates immune signalling and cell death via monoubiquitination of LUBAC.* Nature Cell Biology, 2020. **22**(6): p. 663-673.

267. Peltzer, N., E. Rieser, L. Taraborrelli, et al., *HOIP deficiency causes embryonic lethality by aberrant TNFR1-mediated endothelial cell death.* Cell reports, 2014. **9**(1): p. 153-165.

268. Boisson, B., E. Laplantine, C. Prando, et al., *Immunodeficiency, autoinflammation and amylopectinosis in humans with inherited HOIL-1 and LUBAC deficiency.* Nature immunology, 2012. **13**(12): p. 1178-1186.

269. Lee, I.Y., J.M. Lim, H. Cho, et al., *MST1 negatively regulates TNFα-induced NF-κB signaling through modulating LUBAC activity.* Molecular cell, 2019. **73**(6): p. 1138-1149. e6.

270. Strickson, S., D.G. Campbell, C.H. Emmerich, et al., *The anti-inflammatory drug BAY 11-7082 suppresses the MyD88-dependent signalling network by targeting the ubiquitin system.* Biochemical Journal, 2013. **451**(3): p. 427-437.

271. Sakamoto, H., S. Egashira, N. Saito, et al., *Gliotoxin suppresses NF-κB activation by selectively inhibiting linear ubiquitin chain assembly complex (LUBAC).* ACS chemical biology, 2015. **10**(3): p. 675-681.

272. De Cesare, V., C. Johnson, V. Barlow, et al., *The MALDI-TOF E2/E3 ligase assay as universal tool for drug discovery in the ubiquitin pathway.* Cell chemical biology, 2018. **25**(9): p. 1117-1127. e4.

273. Katsuya, K., Y. Hori, D. Oikawa, et al., *High-throughput screening for linear ubiquitin chain assembly complex (LUBAC) selective inhibitors using homogenous time-resolved fluorescence (HTRF)-based assay system.* SLAS DISCOVERY: Advancing Life Sciences R&D, 2018. **23**(10): p. 1018-1029.

274. Katsuya, K., D. Oikawa, K. Iio, et al., *Small-molecule inhibitors of linear ubiquitin chain assembly complex (LUBAC), HOIPINs, suppress NF-κB signaling.* Biochemical and biophysical research communications, 2019. **509**(3): p. 700-706.

275. Oikawa, D., Y. Sato, F. Ohtake, et al., *Molecular bases for HOIPINs-mediated inhibition of LUBAC and innate immune responses.* Communications Biology, 2020. **3**(1): p. 163.

276. Fiil, B.K. and M. Gyrd-Hansen, *The Met1-linked ubiquitin machinery in inflammation and infection.* Cell Death & Differentiation, 2021. **28**(2): p. 557-569.

277. Sato, Y., E. Goto, Y. Shibata, et al., *Structures of CYLD USP with Met1-or Lys63-linked diubiquitin reveal mechanisms for dual specificity.* Nature structural & molecular biology, 2015. **22**(3): p. 222-229.

278. Lork, M., K. Verhelst, and R. Beyaert, *CYLD, A20 and OTULIN deubiquitinases in NF-κB signaling and cell death: so similar, yet so different.* Cell Death & Differentiation, 2017. **24**(7): p. 1172-1183.

279. Tokunaga, F., H. Nishimasu, R. Ishitani, et al., *Specific recognition of linear polyubiquitin by A20 zinc finger 7 is involved in NF-κB regulation.* The EMBO journal, 2012. **31**(19): p. 3856-3870.

280. Verhelst, K., I. Carpentier, M. Kreike, et al., *A20 inhibits LUBAC-mediated NF-κB activation by binding linear polyubiquitin chains via its zinc finger 7.* The EMBO journal, 2012. **31**(19): p. 3845-3855.

281. Damgaard, R.B., P.R. Elliott, K.N. Swatek, et al., *OTULIN deficiency in ORAS causes cell type-specific LUBAC degradation, dysregulated TNF signalling and cell death.* EMBO molecular medicine, 2019. **11**(3): p. e9324.

282. Damgaard, R.B., H.E. Jolin, M.E. Allison, et al., *OTULIN protects the liver against cell death, inflammation, fibrosis, and cancer.* Cell Death & Differentiation, 2020. **27**(5): p. 1457-1474.

283. Damgaard, R.B., J.A. Walker, P. Marco-Casanova, et al., *The deubiquitinase OTULIN is an essential negative regulator of inflammation and autoimmunity.* Cell, 2016. **166**(5): p. 1215-1230. e20.

284. Elliott, P.R. and D. Komander, *Regulation of Met1-linked polyubiquitin signalling by the deubiquitinase OTULIN.* The FEBS journal, 2016. **283**(1): p. 39-53.

285. Rivkin, E., S.M. Almeida, D.F. Ceccarelli, et al., *The linear ubiquitin-specific deubiquitinase gumby regulates angiogenesis.* Nature, 2013. **498**(7454): p. 318-324.

286. Zhou, Q., X. Yu, E. Demirkaya, et al., *Biallelic hypomorphic mutations in a linear deubiquitinase define otulipenia, an early-onset autoinflammatory disease.* Proceedings of the National Academy of Sciences, 2016. **113**(36): p. 10127-10132.

287. Douglas, T. and M. Saleh, *Post-translational modification of OTULIN regulates ubiquitin dynamics and cell death.* Cell Reports, 2019. **29**(11): p. 3652-3663. e5.

288. Verboom, L., A. Martens, D. Priem, et al., *OTULIN prevents liver inflammation and hepatocellular carcinoma by inhibiting FADD-and RIPK1 kinase-mediated hepatocyte apoptosis.* Cell reports, 2020. **30**(7): p. 2237-2247. e6.

289. Noad, J., A. Von Der Malsburg, C. Pathe, et al., *LUBAC-synthesized linear ubiquitin chains restrict cytosol-invading bacteria by activating autophagy and NF-κB.* Nature microbiology, 2017. **2**(7): p. 1-10.

290. Stangl, A., P.R. Elliott, A. Pinto-Fernandez, et al., *Regulation of the endosomal SNX27-retromer by OTULIN.* Nature communications, 2019. **10**(1): p. 4320.

291. Zuo, Y., Q. Feng, L. Jin, et al., *Regulation of the linear ubiquitination of STAT1 controls antiviral interferon signaling.* Nature communications, 2020. **11**(1): p. 1146.

292. Schlicher, L., M. Wissler, F. Preiss, et al., *SPATA 2 promotes CYLD activity and regulates TNF-induced NF-κB signaling and cell death.* EMBO reports, 2016. **17**(10): p. 1485-1497.

293. Jono, H., J.H. Lim, L.-F. Chen, et al., *NF-κB is essential for induction of CYLD, the negative regulator of NF-κB: evidence for a novel inducible autoregulatory feedback pathway.* Journal of Biological Chemistry, 2004. **279**(35): p. 36171-36174.

294. Haas, T.L., C.H. Emmerich, B. Gerlach, et al., *Recruitment of the linear ubiquitin chain assembly complex stabilizes the TNF-R1 signaling complex and is required for TNF-mediated gene induction.* Molecular cell, 2009. **36**(5): p. 831-844.

295. Tokunaga, F., *Involvement of linear polyubiquitylation of NEMO in NF-kappaB activation. 236.* Nat Cell Biol.

296. Goto, E. and F. Tokunaga, *Decreased linear ubiquitination of NEMO and FADD on apoptosis with caspase-mediated cleavage of HOIP.* Biochemical and biophysical research communications, 2017. **485**(1): p. 152-159.

297. Damgaard, R.B., U. Nachbur, M. Yabal, et al., *The ubiquitin ligase XIAP recruits LUBAC for NOD2 signaling in inflammation and innate immunity.* Molecular cell, 2012. **46**(6): p. 746-758.

298. Bertrand, M.J., K. Doiron, K. Labbé, et al., *Cellular inhibitors of apoptosis cIAP1 and cIAP2 are required for innate immunity signaling by the pattern recognition receptors NOD1 and NOD2.* Immunity, 2009. **30**(6): p. 789-801.

299. Cohen, P. and S. Strickson, *The role of hybrid ubiquitin chains in the MyD88 and other innate immune signalling pathways.* Cell Death & Differentiation, 2017. **24**(7): p. 1153-1159.

300. Tarantino, N., J.-Y. Tinevez, E.F. Crowell, et al., *TNF and IL-1 exhibit distinct ubiquitin requirements for inducing NEMO–IKK supramolecular structures.* Journal of Cell Biology, 2014. **204**(2): p. 231-245.

301. Zak, D.E., F. Schmitz, E.S. Gold, et al., *Systems analysis identifies an essential role for SHANK-associated RH domain-interacting protein (SHARPIN) in macrophage Toll-like receptor 2 (TLR2) responses.* Proceedings of the National Academy of Sciences, 2011. **108**(28): p. 11536-11541.

302. Emmerich, C.H., A. Ordureau, S. Strickson, et al., *Activation of the canonical IKK complex by K63/M1-linked hybrid ubiquitin chains.* Proceedings of the National Academy of Sciences, 2013. **110**(38): p. 15247-15252.

303. Christofferson, D.E., Y. Li, and J. Yuan, *Control of life-or-death decisions by RIP1 kinase.* Annual review of physiology, 2014. **76**: p. 129-150.

304. Peltzer, N., M. Darding, and H. Walczak, *Holding RIPK1 on the ubiquitin leash in TNFR1 signaling.* Trends in cell biology, 2016. **26**(6): p. 445-461.

305. Rickard, J.A., H. Anderton, N. Etemadi, et al., *TNFR1-dependent cell death drives inflammation in Sharpin-deficient mice.* Elife, 2014. **3**: p. e03464.

306. Kumari, S., Y. Redouane, J. Lopez-Mosqueda, et al., *Sharpin prevents skin inflammation by inhibiting TNFR1-induced keratinocyte apoptosis.* Elife, 2014. **3**: p. e03422.

307. Taraborrelli, L., N. Peltzer, A. Montinaro, et al., *LUBAC prevents lethal dermatitis by inhibiting cell death induced by TNF, TRAIL and CD95L.* Nature communications, 2018. **9**(1): p. 3910.

308. Peltzer, N., M. Darding, A. Montinaro, et al., *LUBAC is essential for embryogenesis by preventing cell death and enabling haematopoiesis.* Nature, 2018. **557**(7703): p. 112-117.

309. Chu, Y., Y. Kang, C. Yan, et al., *LUBAC and OTULIN regulate autophagy initiation and maturation by mediating the linear ubiquitination and the stabilization of ATG13.* Autophagy, 2021. **17**(7): p. 1684-1699.

310. Inn, K.-S., M.U. Gack, F. Tokunaga, et al., *Linear ubiquitin assembly complex negatively regulates RIG-I-and TRIM25-mediated type I interferon induction.* Molecular cell, 2011. **41**(3): p. 354-365.

311. Belgnaoui, S.M., S. Paz, S. Samuel, et al., *Linear ubiquitination of NEMO negatively regulates the interferon antiviral response through disruption of the MAVS-TRAF3 complex.* Cell host & microbe, 2012. **12**(2): p. 211-222.

312. Rodgers, M.A., J.W. Bowman, H. Fujita, et al., *The linear ubiquitin assembly complex (LUBAC) is essential for NLRP3 inflammasome activation.* Journal of Experimental Medicine, 2014. **211**(7): p. 1333-1347.

313. Seymour, R., M. Hasham, G. Cox, et al., *Spontaneous mutations in the mouse Sharpin gene result in multiorgan inflammation, immune system dysregulation and dermatitis.* Genes & Immunity, 2007. **8**(5): p. 416-421.

314. Oda, H., K. Manthiram, P. Pimpale Chavan, et al., *Human LUBAC deficiency leads to autoinflammation and immunodeficiency by dysregulation in TNF-mediated cell death.* medRxiv, 2022: p. 2022.11. 09.22281431.

315. Nilsson, J., B. Schoser, P. Laforet, et al., *Polyglucosan body myopathy caused by defective ubiquitin ligase RBCK1.* Annals of neurology, 2013. **74**(6): p. 914-919.

316. Wang, K., C. Kim, J. Bradfield, et al., *Whole-genome DNA/RNA sequencing identifies truncating mutations in RBCK1 in a novel Mendelian disease with neuromuscular and cardiac involvement.* Genome medicine, 2013. **5**(7): p. 1-8.

317. Boisson, B., E. Laplantine, K. Dobbs, et al., *Human HOIP and LUBAC deficiency underlies autoinflammation, immunodeficiency, amylopectinosis, and lymphangiectasia.* Journal of Experimental Medicine, 2015. **212**(6): p. 939-951.

318. Yang, Y., R. Schmitz, J. Mitala, et al., *Essential role of the linear ubiquitin chain assembly complex in lymphoma revealed by rare germline polymorphisms.* Cancer discovery, 2014. **4**(4): p. 480-493.

319. Nakayama, Y., S. Sakamoto, K. Tsuji, et al., *Identification of linear polyubiquitin chain immunoreactivity in tau pathology of Alzheimer's disease.* Neuroscience Letters, 2019. **703**: p. 53-57.

320. Nakayama, Y., K. Tsuji, T. Ayaki, et al., *Linear polyubiquitin chain modification of TDP-43-positive neuronal cytoplasmic inclusions in amyotrophic lateral sclerosis.* Journal of Neuropathology & Experimental Neurology, 2020. **79**(3): p. 256-265.

321. Perera, R.M., S. Stoykova, B.N. Nicolay, et al., *Transcriptional control of autophagy–lysosome function drives pancreatic cancer metabolism.* Nature, 2015. **524**(7565): p. 361-365.

322. Yang, A., N. Rajeshkumar, X. Wang, et al., *Autophagy is critical for pancreatic tumor growth and progression in tumors with p53 alterations.* Cancer discovery, 2014. **4**(8): p. 905-913.

323. Settembre, C., A. Fraldi, L. Jahreiss, et al., *A block of autophagy in lysosomal storage disorders.* Human molecular genetics, 2008. **17**(1): p. 119-129.

324. Seranova, E., K.J. Connolly, M. Zatyka, et al., *Dysregulation of autophagy as a common mechanism in lysosomal storage diseases.* Essays in biochemistry, 2017. **61**(6): p. 733-749.

325. Chen, R.-H., Y.-H. Chen, and T.-Y. Huang, *Ubiquitin-mediated regulation of autophagy.* Journal of Biomedical Science, 2019. **26**: p. 1-12.

326. Doench, J.G., N. Fusi, M. Sullender, et al., *Optimized sgRNA design to maximize activity and minimize off-target effects of CRISPR-Cas9.* Nature biotechnology, 2016. **34**(2): p. 184-191.

327. Zellner, S., M. Schifferer, and C. Behrends, *Systematically defining selective autophagy receptor-specific cargo using autophagosome content profiling.* Molecular cell, 2021. **81**(6): p. 1337-1354. e8.

328. Stojkovska, I., W.Y. Wani, F. Zunke, et al., *Rescue of α-synuclein aggregation in Parkinson's patient neurons by synergistic enhancement of ER proteostasis and protein trafficking.* Neuron, 2022. **110**(3): p. 436-451. e11.

329. Zunke, F., A.C. Moise, N.R. Belur, et al., *Reversible conformational conversion of α-synuclein into toxic assemblies by glucosylceramide.* Neuron, 2018. **97**(1): p. 92-107. e10.

330. Kriks, S., J.-W. Shim, J. Piao, et al., *Dopamine neurons derived from human ES cells efficiently engraft in animal models of Parkinson's disease.* Nature, 2011. **480**(7378): p. 547-551.

331. Livak, K.J. and T.D. Schmittgen, *Analysis of relative gene expression data using real-time quantitative PCR and the 2− ΔΔCT method.* methods, 2001. **25**(4): p. 402-408.

332. Cox, J. and M. Mann, *MaxQuant enables high peptide identification rates, individualized ppb-range mass accuracies and proteome-wide protein quantification.* Nature biotechnology, 2008. **26**(12): p. 1367-1372.

333. Tyanova, S., T. Temu, P. Sinitcyn, et al., *The Perseus computational platform for comprehensive analysis of (prote) omics data.* Nature methods, 2016. **13**(9): p. 731-740.

334. Zein, L., M. Dietrich, D. Balta, et al., *Linear ubiquitination at damaged lysosomes induces local NF-κB activation and controls cell survival.* bioRxiv, 2023: p. 2023.10. 06.560832.

335. Zhao, M., Y. Zhang, Y. Jiang, et al., *YAP promotes autophagy and progression of gliomas via upregulating HMGB1.* Journal of Experimental & Clinical Cancer Research, 2021. **40**: p. 1-15.

336. Huang, T., C.K. Kim, A.A. Alvarez, et al., *MST4 phosphorylation of ATG4B regulates autophagic activity, tumorigenicity, and radioresistance in glioblastoma.* Cancer cell, 2017. **32**(6): p. 840-855. e8.

337. Yoshii, S.R. and N. Mizushima, *Monitoring and measuring autophagy.* International journal of molecular sciences, 2017. **18**(9): p. 1865.

338. Genau, H.M., J. Huber, F. Baschieri, et al., *CUL3-KBTBD6/KBTBD7 ubiquitin ligase cooperates with GABARAP proteins to spatially restrict TIAM1-RAC1 signaling.* Molecular cell, 2015. **57**(6): p. 995-1010.

339. Tumbarello, D.A., P.T. Manna, M. Allen, et al., *The autophagy receptor TAX1BP1 and the molecular motor myosin VI are required for clearance of salmonella typhimurium by autophagy.* PLoS pathogens, 2015. **11**(10): p. e1005174.

340. Huyghe, J., D. Priem, L. Van Hove, et al., *ATG9A prevents TNF cytotoxicity by an unconventional lysosomal targeting pathway.* Science, 2022. **378**(6625): p. 1201-1207.

341. Hyer, M.L., M.A. Milhollen, J. Ciavarri, et al., *A small-molecule inhibitor of the ubiquitin activating enzyme for cancer treatment.* Nature medicine, 2018. **24**(2): p. 186-193.

342. Kavčič, N., M. Butinar, B. Sobotič, et al., *Intracellular cathepsin C levels determine sensitivity of cells to leucyl-leucine methyl ester-triggered apoptosis.* The FEBS journal, 2020. **287**(23): p. 5148-5166.

343. Root, J., P. Merino, A. Nuckols, et al., *Lysosome dysfunction as a cause of neurodegenerative diseases: Lessons from frontotemporal dementia and amyotrophic lateral sclerosis.* Neurobiology of disease, 2021. **154**: p. 105360.

344. Wallings, R.L., S.W. Humble, M.E. Ward, et al., *Lysosomal dysfunction at the centre of Parkinson's disease and frontotemporal dementia/amyotrophic lateral sclerosis.* Trends in neurosciences, 2019. **42**(12): p. 899-912.

345. Udayar, V., Y. Chen, E. Sidransky, et al., *Lysosomal dysfunction in neurodegeneration: emerging concepts and methods.* Trends in neurosciences, 2022.

346. Xia, P., S. Wang, G. Huang, et al., *RNF2 is recruited by WASH to ubiquitinate AMBRA1 leading to downregulation of autophagy.* Cell research, 2014. **24**(8): p. 943-958.

347. Jin, S., S. Tian, Y. Chen, et al., *USP 19 modulates autophagy and antiviral immune responses by deubiquitinating beclin-1.* The EMBO journal, 2016. **35**(8): p. 866-880.

348. Dossou, A.S. and A. Basu, *The emerging roles of mTORC1 in macromanaging autophagy.* Cancers, 2019. **11**(10): p. 1422.

349. Ohnstad, A.E., J.M. Delgado, B.J. North, et al., *Receptor-mediated clustering of FIP200 bypasses the role of LC3 lipidation in autophagy.* The EMBO Journal, 2020. **39**(24): p. e104948.

350. Furthmann, N., L. Angersbach, V. Bader, et al., *NEMO reshapes the protein aggregate interface and promotes aggrephagy by co-condensation with p62.* bioRxiv, 2023: p. 2023.06. 05.543428.

351. Iwata, A., J.C. Christianson, M. Bucci, et al., *Increased susceptibility of cytoplasmic over nuclear polyglutamine aggregates to autophagic degradation.* Proceedings of the National Academy of Sciences, 2005. **102**(37): p. 13135-13140.

352. Dieterich, D.C., J.J. Lee, A.J. Link, et al., *Labeling, detection and identification of newly synthesized proteomes with bioorthogonal non-canonical amino-acid tagging.* Nature protocols, 2007. **2**(3): p. 532-540.

353. Shima, T., M. Ogura, R. Matsuda, et al., *The TMEM192-mKeima probe specifically assays lysophagy and reveals its initial steps.* Journal of Cell Biology, 2023. **222**(12): p. e202204048.

354. Katayama, H., T. Kogure, N. Mizushima, et al., *A sensitive and quantitative technique for detecting autophagic events based on lysosomal delivery.* Chemistry & biology, 2011. **18**(8): p. 1042-1052.

355. Wu, Z., L.A. Berlemann, V. Bader, et al., *LUBAC assembles a ubiquitin signaling platform at mitochondria for signal amplification and transport of NF-κB to the nucleus.* The EMBO Journal, 2022. **41**(24): p. e112006.

356. Moore, A.S. and E.L. Holzbaur, *Dynamic recruitment and activation of ALS-associated TBK1 with its target optineurin are required for efficient mitophagy.* Proceedings of the National Academy of Sciences, 2016. **113**(24): p. E3349-E3358.

357. Matsumoto, G., T. Shimogori, N. Hattori, et al., *TBK1 controls autophagosomal engulfment of polyubiquitinated mitochondria through p62/SQSTM1 phosphorylation.* Human molecular genetics, 2015. **24**(15): p. 4429-4442.

358. Hasan, M., V.K. Gonugunta, N. Dobbs, et al., *Chronic innate immune activation of TBK1 suppresses mTORC1 activity and dysregulates cellular metabolism.* Proceedings of the National Academy of Sciences, 2017. **114**(4): p. 746-751.

359. Ou, Y.-H., M. Torres, R. Ram, et al., *TBK1 directly engages Akt/PKB survival signaling to support oncogenic transformation.* Molecular cell, 2011. **41**(4): p. 458-470.

360. Hahn-Windgassen, A., V. Nogueira, C.-C. Chen, et al., *Akt activates the mammalian target of rapamycin by regulating cellular ATP level and AMPK activity.* Journal of Biological Chemistry, 2005. **280**(37): p. 32081-32089.

361. Kumar, S., Y. Gu, Y.P. Abudu, et al., *Phosphorylation of syntaxin 17 by TBK1 controls autophagy initiation.* Developmental cell, 2019. **49**(1): p. 130-144. e6.

362. Lafont, E., P. Draber, E. Rieser, et al., *TBK1 and IKKε prevent TNF-induced cell death by RIPK1 phosphorylation.* Nature cell biology, 2018. **20**(12): p. 1389-1399.

363. Emmerich, C.H., S. Bakshi, I.R. Kelsall, et al., *Lys63/Met1-hybrid ubiquitin chains are commonly formed during the activation of innate immune signalling.* Biochemical and biophysical research communications, 2016. **474**(3): p. 452-461.

364. Cirman, T., K. Orešić, G.D. Mazovec, et al., *Selective disruption of lysosomes in HeLa cells triggers apoptosis mediated by cleavage of Bid by multiple papain-like lysosomal cathepsins.* Journal of Biological Chemistry, 2004. **279**(5): p. 3578-3587.

365. Droga-Mazovec, G., L. Bojic, A. Petelin, et al., *Cysteine cathepsins trigger caspase-dependent cell death through cleavage of bid and antiapoptotic Bcl-2 homologues.* Journal of Biological Chemistry, 2008. **283**(27): p. 19140-19150.

366. Johansson, A.-C., H. Steen, K. Öllinger, et al., *Cathepsin D mediates cytochrome c release and caspase activation in human fibroblast apoptosis induced by staurosporine.* Cell Death & Differentiation, 2003. **10**(11): p. 1253-1259.

367. Liu, S., Y. Li, H.M. Choi, et al., *Lysosomal damage after spinal cord injury causes accumulation of RIPK1 and RIPK3 proteins and potentiation of necroptosis.* Cell death & disease, 2018. **9**(5): p. 476.

368. Zou, J., T. Kawai, T. Tsuchida, et al., *Poly IC triggers a cathepsin D-and IPS-1-dependent pathway to enhance cytokine production and mediate dendritic cell necroptosis.* Immunity, 2013. **38**(4): p. 717-728.

369. Torii, S., R. Shintoku, C. Kubota, et al., *An essential role for functional lysosomes in ferroptosis of cancer cells.* Biochemical Journal, 2016. **473**(6): p. 769-777.

370. Li, S., Z. Liao, H. Yin, et al., *G3BP1 coordinates lysophagy activity to protect against compression‐induced cell ferroptosis during intervertebral disc degeneration.* Cell Proliferation, 2023. **56**(3): p. e13368.

371. Zhou, B., J. Liu, R. Kang, et al. *Ferroptosis is a type of autophagy-dependent cell death*. in *Seminars in cancer biology*. 2020. Elsevier.

372. Kimura, S., T. Noda, and T. Yoshimori, *Dissection of the autophagosome maturation process by a novel reporter protein, tandem fluorescent-tagged LC3.* Autophagy, 2007. **3**(5): p. 452-460.

373. Kågedal, K., M. Zhao, I. Svensson, et al., *Sphingosine-induced apoptosis is dependent on lysosomal proteases.* Biochemical Journal, 2001. **359**(2): p. 335-343.

374. Werneburg, N.W., M.E. Guicciardi, S.F. Bronk, et al., *Tumor necrosis factor-α-associated lysosomal permeabilization is cathepsin B dependent.* American Journal of Physiology-Gastrointestinal and Liver Physiology, 2002. **283**(4): p. G947-G956.

375. Guicciardi, M.E., J. Deussing, H. Miyoshi, et al., *Cathepsin B contributes to TNF-α–mediated hepatocyte apoptosis by promoting mitochondrial release of cytochrome c.* The Journal of clinical investigation, 2000. **106**(9): p. 1127-1137.

376. Liu, N., S.M. Raja, F. Zazzeroni, et al., *NF-κB protects from the lysosomal pathway of cell death.* The EMBO journal, 2003. **22**(19): p. 5313-5322.

11 Erklärung

Ich erkläre hiermit, dass ich die vorgelegte Dissertation mit dem Titel „New insights in LUBAC- and OTULIN-mediated M1 poly-ubiquitination in the regulation of bulk and selective autophagy“ selbständig angefertigt und mich anderer Hilfsmittel als der in ihr angegebenen nicht bedient habe, insbesondere, dass alle Entlehnungen aus anderen Schriften mit Angabe der betreffenden Schrift gekennzeichnet sind. Alle Beiträge von Kollegen und Kolleginnen werden in der Arbeit explizit erwähnt und sind im Folgenden nochmals aufgeführt:

Fig. 21: M1 poly-Ub accumulation at damaged lysosomes induces local recruitment of NEMO. Marvin Dietrich (medizinischer Doktorand): Behandlung der Zellen, Durchführung der Mikroskopie, Statistische Auswertung und Aufbereitung der Figure; eigener Beitrag: Generierung der *OTULIN* KO Zellen, Konzeption und Supervision.

Fig. 22: Lysosomal damage induces IKK phosphorylation on M1 poly-Ub-modified lysosomes in an OTULIN-dependent manner. Marvin Dietrich (medizinischer Doktorand): Behandlung der Zellen, Durchführung der Mikroskopie, Statistische Auswertung und Aufbereitung der Figure; eigener Beitrag: Generierung der *OTULIN* KO Zellen, Konzeption und Supervision.

Fig. 23: HOIPIN-8-mediated HOIP inhibition decreases LLOMe-induced formation of NEMO puncta. Marvin Dietrich (medizinischer Doktorand): Behandlung der Zellen, Durchführung der Mikroskopie, Statistische Auswertung und Aufbereitung der Figure; eigener Beitrag: Generierung der *OTULIN* KO Zellen, Konzeption und Supervision.

Fig. 24: Inhibition of IKKβ with TPCA-1 prevents IKK phosphorylation at LLOMe-induced M1 poly-Ub puncta. Marvin Dietrich (medizinischer Doktorand): Behandlung der Zellen, Durchführung der Mikroskopie, Statistische Auswertung und Aufbereitung der Figure; eigener Beitrag: Generierung der *OTULIN* KO Zellen, Konzeption und Supervision.

Fig. 25: M1 poly-Ub accumulation at damaged lysosomes induces NF-κB target gene activation in an OTULIN-dependent manner. Marvin Dietrich (medizinischer Doktorand): Behandlung der Zellen, Durchführung der qPCR, Statistische Auswertung und Aufbereitung der Figure; eigener Beitrag: Generierung der *OTULIN* KO Zellen, Konzeption und Supervision.

Fig. 26: Formation of M1 poly-Ub chains at damaged lysosomes relies on K63 poly-Ub. Marvin Dietrich (medizinischer Doktorand): Behandlung der Zellen, Durchführung der Mikroskopie, Aufbereitung der Figure; eigener Beitrag: Generierung der *OTULIN* KO Zellen, Konzeption und Supervision.

Fig. 27: Local recruitment of NEMO to damaged lysosomes and NF-κB activation depends on K63 poly-Ub. Marvin Dietrich (medizinischer Doktorand): Behandlung der Zellen, Durchführung der Mikroskopie und qPCR, Statistische Auswertung und Aufbereitung der Figure; eigener Beitrag: Generierung der *OTULIN* KO Zellen, Konzeption und Supervision.

Fig. 28: Lysophagy serves pro-survival roles during LMP-induced cell death. Marvin Dietrich (medizinischer Doktorand): Behandlung der Zellen, Durchführung der Zelltodmessung, Statistische Auswertung und Aufbereitung der Figure; eigener Beitrag: Generierung der OTULIN KO Zellen, OTULIN Knockdown und Durchführung der Western Blot Analyse zur Bestätigung des OTULIN Knockdown, Konzeption und Supervision.

Das unten aufgeführte Material wurde im Rahmen von Forschungskooperationen erstellt:

Fig. 6: Loss of OTULIN enhances the formation of degradative compartments and autophagosomes. Kollaborationspartner: Muriel C. Mari, Department of Biomedicine, Aarhus University, Denmark; Beitrag des Kollaborationspartners: Elektronenmikroskopie von MZ-54 Zellen, Aufbereitung der Aufnahmen, Quantifizierung und statistische Auswertung; eigener Beitrag: Behandlung und Fixierung der Zellen in Vorbereitung auf die Elektronenmikroskopie, Aufbereitung der Figure.

Fig. 8: APEX2-based autophagosome content profiling identifies OTULIN-dependent autophagy cargo candidates. Kollaborationspartner: Christian Behrends und Susanne Zellner, Munich Cluster for Systems Neurology (SyNergy), Ludwig-Maximilians-University, Munich, Germany; Beitrag des Kollaborationspartners: Proteinase K Verdau, Streptavidin Pulldown, Durchführung, Analyse und statistische Auswertung der Massenspektrometrie im Rahmen des „Autophagosome Content Profiling“; eigener Beitrag: Generierung, Behandlung und Biotinylierung der Zellen in Vorbereitung auf die Massenspektrometrie, Aufbereitung der Figure.

Fig. 29: M1 poly-Ub increases at damaged lysosomes in human dopaminergic neurons and primary mouse cortical neurons. Kollaborationspartner 1: Friederike Zunke, Denise Balta und Julia Vandrey, Department of Molecular Neurology, University Hospital Erlangen, Friedrich-Alexander-University Erlangen-Nürnberg, Germany; Beitrag des Kollaborationspartners: Kultivierung der iPSCs und Differenzierung zu DA-iPSn, Behandlung und Durchführung der Mikroskopie; eigener Beitrag: Statistische Auswertung, Aufbereitung der Figure. Kollaborationspartner 2: Konstanze Winklhofer und Verian Bader, Department of Molecular Cell Biology, Institute of Biochemistry and Pathobiochemistry, Ruhr University Bochum, Germany; Beitrag des

Kollaborationspartners: Kultivierung der Mausneuronen, Behandlung und Durchführung der Mikroskopie; eigener Beitrag: Aufbereitung der Figure.

Die folgenden Teile der Dissertation sind bereits in Teilen veröffentlicht worden:

Aus „Linear ubiquitination at damaged lysosomes induces local NF-κB activation and controls cell survival“ (bioRxiv 2023.10.06.560832; doi: https://doi.org/10.1101/2023.10.06.560832) [334].

Vereinzelte Textpassagen aus den folgenden Kapiteln:

4.2.2 iPSC culture and neuronal differentiation

4.2.3 Culture of primary mouse cortical neurons

4.2.4 Generation of CRISPR/Cas9-derived *OTULIN* KO cells

4.2.5 Generation of myc-APEX2-LC3B expressing MZ-54 cells

4.2.6 Quantification of cell death

4.2.7 RNAi-mediated silencing of protein expression

4.2.8 Immunofluorescence analysis (confocal microscope)

4.2.9 Electron microscopy

4.2.14 APEX2-based autophagosome content profiling

4.2.15 Mass spectrometry (MS) data collection and analysis

5.1 Characterization of the function of OTULIN and LUBAC in autophagy

5.3 Role of OTULIN and M1 poly-Ub in lysophagy

6.1 Function of OTULIN in the control of autophagy

6.2 OTULIN-dependent effects on autophagy cargo proteins

6.4 Role of OTULIN and M1 poly-Ub in the response to lysosomal damage

6.5 TBK1 activation after lysosomal damage is regulated by OTULIN and M1 poly-Ub

6.7 M1 poly-Ub at damaged lysosomes serves as platform for local NF-κB activation

6.8 K63 poly-Ub is required for M1 ubiquitination of damaged lysosomes and local NF-κB activation

6.9 Lysophagy serves pro-survival functions in the response to lysosomal damage

6.10 Modeling the response to lysosomal damage in primary human and mouse neurons

Teile von den folgenden Abbildungen:

Figure 4. Loss of OTULIN enhances LC3 lipidation in response to autophagy induction and increases the autophagic flux.

Figure 5. OTULIN depletion enhances LOP-induced formation of LC3 and M1 poly-Ub puncta.

Figure 6. Loss of OTULIN enhances the formation of degradative compartments and autophagosomes.

Figure 7. Generation and validation of myc-APEX2-LC3B-expressing MZ-54 cells.

Figure 8. APEX2-based autophagosome content profiling identifies OTULIN-dependent autophagy cargo candidates.

Figure 9. Validation of selected cargo candidates.

Figure 10. TAX1BP1 degradation is regulated in an OTULIN-dependent manner.

Figure 16. M1 poly-Ub accumulates at damaged lysosomes.

Figure 17. TAX1BP1 is recruited to damaged lysosomes and colocalizes with LLOMe-induced M1 poly-Ub puncta.

Figure 18. Clearance of galectin-3 puncta after lysosomal damage might be affected by loss of OTULIN.

Figure 19. Loss of OTULIN increases TBK1 phosphorylation in response to lysosomal damage.

Figure 21. M1 poly-Ub accumulation at damaged lysosomes induces local recruitment of NEMO.

Figure 22. Lysosomal damage induces IKK phosphorylation on M1 poly-Ub-modified lysosomes in an OTULIN-dependent manner.

Figure 23. HOIPIN-8-mediated HOIP inhibition decreases LLOMe-induced formation of NEMO puncta.

Figure 24. Inhibition of IKKβ with TPCA-1 prevents IKK phosphorylation at LLOMe-induced M1 poly-Ub puncta.

Figure 25. M1 poly-Ub accumulation at damaged lysosomes induces NF-κB target gene activation in an OTULIN-dependent manner.

Figure 26. Formation of M1 poly-Ub chains at damaged lysosomes relies on K63 poly-Ub.

Figure 27. Local recruitment of NEMO to damaged lysosomes and NF-κB activation depends on K63 poly-Ub.

Figure 28. Lysophagy serves pro-survival roles during LMP-induced cell death.

Figure 29. M1 poly-Ub increases at damaged lysosomes in human dopaminergic neurons and primary mouse cortical neurons.

Ich versichere, die Grundsätze der guten wissenschaftlichen Praxis beachtet, und nicht die Hilfe einer kommerziellen Promotionsvermittlung in Anspruch genommen zu haben.

Frankfurt am Main, den 03.04.2024